Molecular and Cellular Mechanisms Regulating PTH Receptor Signaling and Biology

by

Alex Duncan White

B.S., Butler University, 2015

Submitted to the Graduate Faculty of

School of Medicine in partial fulfillment

of the requirements for the degree of

Doctor of Philosophy

University of Pittsburgh

2020

UNIVERSITY OF PITTSBURGH

SCHOOL OF MEDICINE

This thesis/dissertation was presented

by

Alex Duncan White

It was defended on

December 13, 2019

and approved by

Guillermo Romero, Associate Professor, Pharmacology and Chemical Biology

Alessandro Bisello, Associate Professor, Pharmacology and Chemical Biology

Kunhong Xiao, Associate Professor, Pharmacology and Chemical Biology

Alexander Sorkin, Professor, Cell Biology

Dissertation Director: Jean-Pierre Vilardaga, Professor, Pharmacology and Chemical Biology

Molecular and Cellular Mechanisms Regulating PTH Receptor Signaling and Biology

Alex Duncan White, PhD

University of Pittsburgh, 2020

G protein-coupled receptors (GPCRs) are the largest family of cell surface proteins that initiate intracellular signaling in response to extracellular stimuli. The classical paradigm of GPCR signaling dictates that downstream responses are relatively transient and confined to the cell surface, but this notion has been challenged in recent years following the identification of several receptors that can engage in sustained G protein-dependent signaling responses from early endosomes following internalization of the ligand-receptor complex. This phenomenon was initially discovered for the parathyroid hormone (PTH) type 1 receptor (PTHR), a class B GPCR that mediates the biological effects of endogenous peptide ligands PTH and its related peptide (PTHrP). Despite significant advancements toward understanding the determinants and relevance of PTHR-mediated endosomal cAMP signaling, this aspect of GPCR signaling remains incompletely understood. Here, we utilize a combination of optical, biochemical, cell biological, and physiological approaches to elucidate novel molecular and cellular mechanisms that underlie endosomal cAMP responses by the PTHR, as well as its biological relevance. We demonstrate that extracellular Ca^{2+} acts as a positive allosteric modulator of the PTHR by prolonging ligand residence time and increasing the propensity of ligand-receptor complexes to engage in endosomal cAMP generation. We subsequently utilize biased agonism to decode the biological information encoded in the spatial versus temporal dimension of cAMP signaling. Finally, we identify G_q coupling as a critical determinant in PTH-mediated endosomal cAMP production. These findings

unveil novel insights into mechanisms and biological outcomes of PTHR-mediated signaling that may prove useful in rational drug design.

Table of Contents

1.0 Introduction 1

1.1 G Protein-coupled Receptors 1

1.1.1 Classification of GPCRs 2

1.1.2 GPCR Signaling 3

1.2 The Parathyroid Hormone Type 1 Receptor 4

1.2.1 Biological Effects of the PTHR 5

1.3 New Mode of cAMP Signaling 6

1.3.1 Mechanisms of PTHR Endosomal cAMP Signaling and its Regulation 7

1.3.2 Physiological and Disease Relevance of Endosomal cAMP Signaling 8

1.4 Advancing our Understanding of Endosomal cAMP Regulation and Significance . 9

2.0 Ca^{2+} Allostery in PTH Receptor Signaling 11

2.1 Introduction 11

2.2 Materials and Methods 12

2.2.1 Cell Culture and Transfection 12

2.2.2 Assessment of Receptor Cell Surface Expression by FACS 12

2.2.3 Peptides, Chemicals, Mutagenesis, and Western Blot Analysis 13

2.2.4 Saturation Binding at Equilibrium 14

2.2.5 Laser Scanning Confocal Microscopy 15

2.2.6 Time-course Measurements of cAMP Production in Live Cells 15

2.2.7 Receptor Recycling 16

2.2.8 Endosomal pH 16

2.2.9 Purification of PTHR 17

2.2.10 Assessment of Purified Receptor Functionality 18

2.2.11 Homology Modeling of PTHR 19

2.2.12 Photometric FRET Recordings of Kinetics of Ligand Binding and Receptor Activation 19

2.2.13 Detection of Ca^{2+} Binding PTHR Fragments by Liquid Chromatography with Tandem Mass Spectrometry 21

2.2.14 Statistical Analysis 22

2.3 Results 23

2.3.1 Extracellular Ca^{2+} Prolongs Ligand Residence Time and Promotes Receptor Activation and Endosomal cAMP Production 23

2.3.2 Mass Spectrometry Evidence of Ca^{2+} Binding to Extracellular Loop 1 of the Receptor 26

2.3.3 Positive Ca^{2+} Allostery is Lost for a Hypocalcemia-causing PTH Mutant .. 29

2.4 Discussion 32

3.0 Use of Backbone Modification to Enlarge the Spatiotemporal Diversity of Parathyroid Hormone Receptor-1 Signaling via Biased Agonism 35

3.1 Introduction 35

3.2 Materials and Methods 37

3.2.1 Materials 37

3.2.2 Peptide Synthesis, Purification, and Quantification 37

3.2.3 Glosensor cAMP Assay 38

3.2.4 PTHR-βarr BRET Assay 39

3.2.5 Washout Assay 39

3.2.6 Co-immunoprecipitation 40

3.2.7 Hypothetical Molecular Basis for α/β G_s-biased PTHR Agonists..... 41

3.3 Results..... 42

3.4 Discussion 49

4.0 Biased GPCR Signaling Reveals Endosomal cAMP as Determinant for Vitamin D Homeostasis 50

4.1 Introduction 50

4.2 Materials and Methods 52

4.2.1 Cell Culture and Transfection 52

4.2.2 Chemicals..... 53

4.2.3 Peptide Synthesis, Purification, and Quantification 53

4.2.4 Plasmids 54

4.2.5 Co-immunoprecipitation 54

4.2.6 cAMP Accumulation Assay..... 55

4.2.7 Washout Assay 55

4.2.8 cAMP Time-courses and βarr Recruitment by FRET 56

4.2.9 βarr Recruitment by BRET 57

4.2.10 Saturation and Competition Binding Using PTH^{TMR}..... 57

4.2.11 Receptor Internalization and Recycling 58

4.2.12 Mouse Studies..... 58

4.2.13 Pharmacokinetic Analysis 59

4.2.14 MD simulations 60

4.2.15 Structural Modeling 61

4.2.16 1-α(OH)ase protein expression 61

4.2.17 Photo-crosslinking experiments 62

4.2.18 Stable Isotope Labeling With Amino Acids in Cell Culture (SILAC) 63

4.2.19 HA-PTHR Isolation, Digestion, and Peptide Desalting 64

4.2.20 MS and Data Analyses 65

4.2.21 Statistical Analysis 66

4.3 Results 67

4.4 Discussion 81

5.0 $G_{q/11}$-dependent Regulation of Endosomal cAMP Generation by Parathyroid Hormone Class B GPCR 84

5.1 Introduction 84

5.2 Materials and Methods 85

5.2.1 Cell Culture and Transfection 85

5.2.2 Peptides and Chemicals 86

5.2.3 Plasmids 86

5.2.4 Co-immunoprecipitation 87

5.2.5 Time-course Measurements of cAMP Production and βarr Recruitment in Live Cells 87

5.2.6 Saturation and Competition Binding at Equilibrium 88

5.2.7 Laser Scanning Confocal Microscopy 89

5.2.8 BRET Recordings of PTHR-βarr Interaction. 89

5.2.9 Statistical Analysis 90

5.3 Results **90**

5.4 Discussion **97**

6.0 Final Conclusions **99**

Bibliography **103**

List of Figures

Figure 1. Allosteric Action of Extracellular Ca^{2+} on PTH Signaling. 24

Figure 2. Ligand Residence Time Determined by Ca^{2+} Allostery. 25

Figure 3. Involvement of the Receptor's ECL1 in Ca^{2+} Allostery. 28

Figure 4. Involvement of R25 of PTH in Interaction Stabilization and Receptor Signaling. 31

Figure 5. α/β PTHR Agonists Displaying Significant G_s-biased Agonism Relative to PTH(1-34). 43

Figure 6. Activity Profiles of PTH and α/β G_s-biased PTHR Agonists. 44

Figure 7. Equations Used to Calculate Ligand Bias Factor. 45

Figure 8. Recruitment of Endogenous βarr to PTHR Detected by Co-immunoprecipitation. 46

Figure 9. Effect of Competitive Antagonist and BA1 on Signal Duration. 48

Figure 10. Characterization of Signaling by PTH^{7d}. 68

Figure 11. Localization of Signaling Complexes. 70

Figure 12. SILAC-based quantitative phosphorylation analysis of PTH. 72

Figure 13. Molecular changes induced by PTH^{7d}. 74

Figure 14. Structural basis for impaired βarr coupling by PTH^{7d}. 76

Figure 15. Differential physiological actions of PTH^{7d}, PTH^{WT}, and LA-PTH in mice. 79

Figure 16. Pharmacokinetic Analysis of PTH^{7d} and LA-PTH. 81

Figure 17. $G_{q/11}$-dependent cAMP Production by PTH. 92

Figure 18. Effect of Gq/11 Activation on the Formation of PTHR Endosomal Signaling Complexes. 94

Figure 19. Recruitment of βarr is Regulated by $G_{q/11}$-dependent Activation of PI3Kβ. 96

Figure 20. Ca^{2+} Allostery in PTHR Signaling. 100

Figure 21. Decoding Spatial From Temporal Information of cAMP Signaling via PTH Receptor Biased Agonism 101

Figure 22. $G_{q/11}$-dependent Regulation of Endosomal cAMP Generation by PTH Class B GPCR. 102

1.0 Introduction

1.1 G Protein-coupled Receptors

G protein-coupled receptors (GPCRs) are the largest family of cell surface receptors that regulate an array of physiological processes in response to extracellular stimuli. They consist of an extracellular amino terminus, seven transmembrane (TM) helices, and an intracellular carboxy terminus, and these receptors are highly conserved and represent approximately 1-2% of the human genome. The evolution of multicellular organisms has been partly dependent on the successful evolution of GPCRs, being able to transduce extracellular signals to intracellular functions, and thus, enabling cells to communicate with each other and their environment [1]. GPCRs are also present in insects [2], plants [3], yeast [4], and protozoa [5], as well as in nematodes with the *C. elegans* genome encoding more than 1000 GPCRs [6]. In humans, GPCR function is implicated in the regulation of various physiological systems and their malfunction causes severe disease states such as cancer, pain, cardiovascular disorders, gastrointestinal disorders, and conditions of the central nervous and endocrine systems, among others. The generation of cell-based functional assays in combination with traditional radioligand binding assays and the novel structural information derived from crystal structures of several GPCRs are enabling the translation of fundamental biology into therapeutic applications [7]. Additionally, the cell membrane localization of GPCRs and the diversity of tissue expression have made GPCRs ideal pharmacological targets for drug development. Not surprisingly, around 30% of FDA-approved therapeutics target GPCRs, and there persists a growing interest in this large family of receptors both within the pharmaceutical industry and academia.

1.1.1 Classification of GPCRs

GPCRs in humans are generally classified into five families based on the GRAFS classification system that are based on phylogenetic analyses [8]: Glutamate receptor family (G), rhodopsin family (R), adhesion receptor family (A), frizzled/taste 2 receptor family (F), and secretin receptor family (S).

The glutamate receptor family (formerly class C) is most commonly associated with metabotropic glutamate receptors, Ca^{2+}-sensing receptor, γ-aminobutyric acid B receptors, and type I taste receptors. The N-terminus of these GPCRs is quite large and contains the ligand recognition domain generated by forming two lobes separated by a cavity in which ligands bind to produce the "Venus fly trap" or VFT domain. The VFT domain may also accommodate allosteric binding sites and is connected with the 7-TM core through a cysteine-rich domain, which also plays a role in receptor activation.

The rhodopsin family (formerly class A) is comprised of more than 700 receptors that share high sequence similarity [9] and several structural characteristics with rhodopsin, including an NPXXY motif on TM helix 7 and a DRY motif between TM3 and intracellular loop 2 (ICL2) [10]. Ligand binding for receptors in this class typically takes place within a cavity formed between TM helices. Notable GPCRs in this class that hold significant physiological relevance include muscarinic acetylcholine receptors, dopamine receptors, adrenergic receptors, opioid receptors, adenosine receptors, and histamine receptors.

The adhesion family has recently attracted much attention due to several unique features. These receptors typically possess long N-termini that contain an abundance of serine and threonine residues that constitute sites for O- and N-glycosylation, which act as mucin-like domains to create

rigid structures that protrude from the cell surface. Additionally, many receptors in this family contain a proteolytic domain in their N-termini.

The frizzled/taste 2 receptor family is far less understood as compared to other classes, and their similarity is largely confined to results from phylogenetic analysis. Only recently have frizzled receptors been established as true GPCRs following reports that binding of Wnt ligand can induce G protein coupling. Frizzled receptors are characterized by long N-termini with conserved cysteine residues that are considered critical for Wnt binding.

The secretin family (formerly class B) consists of receptors that have rather long N-termini that contain conserved disulfide bridges formed by cysteine residues, and these N-termini are considered paramount for ligand binding. Secretin receptors are perhaps best well known for binding relatively large peptide ligands that often, but not always, act in a paracrine manner. There are currently 15 identified members of this family in humans, including the parathyroid hormone type 1 receptor that serves as the focus of the dissertation work herein.

1.1.2 GPCR Signaling

Ligand binding induces conformational changes within the receptor that permit coupling to intracellular transducer proteins, including G proteins, GPCR kinases (GRKs), and β-arrestins (βarrs). G proteins are heterotrimeric complexes comprised of one α, β, and γ subunits when in the GDP-bound form [11]. Receptor activation leads to exchange of GDP for GTP on the Gα subunit and its dissociation from the Gβγ obligate heterodimer, with subsequent modulation of second messenger pathways and other downstream effectors. The intrinsic GTPase activity of the Gα subunit hydrolyzes GTP into GDP, leading to reassociation of subunits into the inactive heterotrimeric complex [12]. There are four main classes of Gα subunits that have been identified

based on sequence similarity [13]: G_s that stimulates adenylyl cyclase activity to increase intracellular cyclic adenosine monophosphate (cAMP) levels; $G_{i/o}$ that inhibits adenylyl cyclase activity; $G_{q/11}$ that leads to an increase in intracellular Ca^{2+} levels via activation of phospholipase C (PLC) β; and $G_{12/13}$ that regulates Rho guanine nucleotide exchange factors.

These signals are terminated by the collective work of GRKs, βarrs, and cellular endocytic machinery. Activated GPCRs recruit GRKs that phosphorylate serine and threonine residues within the receptor's third intracellular loop (ICL3) and C-terminal tail

1.2 The Parathyroid Hormone Type 1 Receptor

The parathyroid hormone (PTH) type 1 receptor (PTHR) is a class B GPCR that is expressed in a variety of tissues, predominantly in bone (osteoblasts and osteocytes), the kidney (proximal and distal tubules), and mammary glands [14]. The PTHR serves as the cognate receptor for endogenous peptide ligands PTH and its related peptide (PTHrP), which act in an endocrine and paracrine manner, respectively, to exert distinct biological effects. While PTH is associated with homeostatic control of serum Ca^{2+}, phosphate, and active vitamin D concentrations, PTHrP primarily regulates growth and development of bone, heart, mammary glands, and other tissues. Additionally, both ligands are implicated in dynamic bone remodeling processes, mediating both anabolic and catabolic actions. PTH and PTHrP exert their effects primarily via G_s/cAMP/protein kinase A (PKA) and G_q/PLC/PKC signaling pathways.

1.2.1 Biological Effects of the PTHR

PTH is secreted as an 84-amino acid peptide that serves as the primary regulator of ionized serum Ca^{2+} levels. In response to hypocalcemic conditions when Ca^{2+} concentration falls below the homeostatic set point in blood, or approximately 1.2 ± 0.1 mM, PTH is secreted from the parathyroid glands and acts in an endocrine fashion by exerting effects on specific bone and kidney cells. In bone, PTH-mediated activation of the PTHR expressed by osteoblasts and osteocytes ultimately promotes bone matrix resorption and liberation of Ca^{2+} into the systemic circulation [15-18]. In the kidneys, PTH increases Ca^{2+} reabsorption by distal tubule cells by modulating expression and activity of Ca^{2+} transport proteins [19, 20]. Concomitant with this effect of PTH is a decrease in inorganic phosphate reabsorption in proximal tubule cells via reduction of cell surface sodium-dependent phosphate transporters [21-23], which ensures that Ca^{2+} remains in the ionized state. PTH also acts on renal proximal tubule cells to increase circulating levels of active vitamin D3 via upregulation of the 25-hydroxyvitamin D3 1α-hydroxylase, and active vitamin D3 subsequently serves to increase absorption of Ca^{2+} from the gastrointestinal tract.

PTHrP is secreted as a 141-amino acid peptide that is capable of inducing analogous effects on bone and kidney cells observed for PTH, which is not surprising given the shared amino acid sequence homology within the N-terminal region of these peptides that has been shown to be critical for activity [24-26]. While it was originally associated as a factor responsible for the hypercalcemia frequently observed in cancer patients, PTHrP is now recognized to play a role in the growth and development of a variety of tissues, including bone [27], mammary glands [28], and teeth [29].

1.3 New Mode of cAMP Signaling

In the classical model of GPCR signaling, G protein-dependent signaling by activated receptor is terminated following phosphorylation by GRKs of intracellular receptor domains and recruitment of βarrs, which both sterically occlude G protein binding and promote endocytosis of ligand-bound GPCRs. Thus, signaling responses by these receptors were initially considered transient in nature and confined to the plasma membrane; however, this model has been challenged in recent years by the discovery of GPCRs that can mediate sustained signaling from early endosomes following internalization of the ligand-receptor complex [30, 31]. This unexpected aspect of GPCR signaling has been intensely investigated in the context of the PTHR due to the apparent ligand-dependent nature of endosomal signaling by this receptor. Notably, while PTHrP(1-36) induces only transient cAMP responses from the cell surface that are consistent with the classical model of GPCR signaling, binding of PTH(1-34) and various long-acting analogs promote sustained cAMP generation that arises from ligand-receptor complexes that remain active in early endosomes [31].

Studies involving the PTHR have provided ample evidence that maintenance of sustained G_s signaling from subcellular compartments is dependent upon ligand-specific stabilization of particular active receptor conformations. In the classical GPCR signaling paradigm, high-affinity ligand binding states were believed to exist only upon G protein coupling to the receptor [32]. The PTHR deviates from this model, as this receptor has been shown to form high-affinity complexes in the absence of G protein coupling with PTH and other long-acting ligands [33, 34]. In contrast, PTHrP only forms such complexes in the context of G protein coupling, and these complexes undergo rapid dissociation in the presence of GTPγS, a guanine nucleotide analog that induces G protein uncoupling from the receptor. These findings led to the hypothesis that the PTHR adopts

at least two distinct active conformations: R^G and R^0. Accordingly, whereas the R^G conformation stabilized by PTHrP is G protein-dependent and is associated with transient cAMP responses from the cell surface, the R^0 state is not altered by G protein coupling but nevertheless permits sustained cAMP generation following internalization of the receptor [31, 35-37].

1.3.1 Mechanisms of PTHR Endosomal cAMP Signaling and its Regulation

Sustained cAMP production in response to PTH is initiated by binding of βarrs to activated receptor. Whereas βarr is most commonly associated with inhibition of G protein coupling, previous studies have shown that βarrs contribute to prolonged PTHR-mediated sustained cAMP responses by forming ternary complexes with activated receptor and Gβγ subunits [38]. Indeed, kinetic and biochemical approaches have indicated that the PTHR-Gβγ-βarr complex in endosomes provides a scaffold by which G_s activation is accelerated, leading to prolonged cAMP generation by PTH-bound receptor. This conclusion is supported by additional mutation analyses that have shown that the site of interaction of Gβγ subunits with the receptor does not overlap with that of βarr [39].

In addition to the role of forming these ternary complexes, βarrs have also been implicated in downstream regulation of PTHR endosomal cAMP production. It is well-established that βarrs have the capacity to activate extracellular signal-regulated kinases (ERK), which, in turn, can lead to phosphorylation and inhibition of cAMP-specific phosphodiesterase (PDE4) enzymatic activity [40]. The Vilardaga lab has previously reported that endosomal cAMP responses by PTH are prolonged when cells are treated with PDE4 inhibitors but blunted when cells are treated with inhibitors of ERK1/2 [41], suggesting a positive feedback loop whereby PTHR-βarr complexes induce ERK1/2 signaling from endosomes to promote sustained cAMP generation.

Termination of sustained cAMP responses by the PTHR is predominantly controlled by mechanisms instilled within the endosomal trafficking pathway. Previous work has highlighted that the release of βarrs from the PTHR localized in endosomes is concomitant with association of the retromer complex with the receptor [41]. The retromer complex is comprised of two membrane-bound sorting nexins (SNX1 and SNX2) as well as a heterotrimer consisting of vesicle protein sorting (Vps) 26, 29, and 35, which collectively serve to regulate the sorting of cargo proteins from early endosomes to the *trans*-Golgi network [42, 43]. Examination of this complex in the context of PTHR-mediated cAMP showed that overexpression of Vps subunits reduces the duration of cAMP generation, whereas siRNA targeting of the subunits prolonged cAMP signaling time courses [41]. This process was recently shown to be dependent upon PKA activation and subsequent v-ATPase phosphorylation and endosomal acidification, which promotes dissociation of active PTH-PTHR-βarr complexes and the assembly of inactive PTHR-retromer complexes [44].

1.3.2 Physiological and Disease Relevance of Endosomal cAMP Signaling

PTH and PTHrP are implicated in bone remodeling processes, mediating both anabolic and catabolic effects, but previous studies have shown that PTH(1-34) stimulates more prolonged increases in serum levels of 1,25-dihydroxy-vitamin D, Ca^{2+}, and bone resorption markers than does PTHrP(1-36) when the ligands are injected by continuous infusion [45-47]. The anabolic effects of the PTHR on bone have led to its clinical targeting for the treatment of osteoporosis by once daily subcutaneous injection of the FDA-approved agents PTH(1-34) (teriparatide) [48] or abaloparatide (ABL) [49], a modified PTHrP(1-34) analog. While PTH and ABL stimulate transient cAMP production derived from ligand-receptor complexes at the plasma membrane, only

PTH causes sustained signaling via the internalization of PTHR in complex with βarr and Gβγ subunits. Observation that ABL can stimulate bone anabolic responses that are comparable with those induced by PTH but with a significantly reduced hypercalcemic effect led to the hypothesis that transient cAMP production from the cell surface might favor the formation of new bone, while sustained cAMP production from endosomes may promote bone breakdown. In agreement with this hypothesis, previous studies have shown that a modified PTH/PTHrP chimera that triggers substantially longer endosomal cAMP responses than PTH also induces enhanced and prolonged blood Ca^{2+} elevation in mice and monkeys compared to PTH [36, 50]. This link is further strengthened by a recent study demonstrating that chronic hypocalcemia in patients with idiopathic hypoparathyroidism can be caused by a single point mutation in residue 25 of PTH that fails to engage in endosomal cAMP [51, 52]. Implicit in these observations is that endosomal cAMP production in PTHR signaling has both physiological and disease relevance.

1.4 Advancing our Understanding of Endosomal cAMP Regulation and Significance

Since its initial discovery, significant advancements have been made toward elucidating the molecular and cellular determinants that underlie PTHR endosomal cAMP and its biological outcomes. Even so, several outstanding questions remain regarding this unexpected aspect of GPCR signaling. Are there extracellular factors that regulate the propensity of ligand-receptor complexes to engage in endosomal cAMP production? What ligand-dependent determinants exist that dictate spatiotemporal regulation of cAMP responses? What biological information is encoded within the spatial versus temporal dimension of cAMP signaling? Are there additional

intracellular transducer proteins that can modulate this process? Here, we utilize a combination of optical, biochemical, cell biological, and physiological approaches to address each of these questions.

2.0 Ca^{2+} Allostery in PTH Receptor Signaling

2.1 Introduction

Recent studies revealed altered modes of cAMP signaling for GPCRs where transient cAMP responses originate from cell membrane receptors, whereas internalized receptors prolong cAMP production from intracellular membranes [31, 53-55]. Initially uncovered for the PTHR, a class B GPCR that primarily couples of G_s/cAMP and G_q/Ca^{2+} signaling pathways and plays a central role in regulating Ca^{2+} homeostasis and bone turnover, this model is considered a new paradigm for GPCR signaling that can be viewed as a new form of signaling bias as it relates to distinct location and duration of cAMP generation [55-57]. Parts of cellular mechanisms of this unexpected process have been determined for the PTHR [38, 41, 44, 58], but its structural determinants and relevance for human disease remain unknown. Given that large fluctuations in extracellular Ca^{2+} observed in bone can reach up to 40 mM due to dynamic bone remodeling processes [59] and the reported effect of Ca^{2+} on PTH binding to purified receptor [60], we questioned whether changes in local extracellular Ca^{2+} concentrations could affect PTHR signaling in live cells. Here, we show through a series of biochemical and cell biological approaches that extracellular Ca^{2+} binds to the first extracellular loop of the receptor and acts as a positive allosteric modulator of PTHR signaling by increasing ligand residence time on the receptor and amplifying sustained cAMP production. We also show that the sensitivity to Ca^{2+} is lost for the recently identified homozygous PTH variant (R25C), implicated as a novel cause of chronic hypocalcemia in humans [52].

2.2 Materials and Methods

2.2.1 Cell Culture and Transfection

Cell culture reagents were obtained from Corning (CellGro). Human embryonic kidney cells (HEK293; ATCC, Georgetown, DC) stably expressing the recombinant human PTHR were grown in selection medium (DMEM, 5% FBS, 1% penicillin/streptomycin, 500 µg/mL neomycin) at 37 °C in a humidified atmosphere containing 5% CO_2. Primary mouse calvarial osteoblast (Ob) cells were isolated and cultured as described [58]. Human renal proximal tubule epithelial cells (RPTEC) were grown in DMEM/F12 supplemented with 5 pM triiodo-L-thyronine, 10 ng/mL recombinant human epidermal growth factor, 25 ng/mL prostaglandin E_1, 3.5 µg/mL ascorbic acid, 1 mg/mL insulin, 0.55 mg/mL transferrin, 0.5 µg/mL sodium selenite, 25 ng/mL hydrocortisone, and 1% penicillin/streptomycin. For transient transfection, cells were seeded on glass coverslips coated with poly-D-lysine in six-well plates and cultured for 24 hours prior to transfection with the appropriate cDNAs using Fugene-6 (Promega) or Lipofectamine 3000 (Life Technologies) for 48-72 hours before experiments. We optimized expression conditions to ensure expression of fluorescently labeled proteins was similar in examined cells by performing experiments in cells displaying comparable fluorescence levels.

2.2.2 Assessment of Receptor Cell Surface Expression by FACS

HEK293 cells were grown on 10 cm tissue culture plates and transfected with HA-tagged wild-type or ECL1 mutant PTHR constructs, as described above, using equal amounts of plasmid DNA for each construct. After 48 hours, the plates with cells were placed on ice, and cells were

washed with cold phosphate-buffered saline (PBS) (Lonza, #17517Q). Cells were detached by applying PBS supplemented with 0.5 mM EDTA, transferred to microcentrifuge tubes and spun down at 100x*g* for 2 min. Cell pellets were washed with blocking buffer (PBS with 0.5% BSA and 0.5% FBS), then resuspended in 0.75 mL blocking buffer with mouse anti-HA antibody (BioLegend, #901513) at 1:1000 dilution and incubated for 1 hour at 4 °C. After two washes with blocking buffer, cells were resuspended in blocking buffer with anti-mouse Alexa Fluor 568 antibody (Abcam, #ab175473) at 1:300 dilution and incubated for 1 hour at 4 °C. Cells were washed with blocking buffer and resuspended in 0.25 mL of blocking buffer for FACS measurements. FACS analysis was performed on BD FACSCalibur instrument and CellQuestPro software (BD Biosciences) taking 100,000 cells per analysis.

2.2.3 Peptides, Chemicals, Mutagenesis, and Western Blot Analysis

PTH(1-34), PTH(1-34)^{R25C}, PTH(1-34)^{R25S}, PTH(1-34)^{R25A}, PTH(1-34)^{TMR}, PTH(1-34)^{R25CTMR}, and [M]-PTH(1-14) (M=BVBEIQLOHQZAKWY-NH_2, where B = aminoisobutyric acid; O = norleucine, Z = homoarginine) were synthesized and characterized as previously described [44]. Abaloparatide (#H-8334) was purchased from Bachem. Dynasore (#324410) and forskolin (#344270) were purchased from EMD-Millipore.

Receptor mutagenesis converting ^{251}DEAE^{254}→SSAS (ECL1-1) and ^{257}EEE^{259}→SSS (ECL1-2) were performed using the QuikChange II Site-Directed Mutagenesis Kit (Agilent Technologies, #200523) using the provided protocol and the following primers: GGCGCCACGCTTTCTTCTGCTTCGCGCCTCACCGAGG for ECL1-1, and GCTGAGCGCCTCACCTCTTCTTCTCTGCGCGCCATCG for ECL1-2, and their corresponding reverse complement primers.

For Western blot analysis, total protein extracts were prepared using cell lysis buffer (1% NP40, 0.5% sodium deoxycholate, 0.1% SDS, 50 mM Tris pH 7.4, 100 mM NaCl, 2 mM EDTA, 50 mM NaF) containing EDTA-free Protease Inhibitor Cocktail (Roche Diagnostic GmbH). Protein concentrations were quantified by the Micro BCA protein assay kit (ThermoFisher scientific #23225) according to the manufacturer's instructions. Equal amounts of protein were separated by SDS-PAGE (10% SDS) and transferred to a nitrocellulose membrane. Membranes were blocked for 1 hour in TBS containing 5% non-fat milk, 1% BSA, and 0.1% Tween20, then incubated overnight with mouse anti-HA antibody (Covance). Membranes were then incubated with HRP-conjugated polyclonal goat anti-mouse antibody (Dako). The same membranes were subsequently stripped for 5 minutes at room temperature in Western blot stripping buffer (10% SDS, 0.5 M Tris pH 6.8, 0.8% β-mercaptoethanol), and then reprobed with mouse anti-βactin antibody (Cell signaling) and HRP-conjugated secondary antibody.

2.2.4 Saturation Binding at Equilibrium

Stably or transiently transfected HEK293 cells grown in 96-well plates were incubated in Hepes buffer (137 mM NaCl/5 mM KCl/1 mM $MgCl_2$/20 mM HEPES, pH 7.4) for 1 hour at 4 °C, followed by 17 hour incubation at 4 °C in the presence of increasing concentrations of TMR-labeled PTH or PTH^{R25C} and distinct [Ca^{2+}] as indicated in figures. Cells were washed twice with the same buffer, and fluorescence intensities were recorded at 580 ± 20 nm using an excitation wavelength of 525 ± 20 nm on a Tecan Spark 20M multimode microplate reader. Non-specific binding was determined using 1 µM of unlabeled ligand. Data were subsequently analyzed using GraphPad Prism 7.0 (GraphPad Software Inc., La Jolla, CA).

2.2.5 Laser Scanning Confocal Microscopy

Cells plated on coverslips were mounted in Attofluor cell chambers (Life Technologies) and incubated with HEPES buffer (150 mM NaCl, 20 mM HEPES, 2.5 mM KCl, varied [Ca^{2+}], 0.1% BSA, pH 7.4) and transferred on the Nikon Ti-E microscope (Nikon) equipped with a Z-driven piezo motor. Imaging was performed using Nikon A1 confocal unit, through a 60X N.A. = 1.45 objective (Nikon). Fluorescent antibody (anti-HA-Alex488, Cell Signaling, #2350), proteins or peptides containing CFP, Turqoise, GFP, FITC, YFP, tetramethylrhodamine (TMR) were excited with 440 nm (CFP, Turquoise), 488 nm (Alexa488, GFP, FITC), 514 nm (YFP) or 561 nm (TMR) lasers (Melles Griot). Data acquisitions were done using Nikon Element Software (Nikon Corporation). After acquisition, raw data were analyzed using ImageJ software. Each different analysis was done at the single-cell level.

2.2.6 Time-course Measurements of cAMP Production in Live Cells

cAMP was assessed using FRET-based assays. Cells were transiently transfected with the FRET-based biosensor $Epac1^{CFP/YFP}$ [61] for measuring cAMP. Measurements were performed and analyzed as previously described [62]. In brief, cells plated on poly-D-lysine coated glass coverslips were mounted in Atoofluor cell chambers (Life Technologies), maintained in a HEPES buffer containing 150 mM NaCl, 20 mM HEPES, 2.5 mM KCl, 0.1-10 mM $CaCl_2$, 0.1% BSA, and pH 7.4 and transferred on the Nikon Ti-E equipped with an oil immersion 40X numerical aperture 1.30 Plan Apo objective and a moving stage (Nikon Corporation). CFP and YFP were excited using a mercury lamp. Fluorescence emissions were filtered using a 480 ± 20 nm (CFP) and 535 ± 15 nm (YFP) filter set and collected simultaneously with a LUCAS electron-multiplying

charge-coupled device camera (Andor Technology) using a DualView 2 (Photometrics) with a beam splitter dichroic long pass of 505 nm. Fluorescence data were extracted from a single cell using Nikon Element Software (Nikon Corporation). The FRET ratio for single cells was calculated and corrected as previously described [63]. Individual cells were perfused with buffer or with ligand for the time indicated by the horizontal bar.

2.2.7 Receptor Recycling

Live-image trafficking of SEP-PTHR was done as described [64] using a Nikon A1 confocal microscope. Briefly, HEK293 cells stably expressing a pH-sensitive GFP variant, superecliptic pHluorin, inserted in the N-terminal domain of the human PTHR (SEP-PTHR) were seeded onto glass coverslips coated with poly-D-lysine (Sigma #P7280) for 24 hours. Experiments were carried out at 37 °C in FRET buffer used for cAMP experiments. Cells were stimulated by the ligand for 10 minutes then washed out to allow recycling. Images were acquired every 30 seconds.

2.2.8 Endosomal pH

Estimates were made using FITC fluorescence data together with the pH standard plot as previously described [44].

2.2.9 Purification of PTHR

Human PTHR construct comprising amino acid residues 27-483, with HA signal peptide for cell surface expression and with residues 58-106 replaced by GSGS linker, carrying N-terminal Flag tag and C-terminal 8x His tag was cloned into pFastBac1 vector. The baculovirus was generated according to procedures provided by Bac-to-Bac Expression Systems (Thermfisher). The receptor was expressed in Sf9 insect cells, grown in protein-free insect cell media ESF-921 (Expression Systems, #96-001-01) supplemented with penicillin/streptomycin. Cells were infected when density reached $5x10^6$/mL with 60X dilution of P2 baculovirus and cultured at 27 °C for 50 hours. Cells were harvested by centrifugation and stored at -80 °C until used. Cells were lysed by dounce-homogenization in lysis buffer consisting of 50 mM Tris-HCl pH 8.0, 100 µM TCEP, and protease inhibitors. To the lysate, 0.3% DDM, 0.3% DMNG, 0.06% CHS, 30 mM imidazole, 0.4 M NaCl, and 8% glycerol were added, and receptor extraction was carried out for 1 hour at 4 °C. After clearing the extract by centrifugation at 29,000x*g* for 30 min, the PTHR was captured onto Ni 6 Fast Flow sepharose (GE Healthcare, #17531801) by batch-binding for 2 hours at 4 °C. The beads were washed with Ni buffer consisting of 20 mM HEPES pH 7.5, 0.4 M NaCl, 30 mM imidazole, 2% glycerol, 0.008% DMNG, 0.0008% CHS, 100 µM TCEP, and protease inhibitors, then eluted with Ni buffer supplemented with 0.4 M imidazole and 4 mM $CaCl_2$. Ni eluate was incubated with anti-Flag-M1 agarose (Sigma-Aldrich, #4596) for 1 hour at 4 °C, washed with buffer consisting of 20 mM HEPES pH 7.5, 150 mM NaCl, 4 mM $CaCl_2$, 1% glycerol, 0.008% DMNG, 0.0008% CHS, then eluted with 20 mM HEPES pH 7.5, 150 mM NaCl, 10 mM EDTA, 0.1 mg/mL Flag peptide, 1% glycerol, and 0.008% DMNG. The eluted receptor was concentrated using Amicon Ultra-15 50 kDa MWCO spin-concentrators (Millipore-Sigma, #UFC905008) to 1 mL, and then injected to Superose 6 10/300 GL (GE Healthcare) gel-filtration

column equilibrated in 20 mM HEPES pH 7.5, 150 mM NaCl, 0.008% DMNG, and 0.0008% CHS. The yield of purified receptor was 0.2-0.5 mg from 1 L insect cell culture.

2.2.10 Assessment of Purified Receptor Functionality

The functionality of purified receptor was tested in terms of its ability to form complex with Gs protein. To this end, the PTHR was incubated with 2-3 fold molar excess of LA-PTH, Gs heterotrimer, and nanobodies Nb35 and $Nb37^{GFP}$ for 40 minutes at room temperature. Then 2 µL of apyrase (NEB, #M0398S) was added, and the reaction mixture was incubated at room temperature for 40 minutes. The formed complex was captured onto anti-Flag-M1 agarose beads packed in an Econo column, washed, and eluted using the same buffers as for receptor purification, but supplemented with 50 nM LA-PTH. The eluted sample was concentrated using Amicon Ultra-4 100 kDa MWCO spin-concentrators (Millipore-Sigma, #UFC810008) to 1 mL, then injected to Superose 6 10/300 GL gel-filtration column equilibrated in 20 mM HEPES pH 7.5, 150 mM NaCl, 0.008% DMNG, and 0.0008% CHS. The constructs of Gs heterotrimer and Nb35 were provided by Dr. Cheng Zhang (University of Pittsburgh) and purified as described previously [65]. The $Nb37^{GFP}$ construct was a kind gift from Dr. Mark zon Zastrow (UCSF). The 10xHis tag was inserted at the C-terminus of GFP and the construct was subcloned to pEt21a. The $Nb37^{GFP}$ was expressed in Shuffle T7 Express Competent E. coli strain (NEB #C3029J) that is engineered to aid correct disulfide folding of target proteins in the cytoplasm. The cells were cultured at 37 °C in LB media supplemented with ampicillin. When cell density reached OD_{600} 0.75, the temperature was lowered to 18 °C and protein expression was induced with 0.4 mM IPTG. After induction, the cells were grown for 20 hours at 18 °C, and then harvested by centrifugation and resuspended in buffer consisting of 50 mM Tris-HCl pH 8.0, 0.4 M NaCl, 30 mM imidazole, and protease

inhibitors. Cells were lysed by sonication, then spun down 50,000x*g* for 25 minutes to clear the lysate. The $Nb37^{GFP}$ was captured onto Ni 6 Fast Flow sepharose beads by batch-binding for 1.5 hours at 4 °C. Beads were excessively washed with Ni buffer (25 mM Tris-HCl pH 8.0, 0.4 M NaCl, 30 mM imidazole, and protease inhibitors), then eluted with Ni buffer supplemented with 0.4 M imidazole. Ni eluate was concentrated using Amicon Ultra-15 30 kDa MWCO spin-concentrators (Millipore-Sigma, #UFC903008) to 1 mL, then injected to Superose 6 10/300 GL gel-filtration column equilibrated in 25 mM Tris-HCl pH 8.0, 150 mM NaCl, and protease inhibitors. The purified protein was aliquoted, flash-frozen, and stored at -80 °C until used.

2.2.11 Homology Modeling of PTHR

To model PTH binding to PTHR, we generated a homology model of PTHR via GPCR-I-TASSER [66]. We first aligned the N-PTHR/PTH(15-34) crystal structure (PDB 3C4M) [67] with the ECD of the highest scoring PTHR model. Next, we aligned the crystal structure of PTH(1-34) alone (PDB 1ET1) [68] with PTH(15-34) from N-PTHR/PTH(15-34). Backbone-dependent conformers of R25 were assessed, revealing R25 could be oriented toward ECL1, and figures were generated in PyMOL (Molecular Graphics System, Version 2.0 Schrödinger, LLC).

2.2.12 Photometric FRET Recordings of Kinetics of Ligand Binding and Receptor Activation

FRET experiments were performed as previously described [63]. In brief, cells grown on glass coverslips were maintained in buffer A (137 mM NaCl, 5 mM KCl, 1 mM $MgCl_2$, 20 mM HEPES, pH 7.4) at room temperature and placed on a Zeiss inverted microscope (Axiovert 200)

equipped with an oil immersion X100 objective and a dual emission photometric system (TILL Photonics, Germany). Cells were excited with light from a polychrome V (TILL Photonics). To minimize photobleaching, the illumination time was set to 5-15 ms applied with a frequency between 1 and 75 Hz. For binding events, the illumination time was typically set to 5 ms applied with a frequency of 40 Hz. FRET was monitored as the decrease in emission of GFP (F_{GFP}) from the PTHR N-terminally tagged with GFP (PTHR-GFP) in the presence of TMR-labeled peptides, recorded at 520 ± 20 nm (beam splitter 530 DCLP) upon excitation at 480 ± 20 nm (beam splitter 498 DLCP). Because the diminution of GFP fluorescence was due to FRET between GFP and TMR [69], we used the decline of GFP fluorescence as readout for the binding event. The spillover of TMR into the 520 nm channel (1.5%) was negligible. For receptor activation, the emission fluorescence intensities were determined at 535 ± 15 and 480 ± 20 nm (beam splitter dichroic long-lass (DCLP) 505 nm) upon excitation at 436 ± 10 nm (DCLP 460 nm) and were corrected for the spillover of CFP into the 535 nm channel, the spillover of YFP into the 480 nm channel, and the direct YFP excitation to give a corrected FRET emission ratio F_{YFP}/F_{CFP}. Changes in fluorescence emissions due to photobleaching were systematically subtracted. To determine agonist-induced changes in FRET, cells were continuously superfused with the buffer A with a range of $CaCl_2$ concentrations and agonist was applied using a computer-assisted solenoid valve-controlled rapid superfusion device ALA-VM8 (ALA Scientific Instruments) (solution exchange 5-10 ms). Signals detected by avalanche photodiodes were digitized using a converter (Digidata1322A; Axon Instruments) and stored on PC computer using Clampex 9.0 software (Axon Instruments). Data were analyzed using the program Origin (OriginLab Corp.).

2.2.13 Detection of Ca^{2+} Binding PTHR Fragments by Liquid Chromatography with Tandem Mass Spectrometry

For non-SILAC experiments, HEK293S cells stably expressing HA-tagged PTHR (HA-PTHR) were grown in regular DMEM supplemented with 5% FBS and 1% penicillin/streptomycin. For SILAC experiments, HEK293S cells stably expressing HA-PTHR were grown in SILAC DMEM. The SILAC medium was prepared from custom-ordered DMEM powder without arginine and lysin (ThermoFisher #88425). L-lysine-[$^{13}C_6$,$^{15}N_2$] (50 mg/L) and L-arginine-[$^{13}C_6$, $^{15}N_4$] (25 mg/L) were added to the "heavy" medium, whereas equal concentration of conventional L-lysine-[$^{12}C_6$, $^{14}N_2$] and L-arginine-[$^{12}C_6$, $^{14}N_4$] were added to the "light" medium. Cells were maintained in heavy and light SILAC media side-by-side for at least 7 doubling until the isotope incorporation efficiency achieved >95% as determined by mass spectrometry. The cells were then grown to ~80% confluence. The heavy cells were stimulated with 100 nM PTH for 15 minutes before harvesting, and the light cells werved as control without any treatment. After treatment, equal numbers of heavy and light cells were mixed and served as SILAC cell samples. Non-SILAC and SILAC cell samples were lysed in buffer containing 50 mM HEPES pH 7.5, 0.5% NP-40, 250 mM NaCl, 10% (v/v) glycerol. The HA-PTHR was isolated from cell lysates using anti-HA agarose beads. Purified HA-PTHR samples were digested by trypsin using an in-solution trypsin digestion protocol was described previously [70]. For *in vitro* Ca^{2+} binding experiments, PTHR was purified from Sf9 cells was described above and diluted to 0.1 µg/µL in 50 mM Tris-HCl pH 7.5, 150 mM NaCl, 0.1% DDM. The purified PTHR was then incubated with or without 1 mM $CaCl_2$ at room temperature for 30 minutes before subjection to in-solution trypsin digestion. After peptide desalting with in-house prepared stage-tip, tryptic peptides were reconstituted in a solution containing 0.1% formic acid and 2% acetonitrile and

analyzed on a nanoACQUITY (Waters)-LTQ Orbitrap Velos mass spectrometer (Thermofisher) system. The LTQ Orbitrap Velos was operated in the data dependent mode using the TOP_{10} strategy. In brief, each scan cycle was initiated with a full MS scan of high mass accuracy 375-1,800 m/z, acquired in the Orbitrap at $6x10^4$ resolution setting and automatic gain control (AGC) target of 10^6, which was followed by MS/MS scans (AGC target 5,000; threshold 3,000) in the linear ion trap on the ten most abundant precursor ions. Selected ions were dynamically excluded for 30 seconds. MS data analysis was performed using SEQUEST software against Uniprot Homo sapiens forward and reverse protein sequences. To search for evidence of Ca^{2+} containing peptides, each LC-MS/MS data set was manually examined to look for additional MS peaks matching exactly the possible theoretical m/z change ($\Delta m/z = 37.946941$, $z = 1$; $\Delta m/z = 18.97347$, $z = 2$; $\Delta m/z = 12.64898$, $z = 3$) when a single Ca^{2+} ion binds to the PTHR. For SILAC data, the m/z differences between the light and heavy version of free peptides and Ca^{2+} binding peptides were examined to ensure they matched.

2.2.14 Statistical Analysis

Data were processed using Excel 2013 (Microsoft Corp. Redmond, WA) and Prism 7.0 (GraphPad Software Inc., La Jolla, CA). Data are expressed as mean ± SEM. Curves were fit to the data using a four-parameter, non-linear regression function. Statistical analyses were performed using unpaired, 2-tailed Student's t tests for comparisons between 2 groups.

2.3 Results

2.3.1 Extracellular Ca^{2+} Prolongs Ligand Residence Time and Promotes Receptor Activation and Endosomal cAMP Production

Both in human and embryonic kidney 293 (HEK293) cells and primary osteoblasts expressing recombinant and native PTHR, respectively, we observed a significant ($P < 0.01$) difference in magnitude and duration of cAMP production when a range of Ca^{2+} concentrations (0.1-10 mM) were co-applied with PTH (**Fig. 1A**,**C**). The effective concentration that gives half maximal response (EC_{50}) for PTH-induced cAMP decreased 30-fold when the Ca^{2+} concentration was increased from 0.1 to 10 mM (**Fig. 1B**, **left**). Ca^{2+} had no effect by itself but caused a concentration-dependent increase in PTH-mediated cAMP response with an EC_{50} value (1.01 mM) near the physiological range of ionized serum Ca^{2+} levels (1.1-1.3 mM) (**Fig. 1B**, **right**). These data show that Ca^{2+} significantly enhances both the magnitude and the duration of PTH-induced cAMP generation. Surprisingly, potentiation of PTHR signaling was ligand-dependent, as PTHrP-induced cAMP lacked sensitivity to Ca^{2+} (**Fig. 1D**), whereas its analog ABL, recently Food and Drug Administration approved to treat osteoporosis, showed sensitivity similar to that of PTH (**Fig. 2A**). We thus utilized either PTH or ABL as ligand in subsequent experiments.

To further interrogate the mechanism by which extracellular Ca^{2+} regulates receptor signaling, effects on ligand binding were assessed via equilibrium and kinetic analyses. Saturation binding experiments using tetramethylrhodamine (TMR)-labeled PTH (PTH^{TMR}) revealed moderate increases in ligand binding affinity in the presence of increasing extracellular Ca^{2+}, a defining characteristic of a positive allosteric modulator (**Fig. 1E**). In an effort to confirm that Ca^{2+}-mediated effects on ligand binding are responsible for the observed modulation of cAMP

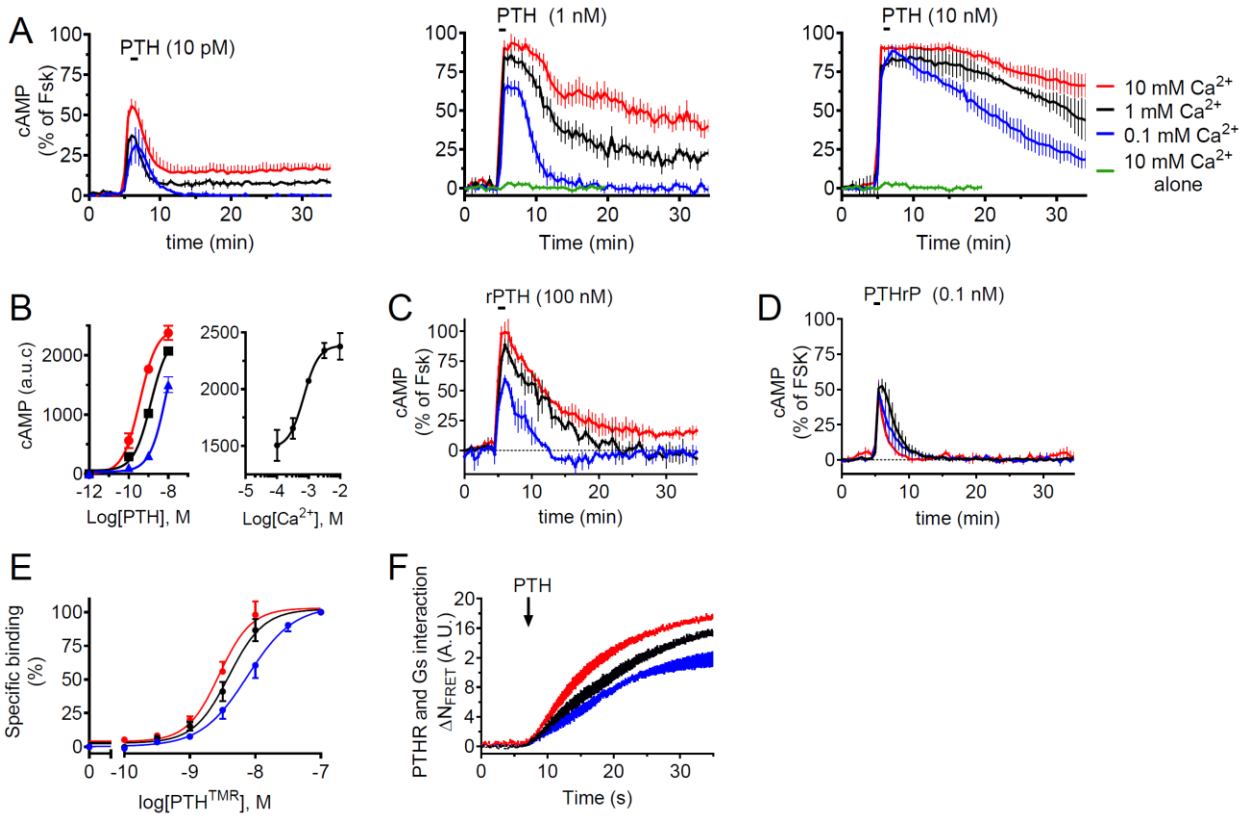

Figure 1. Allosteric Action of Extracellular Ca^{2+} on PTH Signaling.

(A) Averaged cAMP responses over 35 min in HEK293 cells stably expressing the PTHR stimulated with 10 pM, 1 nM, and 10 nM PTH in the presence of a range of [Ca^{2+}]. (B) cAMP responses for experiments represented in A, determined by measuring the area under the curve (a.u.c) from 0 to 35 min (left). The effect of increasing concentration of Ca^{2+} on PTH (10 nM)-mediated cAMP (right). (C) Averaged time courses of cAMP production rat primary osteoblasts upon stimulation with 100 nM rat PTH (rPTH) in the presence of increasing Ca^{2+} concentrations. (D) PTHrP-induced cAMP responses are insensitive to Ca^{2+} modulation. (E) Saturation binding isotherms of PTH^{TMR} to the PTHR stably expressed in HEK293 cells with a range of [Ca^{2+}]. (F) Averaged time-courses of venus-tagged mini G_s (mG_s^{venus}) recruitment to $PTHR^{CFP}$ in response to PTH in the presence of a range of extracellular [Ca^{2+}] measured by FRET in HEK293 cells. Data represent the mean ± SEM of N=3 experiments carried out in triplicate for E and n = 8-30 cells/experiments for other panels.

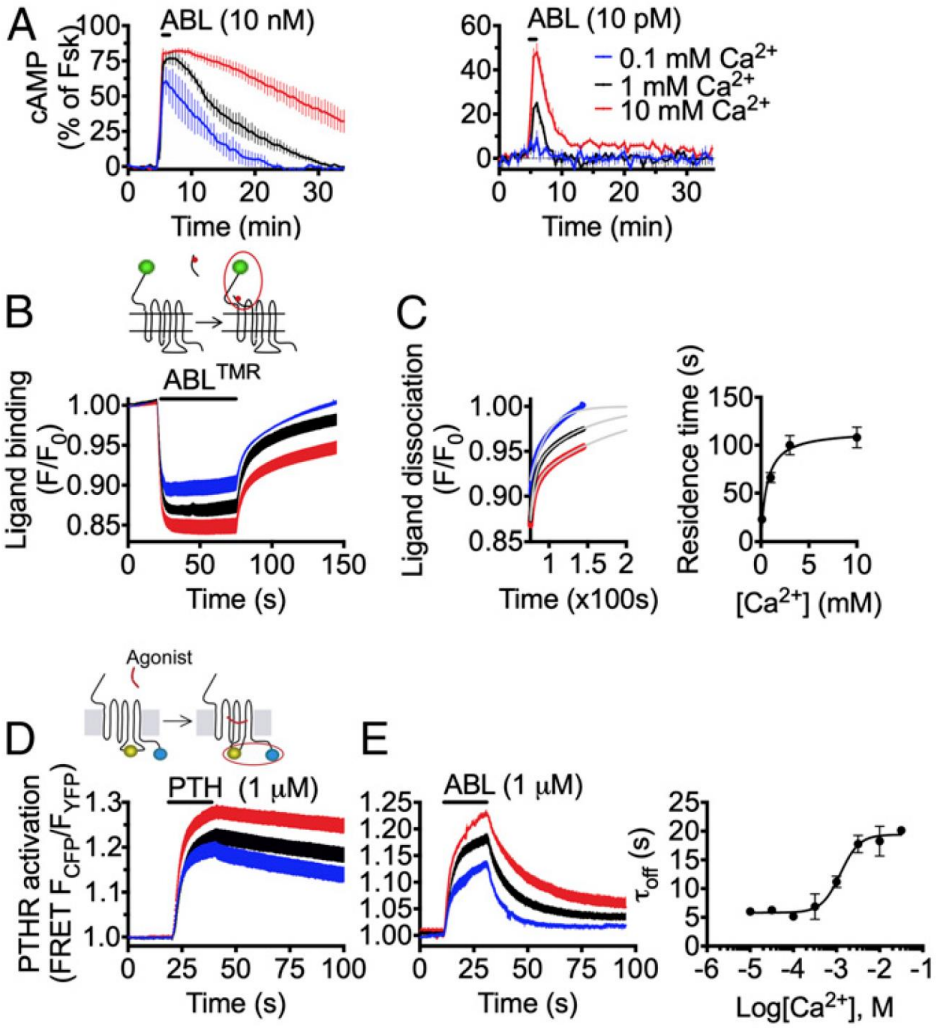

Figure 2. Ligand Residence Time Determined by Ca^{2+} Allostery.

(A) Averaged cAMP response over 35 minutes in HEK293 cells stably expressing the PTHR stimulated with 10 nM and 10 pM ABL in the presence of a range of $[Ca^{2+}]$. (B) Time courses of ABL^{TMR} binding to $PTHR^{GFP}$ expressed in HEK293 cells. Measurements were recorded in single cells continuously perfused with buffer or 1 µM ABL^{TMR} (horizontal bar) in the presence of varying $[Ca^{2+}]$. (C) Comparison of ligand dissociation time courses from experiments in B (left) and the corresponding residence time of the ligand, calculated as the inverse of the rate constant of ligand dissociation ($1/k_{off}$) as a function of $[Ca^{2+}]$ (right). (D and E) Effects of Ca^{2+} on time courses of receptor activation/deactivation using $PTHR^{CFP/YFP}$ stably expressed in HEK293 cells. Single cells were continuously perfused with buffer or 1 µM PTH (D) or ABL (E, left) indicated by the horizontal bar. Time constants (τ_{off}) of receptor deactivation (E, right) as a function of $[Ca^{2+}]$ calculated from experiments similar to E (left). Data represent the mean ± SEM of N=3 experiments and n=8-30 cells/experiment.

responses, G_s recruitment to the receptor was measured by Förster Resonance Energy Transfer (FRET) using mini-G_s^{venus} and CFP-tagged PTHR ($PTHR^{CFP}$). Even at saturating concentration of ligand, increasing extracellular Ca^{2+} concentration resulted in enhanced recruitment of G protein with faster kinetics (**Fig. 1F**).

Consistent with a positive allosteric action, increasing extracellular Ca^{2+} concentration also prolonged ligand residence time ($(1/k_{off}$, where k_{off} is the dissociation rate constant) following washout as measured by changes in FRET between TMR-labeled ABL (ABL^{TMR}) and GFP fused N-terminally to PTHR ($PTHR^{GFP}$) (**Fig. 2B,C**). We reasoned that slower ligand dissociation kinetics should, in turn, impact the duration of receptor activation. Accordingly, we utilized a previously characterized FRET-based conformational biosensor ($PTHR^{CFP/YFP}$) to measure the time-course of receptor activation and deactivation by monitoring changes in the FRET ratio upon stimulation and washout, respectively. We observed that increasing extracellular Ca^{2+} concentration resulted in an increased magnitude of PTHR activation by PTH and ABL, suggesting a key role in stabilizing the agonist-bound PTHR in an active conformation (**Fig. 2D**; **E**, **left**). Ca^{2+} also caused a concentration-dependent increase in the deactivation time constant (τ_{off}) after ABL washout (**Fig. 2E**, **right**), reflective of prolonged receptor activation. Collectively, these results demonstrate that extracellular Ca^{2+} acts as a positive allosteric modulator of the PTHR by prolonging ligand residence time and receptor activation, which, in turn, significantly alters the magnitude and kinetics of the cAMP response.

2.3.2 Mass Spectrometry Evidence of Ca^{2+} Binding to Extracellular Loop 1 of the Receptor

We next sought to identify Ca^{2+} binding sites on the PTHR via liquid chromatography coupled to tandem mass spectrometry (LC-MS/MS). To this end, two populations of HEK293S

cells stably expressing HA-tagged PTHR (HA-PTHR) were cultured side-by-side in stable isotope labeling with amino acids in cell culture (SILAC) media containing either "light" (Lys-[$^{12}C_6$, $^{14}N_2$] and Arg-[$^{12}C_6$, $^{14}N_4$]) or "heavy" (Lys-[$^{13}C_6$, $^{15}N_2$] and Arg-[$^{13}C_6$, $^{15}N_4$]) isotopic forms of amino acids. The heavy cells were stimulated with 100 nM PTH(1-34) for 15 minutes, and the light cells served as control. Upon mixing lysates from equal numbers of light and heavy cells, HA-PTHR was immunoprecipitated and enzymatically digested by trypsin and subjected to LC-MS/MS analysis using a high-resolution and mass accuracy linear trap quadrupole Orbitrap Velos mass spectrometer. We identified MS peaks (charge state z = 2) corresponding to light and heavy version of the free peptides ^{241}DAVLYSGATLDEAER^{255} (monoisotopic m/z = 805.39252 for light and m/z = 810.39624 for heavy) and ^{256}LTEEELR^{262} (monoisotopic m/z = 445.23596 for light and m/z = 450.23998 for heavy) covering parts of the PTHR's extracellular loop 1 (ECL1) (**Fig. 3A**). Additional peaks matching exactly the theoretical mass-to-charge change (Δm/z) when a single Ca^{2+} ion binds to these peptides (Δm/z = 18.97347) were simultaneously detected for their corresponding light and heavy versions with monoisotopic m/z = 824.36597 (light) and 829.36926 (heavy) for ^{241}DAVLYSGATLDEAER^{255} and monoisotopic m/z = 464.20917 (light) and 469.21348 (heavy) for ^{256}LTEEELR^{262} (**Fig. 3A**). Furthermore, the extent of Ca^{2+} binding was not significantly altered by PTH stimulation.

Given the well-known ability of acidic amino acid clusters to chelate Ca^{2+} and the presence of such clusters in each of the peptides identified by MS, we then generated two PTHR mutants wherein negatively charged aspartates (D) or glutamates (E) were substituted with serine (S) side chains to impair Ca^{2+} chelation without significant impact on overall polarity: ^{251}DEAE^{254}→SSAS (noted ECL1-1), and ^{257}EEE^{259}→SSS (noted ECL1-2). Interestingly, both ECL1 mutants were unable to engage in sustained cAMP production was efficiently as the wild-type (WT) receptor

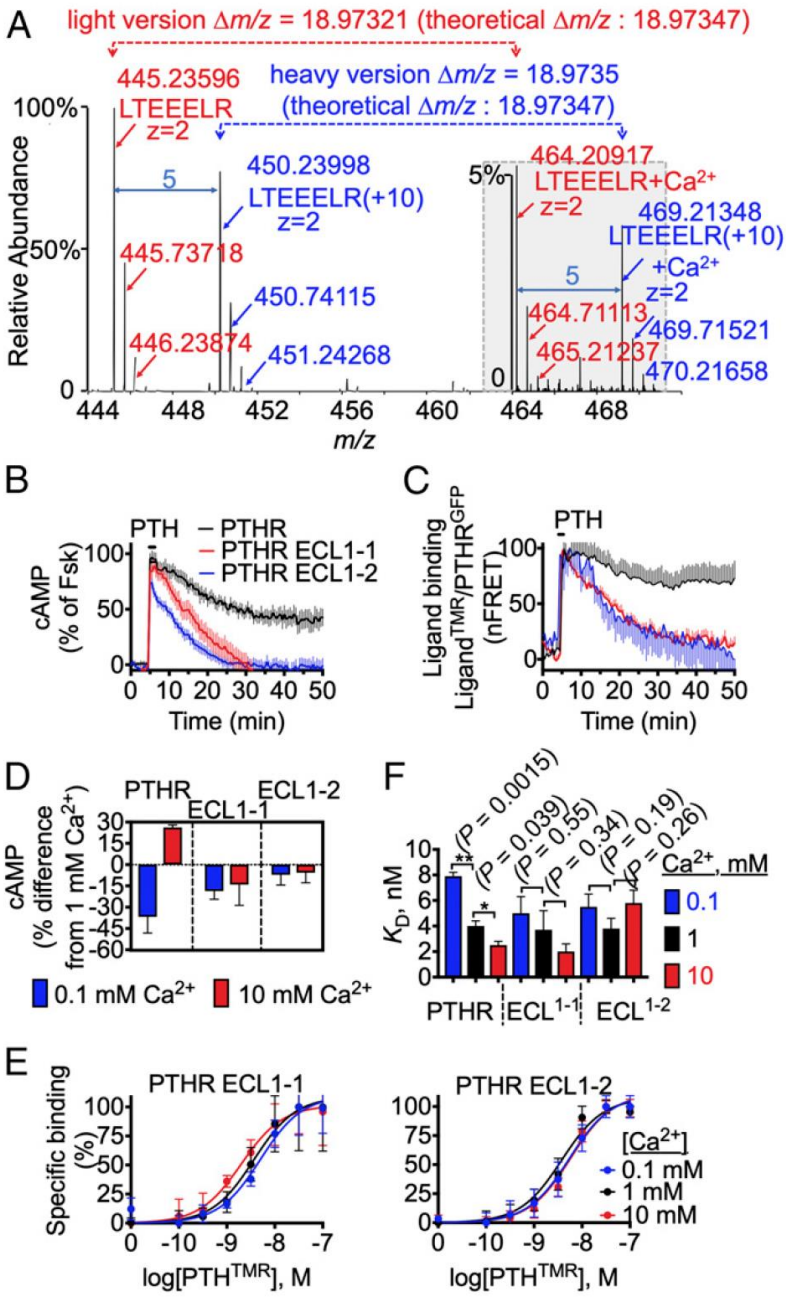

Figure 3. Involvement of the Receptor's ECL1 in Ca^{2+} Allostery.

(A) Representative MS of the tryptic digest of the PTHR from SILAC experiments showing the identified peptide ^{256}LTEEELR^{262} located within the ECL1 of the receptor. The free and Ca^{2+}-bound versions of the peptide were detected simultaneously. The red and blue colors represent light and heavy versions of the peptide. The theoretical mass-to-charge differences (Δm/z) between free and Ca^{2+}-bound peptides are shown for both light and heavy versions. The Δm/z values of the corresponding light and heavy peptides are 5. For clarity, the MS peaks for Ca^{2+}-bound

peptides are enlarged and highlighted in a gray box. (B) Averaged time courses of cAMP production in response to PTH in HEK293 cells expressing wild-type (WT) PTHR or PTHR-ECL1 mutants measured by FRET in response to 10 nM PTH. (C) Averaged dissociation time courses of PTH^{TMR} from GFP-tagged PTHR WT (black), ECL1-1 (red), or ECL1-2 (blue). FRET recordings from HEK293 cells are shown as a normalized ratio. (D) The effect of 0.1 and 10 mM Ca^{2+} on cAMP response mediated by 10 nM PTH in HEK293 cells expressing PTHR WT or ECL1 mutants. cAMP responses were quantified by measuring the area under the curve from 0 to 35 minutes and are represented as percentage differences from the 1 mM Ca^{2+} condition. (E) Saturation binding isotherms of PTH^{TMR} to ECL1 mutants stably expressed in HEK293 cells. The mean ± SEM of N=3 experiments carried out in triplicate. (F) The bars represent the mean of the K_D values ± SEM of binding experiments shown in 1C and 3E. *Significantly different when $P < 0.05$. cAMP time courses represent the mean value ± SEM of N=3 with n=14-26 cells/experiment.

(**Fig. 3B**). Despite normal internalization, PTH dissociated with markedly faster kinetics from receptor mutants compared with WT receptor, consistent with more transient cAMP responses (**Fig. 3C**). Time courses of cAMP measurements for ECL1-1 and ECL1-2 receptor mutants in response to PTH revealed markedly reduced sensitivity to Ca^{2+}, particularly for ECL1-2 (**Fig. 3D**). Similarly, receptor mutants failed to mimic the effects of Ca^{2+} concentration on ligand binding that were observed for WT receptor in saturation binding experiments (**Fig. 3E**,**F**). These results suggest that acidic residues within ECL1 of the PTHR serve as key determinants for mediating Ca^{2+} allostery and endosomal signaling by PTH.

2.3.3 Positive Ca^{2+} Allostery is Lost for a Hypocalcemia-causing PTH Mutant

Although negatively-charged amino acids within ECL1 of the PTHR clearly play a role in mediating allosteric modulation by Ca^{2+}, the lack of sensitivity to Ca^{2+} concentration observed in PTHrP-induced cAMP responses suggests an additional ligand-dependent component. We next

examined PTH^{R25C}, a recently identified homozygous PTH variant wherein arginine (R) at position 25 has been substituted with cysteine (C). Patients harboring this mutation present with severe hypocalcemia despite normal or even excess levels of the circulating hormone, likely due to the reduced efficacy of PTH^{R25C} in stimulating cAMP production [52], but the molecular basis for impaired signaling remains poorly understood. Given the apparent correlation between PTHR sensitivity to Ca^{2+} concentration and the ability to promote normal cAMP responses, we questioned whether position 25 of PTH plays a role in mediating Ca^{2+} allostery and thus endosomal signaling. Indeed, saturation binding analysis and cAMP time-course experiments in HEK293 cells revealed that PTH^{R25C} completely lacks sensitivity to extracellular Ca^{2+} concentration (**Fig. 4A**,**B**). Moreover, PTH^{R25C}-induced cAMP generation was markedly shorter in duration than that of WT hormone (**Fig. 4B**). Preventing PTHR internalization by expressing DynK44A had only minimal effect on cAMP induced by PTH^{R25C} (**Fig. 4C**), suggesting that this signaling is mainly restricted to the cell surface. Surprisingly, the inability of PTH^{R25C} to sustain cAMP was not due to defective internalization and trafficking of ligand-bound PTHR into endosomes, as revealed by similar Pearson's correlation coefficients between TMR-labeled ligands and either PTHR detected with anti-HA Alexa488 conjugated antibody or Rab5 labeled with GFP (Rab5-GFP) (**Fig. 4D**). We considered the possibility that R25 of PTH engages in ionic interactions with the negatively charged residues within ECL1 of PTHR because the reduced Ca^{2+} allostery and endosomal signaling observed with PTH^{R25C} were mimicked by ECL receptor mutants (**Fig. 4E**). The R25 interaction with acidic residues within ECL1 is, indeed, supported by our homology model of the PTHR built to investigate possible structural interactions between PTH and ECL1 of the receptor (**Fig. 4F**). In this model, R25 faces the acidic regions of ECL1 of the PTHR at a distance compatible with salt bridge formation. The lack of R25 interaction with ECL1 acidic residues

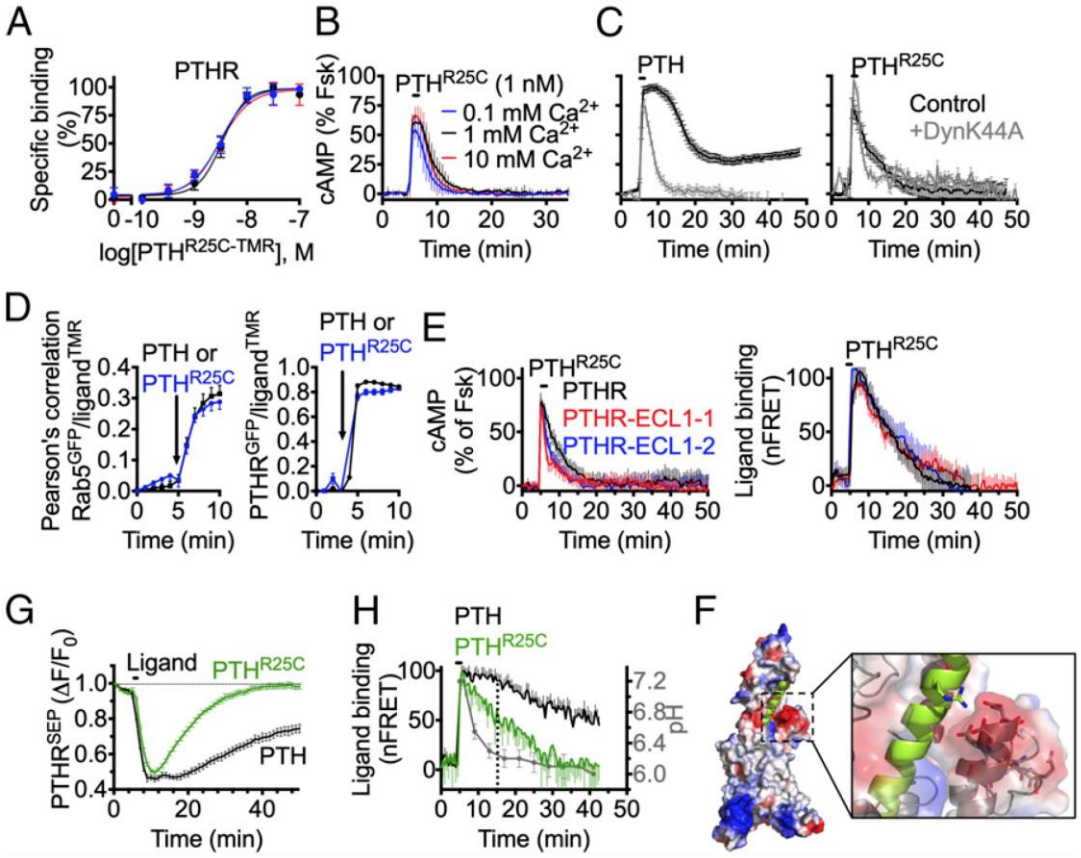

Figure 4. Involvement of R25 of PTH in Interaction Stabilization and Receptor Signaling.

(A) Saturation binding isotherms of TMR-labeled PTH^{R25C} to PTHR stably expressed in HEK293 cells with [Ca^{2+}] = 0.1 (blue), 1 (black), or 10 (red) mM. The mean ± SEM of N=3 experiments carried out in triplicate. (B) Averaged time courses of cAMP production in response to PTH^{R25C} in HEK293 cells expressing the PTHR in the presence of a range of [Ca^{2+}] measured by FRET. (C) Time courses of cAMP production in response to PTH (right) or PTH^{R25C} (left) in HEK293 cells expressing the PTHR. Experiments were run in two conditions: cells expressing only the PTHR (black), and cells co-expressing the PTHR and DynK44A (gray). (D) Pearson's correlation values obtained from colocalization experiments between TMR-labeled PTH or PTH^{R25C} with anti-HA Alexa488 (HA-PTHR, right) or the early endosome marker Rab5^{GFP} (left). The arrows indicate the time of ligand stimulation. (E) Averaged time courses of cAMP production in response to PTH^{R25C} in HEK293 cells expressing WT PTHR or ECL1 mutants (left), and dissociation time courses of TMR-labeled PTH^{R25C} from WT or mutant PTHR^{GFP} expressed in HEK293 cells (right) measured by FRET. (F) Homology model of the PTHR generated from GPCR-I-TASSER with the modeled PTH. The PTHR is shown as an electrostatic surface, and PTH is represented as a green helix. R25 of PTH points

toward an acidic face of the PTHR, which consists of ECL1-1 and ECL1-2 residues; R25 of PTH and residues of ECL1-1 and ECL1-2 are shown as sticks. (G) Time courses of internalization and recycling of $PTHR^{SEP}$ in response to ligand, measured by time-lapse confocal microscopy with images acquired every 30 seconds. The baseline was established, and cells were stimulated with 100 nM ligand for 10 minutes then washed out. (H) Averaged dissociation time courses of TMR-labeled PTH or PTH^{R25C} from $PTHR^{GFP}$. FRET recordings from HEK293 cells are shown as normalized ratios. Cells were stimulated with 50 nM ligand for 30 seconds. The gray line is a recording of pH using PTH-fluorescein isothiocyanate (FITC) in HEK293 cells expressing the PTHR C-terminally tagged with CFP. Time courses represent the mean value ± SEM of N=3 experiments with n=8-20 cells/experiment.

resulted in faster receptor recycling (**Fig. 4G**), likely due to faster dissociation of PTH^{R25C} and increased pH sensitivity of this mutant hormone (**Fig. 4H**). Collectively, these results provide strong evidence that ionic interactions between R25 of PTH and ECL1 residues of receptor are required for positive allosteric modulation by Ca^{2+} that likely stabilize hormone interaction with the receptor and thus are prerequisite for endosomal cAMP production.

2.4 Discussion

Over the past decades, it has been well-established that Na^+ acts as a negative allosteric modulator of numerous class A GPCRs, wherein it binds to a conserved site within the seven transmembrane helix bundle and stabilizes an inactive state of the receptors [71]. In contrast, the divalent cations, such as Mg^{2+}, Ca^{2+}, and Mn^{2+}, have been found to positively modulate class A GPCRs [72-77], and Ca^{2+} is a known allosteric regulator of several class C GPCRs [78]. Here, we reveal cellular and molecular mechanisms of positive allosteric actions of Ca^{2+} on a medically important class B GPCR, the PTHR.

Indeed, PTH is an indispensable endocrine hormone regulating blood levels of Ca^{2+} and phosphate ions. PTH binds to and activates its cognate receptor in bone, where it induces bone resorption that, in turn, releases ionized Ca^{2+} from the mineralized bone matrix. Consequently, the receptor encounters elevated extracellular Ca^{2+} concentrations that can reach up to 40 mM [59]. Here, we studied the effects of extracellular Ca^{2+} on PTHR ligand binding and signaling. Our findings identify the ability of extracellular Ca^{2+} to act as an allosteric modulator of PTHR activation by promoting cAMP signaling when Ca^{2+} concentration is greater than 1 mM, and attenuating signaling when less than 1 mM. We demonstrated that the sensitivity of PTHR signaling to Ca^{2+} allostery is dependent upon two acidic residue clusters in ECL1 of the receptor where possible Ca^{2+} coordination may promote interaction with ligands, and thus increasing their residence time on the receptor.

Our investigation of the cellular and molecular bases of hypocalcemia caused by a novel PTH variant where the arginine residue at position 25 is mutated to cysteine [52] revealed that this mutant has an impaired capacity to prolong cAMP responses from endosomes. The mutant hormone's conformation, binding affinity to the extracellular domain of the PTHR, and trafficking properties were comparable to WT PTH; however, we showed that mutation of R25 in PTH^{R25C} renders this mutant insensitive to Ca^{2+} allostery and short-acting. Our findings allow us to infer that R25 in PTH might be a key residue interacting with acidic clusters of receptor ECL1, and Ca^{2+} coordination at this site may further promote and stabilize this interaction. We propose that Ca^{2+} allostery is a determinant of biased PTH agonism as it relates to the duration of PTHR signaling. Furthermore, the observed loss of sensitivity to Ca^{2+} in the disease-causing PTH variant unveils an unexpected role of Ca^{2+} in the etiology of hypocalcemia.

Prolonged cAMP generation from endosomes was originally discovered for the PTHR [31], but its physiological relevance remained unknown until recently. The first reliable link between endosomal cAMP responses and its physiological outcomes was provided by the finding that a long-acting PTH analog (LA-PTH), which triggers substantially longer endosomal cAMP responses than PTH, is also able to induce enhanced and prolonged blood Ca^{2+} elevation in mice and in monkeys compared with PTH [50, 79]. This link is further strengthened by this study demonstrating that the hypocalcemia-causing mutation in PTH displays defective endosomal PTHR signaling. The opposing actions of PTH and PTH^{R25C} as they relate to endosomal cAMP production in cells and calcemic responses in a human patient provide a better understanding of the disease relevance of endosomal PTHR signaling., which is likely the primarily signaling component of the PTH-mediated regulation of Ca^{2+} homeostasis in vertebrates.

3.0 Use of Backbone Modification to Enlarge the Spatiotemporal Diversity of Parathyroid Hormone Receptor-1 Signaling via Biased Agonism

3.1 Introduction

Information transfer at the molecular level is critical in living systems, and many natural messages are encoded in amino acid sequences. Evolutionary modulation of these message is focused on side chains of proteins and peptides. Chemical synthesis enables an expansion in polypeptide language via backbone modification, which can be implemented without change side chains. We have begun to explore this approach in the context of polypeptide hormones that activate class B GPCRs, many of which are targets of therapeutic interest [80-83]. Previously, β-amino acids have been used to modulate proteolytic stability, receptor-subtype selectivity, and signaling profiles of peptidic GPCR agonists [84-88]. The present study introduces a new capability of α→β substitution: modulation of the spatiotemporal characteristics of signal transduction.

Agonist binding to a GPCR induces conformational changes that are sensed by cytosolic binding partners. Different intracellular partners, such as G_s or βarrs, are predicted to engage distinct receptor conformations [89]. Biased agonism [90] is observed when a ligand favors a receptor conformation attractive to one partner relative to others. Our group previously discovered that replacing multiple α-amino acid residues of glucagon-like peptide-1 (GLP-1) with cyclic β-amino acid residues generated biased agonists favoring receptor interaction with βarrs relative to G_s. However, these α/β-peptides were less potent agonists than the original α-peptide (GLP-1) [88]. Here, we show that minimal backbone alteration enabled by the use of homologous β-

residues can generate potent agonists with high signaling selectivity at the PTHR and an altered spatiotemporal signaling profile relative to α-peptide prototypes.

The PTHR is an important target for the treatment of osteoporosis and hypoparathyroidism. Activation of the PTHR by its two native ligands, PTH and PTHrP, initiates G_s/cAMP/PKA signaling and βarr recruitment [91, 92]. PTH and PTHrP differ, however, in their spatiotemporal signaling profiles [93]. PTHrP causes transient cAMP production from receptors on the cell surface, while PTH triggers prolonged cAMP production after the receptor-agonist complex has translocated to endosomes [31, 44, 55].

Signaling duration is an important determinant of the physiological effects exerted by PTHR agonists [36], but the subcellular location of GPCR signaling can also influence physiological outcomes [94]. Therefore, molecular tools that enable dissection of the spatial and temporal dimensions of PTHR signaling would be useful for elucidating the physiological roles of this receptor [45, 95]. We asked whether backbone modification could provide a PTHR agonist with a unique spatiotemporal signaling profile relative to natural hormones, specifically, an agonist that would induce prolonged receptor activation that occurs only at the cell surface.

Because binding of βarr to the PTHR is necessary for receptor internalization and attenuates cell-surface G_s/cAMP signaling [96], PTHR engaged by a G_s-biased agonist might persist at the cell surface and cause prolonged cAMP production from that location. Previous approaches to G_s-biased agonists of the PTHR have involved amino acid side chain modification and achieved only limited success [92, 97, 98]. We pursued α→β backbone modification [84, 87, 99, 100] with PTH(1-34) and with PTHrP analog abaloparatide (ABL), both of which are used to treat osteoporosis [101, 102].

3.2 Materials and Methods

3.2.1 Materials

Fmoc-protected α-amino acids and O-(7-azabenzotriazol-1-yl)-N,N,N',N'-tetramethyluronium hexafluorophosphate (HATU) were purchased from Chem-Impex International. Fmoc-protected β^3 amino acids were purchased from Chem-Impex International and PepTech Corporation. Fmoc-protected β^2 amino acids were synthesized by a previously reported method [103, 104] or using a modification of that method; details will be described elsewhere. NovaPEG Rink amide resin was purchased from Millipore Sigma. The other reagents used for peptide synthesis and purification were purchased from Sigma-Aldrich. For cell culture, Dulbecco's Modified Eagle Medium (DMEM) and Fetal Bovine Serum (FBS) were purchased from Thermofisher Scientific. For glosensor assays, the luciferase substrate (D-luciferin) was purchased from Goldbiotechnology.

3.2.2 Peptide Synthesis, Purification, and Quantification

Peptides were synthesized by microwave-assisted reactions on NovaPEG Rink amide resin. For the coupling step, the resin was treated with 4 equivalents of protected amino acids, 4 equivalents of HATU, and 8 equivalents of *N,N*-diisopropylethylamine (DIEA) in DMF. The Fmoc deprotection was carried out by using 20% (v/v) piperidine with 0.1 M HOBT in DMF. Upon completion of the synthesis, peptides were cleaved from the resin using a solution of 94% trifluoroacetic acid (TFA), 2.5% H_2O, 2.5% 1,2-ethanedithiol (EDT), and 1% triisopropylsilane (TIS). After the cleave, the crude peptides were precipitated in cold diethyl ether and purified by

preparative HPLC. Peptide purity was assessed by UPLC (BEH C18 stationary phase, 2.1 mm x 100 mm, the solvent gradient is 10-60% acetonitrile over 5 minutes), and peptide mass was checked by MALDI-TOF MS. All the peptides reported here were >90% pure as determined by UPLC. Each α/β analogue of PTH(1-34) contains on tryptophan, and concentration was determined by UV spectroscopy using the absorbance at 280 nm. For abaloparatide and its α/β analogues, there is neither tryptophan nor tyrosine in the sequence. Concentrations in these cases were determined by UV spectroscopy using the absorbance at 214 nm [105]. After concentration determination, each peptide was aliquoted, lyophilized to dry powder, and stored at -20 °C. For cell assays, each peptide was dissolved in 10 mM aqueous acetic acid to the final concentration of 1 mM stock solution.

3.2.3 Glosensor cAMP Assay

HEK293 cells stably expressing the Glosensor cAMP reporter and human PTHR were cultured in DMEM supplemented with 10% FBS. Cells were seeded into 96-well corning plates and used for cAMP assays after forming a confluent monolayer. Upon the removal of culture medium, the intact cells in 96-well plates were incubated in CO_2-independent medium containing D-luciferin (0.5 mM) for 20 minutes at room temperature. After this period, cells in each well were treated with peptides at various concentrations, and luminescence resulting from cAMP production was measured for 30 minutes on a BioTek Synergy 2 plate reader. The peak luminescence signaling (which usually appeared 14-20 minutes after peptide addition) were used to generate concentration-response curves. The concentration-response curves were fit to the data by using the sigmoidal dose-response equation in Prism 6.0. Reported EC_{50} and E_{max} values represent mean ± s.e.m of $n \geq 3$ independent measurements.

3.2.4 PTHR-βarr BRET Assay

CHO-FlpIn cells transfected with PTHR-Rluc8 and βarr-1^{venus} or βarr-2^{venus} were cultured in DMEM supplemented with 10% FBS and 0.7 mg/mL hygromycin-B. Cells were seeded into 96-well plates at a density of $4x10^4$ cells/well and cultured for 24 hours before the BRET assay. Cells were rinsed twice with DPBS to remove traces of phenol red and incubated in fresh DPBS containing coelenterazine-h (at a final concentration of 5 μM) at 37 °C for 10 minutes. After this period, cells in each well were treated with peptides at various concentrations and BRET readings were collected for 25 minutes on a BioTek Synergy 2 plate reader with 460/40 and 528/20 nm emission filters. The BRET signal was calculated by subtracting the ratio of 528/20 emission over 460/40 emission for vehicle-treated cells from the same ratio for ligand-treated cells. The peak BRET signals (which usually appeared within the initial 5 minutes after the peptide addition) were used to generate concentration-response curves. The concentration-response curves were fit to the data by using sigmoidal dose-response equation in Prism 6.0. Reported EC_{50} and E_{max} values represent mean ± s.e.m of $n \geq 3$ independent experiments.

3.2.5 Washout Assay

For the washout experiments, cells preloaded with D-luciferin were treated with medium (vehicle) or agonists at the concentration of 1 nM for 14 minutes (ligand-on phase). After this period, the medium in each well was removed and the cells were rinsed twice with CO_2-independent medium to remove unbound ligand. After the addition of D-luciferin-containing fresh medium to each well, the luminescence was recorded for an additional 150 minutes (ligand-off phase). For competitive antagonist-modified washout assays, the experimental protocol was as

described above except that the competitive antagonist (0.5 μM) was introduced during the ligand-off phase. For Bafilomycin A1 (BA1) and competitive antagonist-modified washout experiments, the cells were pretreated with medium containing 0.5 mM D-luciferin for 20 minutes in the presence or absence of 50 nM BA1. After the ligand-on phase, as described above, the rinsed cells were incubated in D-luciferin-containing fresh medium with or without BA1 and competitive antagonist, and luminescence was monitored for 150 minutes.

3.2.6 Co-immunoprecipitation

HEK293 cells stably expressing HA-PTHR and cultured on a 10-cm dish were stimulated with PTH(1-34) or analogues at 100 nM at 5 minutes. Cells were then washed with ice-cold PBS prior to cross-linking for 2 hours with DSP (Covachem, #13301) in PBS at 4 °C. The reaction was stopped by addition of 10 mM Tris-HCl for 10 minutes and cell lysates were prepared using lysis buffer (1% Triton X-100, 50 mM Tris-HCl pH 7.4, 140 mM NaCl, 0.5 mM EDTA) containing protease and phosphatase inhibitors (Roche, #11873580001). Protein concentration was determined using BCA protein assay kit (ThermoFisher, #23225), and lysates were incubated with anti-HA agarose antibody beads (Sigma-Aldrich; #A2095 clone HA-7) overnight at 4 °C. Elution was done using LDS loading buffer (Life Technologies) and samples loaded on 10% SDS-PAGE and transferred to nitrocellulose membrane. We used antibodies against HA (Covance, clone 16B12), and βarr-1/2 (Cell Signaling; #4674, clone D24H9). Immunoreactive bands were visualized with Luminata Forte (EMD Millipore) and autoradiography film.

3.2.7 Hypothetical Molecular Basis for α/β G_s-biased PTHR Agonists

Several structures of class B GPCRs bound to an agonist and G_s have been reported in recent years [106-109], but only one of these structures involves a biased agonist [106]. Comparison of the GLP-1R TMD bound to GLP-1 versus a G_s-biased agonist peptide reveals several structural features that are potentially responsible for G_s-biased agonism of this receptor. The largest structural differences observed between these two ligand-bound GLP-1R TMDs involve TM helices 1, 6, and 7, as well as ECL3. Due to the structural conservation among class B GPCRs, we speculate that conformational perturbations in these portions of other receptors may result in G_s-biased agonism in these cases as well.

We integrate the structural information for the GLP-1R discussed above with the recently solved structure of full-length PTHR bound to LA-PTH and G_s to formulate a hypothesis to explain the G_s bias displayed by our β-containing PTHR agonists. Since the N-terminal portion of LA-PTH largely corresponds to PTH(1-14), we hypothesize that PTH(1-34) is similar to LA-PTH in the manner in which the TMD of the PTH1R is engaged. Backbone modification of PTH(1-34) at position 5, 7, or 8 results in significant signal bias. In the PTHR structure, Leu7 of LA-PTH forms nonpolar contacts with TM1 and TM7 of the receptor, which seems consistent with "hot spot regions" proposed for G_s-biased agonism of GLP-1R [106]. Both Ile5 and Met8 of LA-PTH form nonpolar contacts with TM3 of PTHR, and the bottom of TM3 interfaces with the α5 helix of $G\alpha_s$. Previous studies of the GLP-1R showed that a G_s-biased agonist of this receptor induced faster conformational change of G_s and greater efficacy of G_s-mediated cAMP signaling than did GLP-1. Such a functional distinction was suggested to arise because the biased agonist altered the positioning of the $G\alpha_s$ α5 helix by enhancing the conformational flexibility of the intracellular portion of the GLP-1R. Thus, we speculate that the effect of backbone modification of PTH(1-

34) at position 5 or 8 might propagate to G_s via TM3 of the PTHR, resulting in G_s-biased agonism upon backbone modification at either of these agonist positions.

The PTHR complex structure reveals that LA-PTH residue 1 forms hydrogen bonds with TM6 and ECL3 of the receptor. These contacts could explain why side chain modification of residue 1 in PTH(1-34) scaffold can lead to G_s-biased agonism [98].

We note that it is not possible to speculate about the effects of backbone modification in ABL scaffold at this time because no structural data are available. ABL is a derivative of PTHrP(1-34); these two peptides have the same N-terminal sequence, which differs from the N-terminal sequence of PTH(1-34). Studies with PTH/PTHrP hybrid peptides reveal that the N-termini of PTH and PTHrP have very different affinities for the PTHR TMD [35, 110]. The different affinities may arise from distinct binding modes of PTH and PTHrP to the PTHR TMD.

3.3 Results

The N-terminal region of peptidic PTHR agonists inserts deeply into the transmembrane domain (TMD) and causes conformational changes to which transducers respond [109]. The PTHR conformation required for G_s activation appears to differ from that needed for recruitment of βarrs [111]. We hypothesized that backbone modification in the N-terminal region of PTH(1-34) might induce PTH1R conformations that differentially affect G_s activation and βarr recruitment. Our search for G_s-biased agonists based on PTH(1-34) began with a set of previously described analogues generated by replacing each of the first eight residues, individually, with the (*S**)-β^3, (*S**)-β^2, or (*R**)-β^2 homologue (**Fig. 5**; *S** and *R** defined in **Fig. 5**). Several of these

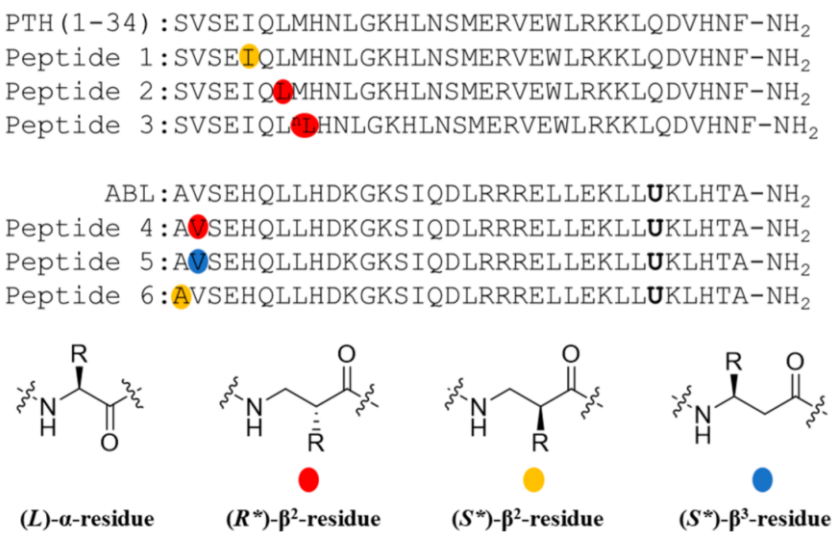

Figure 5. α/β PTHR Agonists Displaying Significant G_s-biased Agonism Relative to PTH(1-34).

β^3 homoamino acids stereospecifically prepared from proteinogenic L-α amino acids are designated *S**, based on the absolute configuration for (*S*)-β^3-hAla. *S** and *R** are applied to β^2 residues as shown above, based on the absolute configurations of the two β^2-hAla enantiomers. ^{n}L denotes norleucine. U denotes 2-aminoisobutyric acid.

backbone-modified analogues (**Fig. 6A**) were indistinguishable from PTH(1-34) in stimulating cAMP production, as evaluated in HEK293 cells stably expressing human PTHR and the Glosensor for cAMP detection. We evaluated these analogues for their ability to recruit βarrs to the receptor via bioluminescence resonance energy transfer (BRET) in CHO-FlpIn cells stably transfected with PTHR^{Rluc8} and venus-tagged βarr-1 or βarr-2. Considerable variation in recruitment of βarrs to the PTHR was observed, with incorporation of the (*S**)-β^2 homologue at position 5 or the (*R**)-β^2 homologue at position 7 or 8 (peptides 1-3) causing the most significant BRET reductions (**Fig. 6A**).

With PTH(1-34) as the reference agonist, we quantified the signaling bias of peptides 1-3 based on the Black-Leff operational model (**Fig. 6C**, **7**), in which $\Delta\Delta\log(\tau/K_A)$ denotes the bias factor [112, 113]. This quantification method minimizesthe dependence of bias factor on cell type

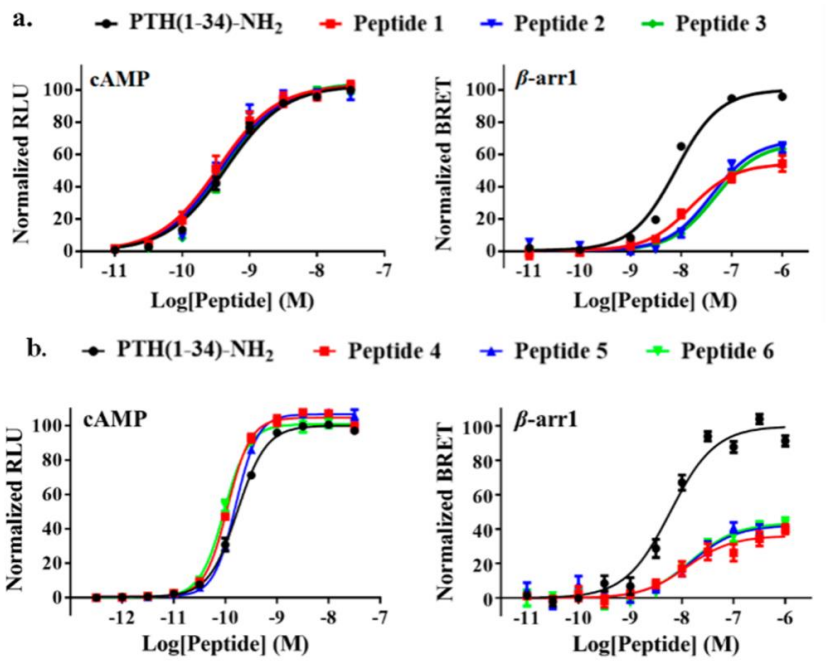

c.

Peptide	$\Delta\Delta\log(\tau/K_A)_{cAMP/\beta arr1}$	$\Delta\Delta\log(\tau/K_A)_{cAMP/\beta arr2}$
PTH (1-34)-NH_2	0	0
1	0.70* ± 0.18	0.57# ± 0.22
2	1.02* ± 0.10	1.06* ± 0.11
3	1.03* ± 0.11	0.96* ± 0.11
4	1.02* ± 0.12	1.26* ± 0.24
5	0.88* ± 0.14	1.14* ± 0.14
6	1.23* ± 0.15	1.15* ± 0.10

Figure 6. Activity Profiles of PTH and α/β G_s-biased PTHR Agonists.

(A,B) Concentration-response effects of PTH and peptides 1-6 for cAMP production and βarr-1 recruitment. Data represent mean ± s.e.m from N≥6 independent experiments. (C) Calculated bias factors of 1-6 relative PTH(1-34). *, # Statistically significant difference from PTH using one-way ANOVA (* $P < 0.0001$; # $P < 0.001$).

$$E = \frac{E_{max}\tau[A]}{[A](1+\tau) + K_A} \quad (1)$$

$$E = \frac{E_{max}}{1 + \frac{\left(\frac{[A]}{10^{\log K_A}} + 1\right)}{10^{\log R} * [A]}} \quad (2)$$

$$\Delta\log(\tau/K_A) = \log(\tau/K_A)_{ligand} - \log(\tau/K_A)_{PTH} \quad (3)$$

$$\Delta\Delta\log(\tau/K_A)_{cAMP/\beta arr} = \Delta\log(\tau/K_A)_{cAMP} - \Delta\log(\tau/K_A)_{\beta arr} \quad (4)$$

Figure 7. Equations Used to Calculate Ligand Bias Factor.

To quantify the relative capacity of PTHR agonists at stimulating cAMP production and βarr recruitment, the concentration-response data obtained in the Glosensor cAMP assay and PTHR-βarr BRET assay were fitted to the Black-Leff operational model, as shown in eq. 1. [A] is the agonist concentration, E is the observed signal in each assay, K_A is the functional affinity of the agonist, and τ is a parameter operationally describing the agonist efficacy. τ is dependent on both the receptor density and the intrinsic efficacy of the agonist in activating cellular pathways. From eq. 1, a single parameter, $\log(\tau/K_A)$, is defined as the transduction ratio, which characterizes the agonist capacity to activate a specific pathway. For curve-fitting purposes, eq. 1 is rewritten into eq. 2, in which $R = \tau/K_A$. For a given analogue, the transduction ratio of each signaling pathway, cAMP production or βarr recruitment, was compared to that of PTH(1-34) by calculating the difference in their $\log(\tau/K_A)$ values (eq. 3). The resulting $\Delta\log(\tau/K_A)$ values were used to determine the bias factor $\Delta\Delta\log(\tau/K_A)$ by substracting the $\Delta\log(\tau/K_A)$ value in the arrestin pathway from that in the cAMP pathway (eq. 4). For each peptide, S.E.M. was calculated for the transduction ratio in both pathways. Standard error (S.E.) in the bias factor was calculated by propagating the error in the $\log(\tau/K_A)$ values. To determine whether the bias factor for a given analogue was statistically significant, $\Delta\Delta\log(\tau/K_A)$ values were compared using one-way ANOVA followed by Dunnett's test. $P<0.05$ denotes statistical significance.

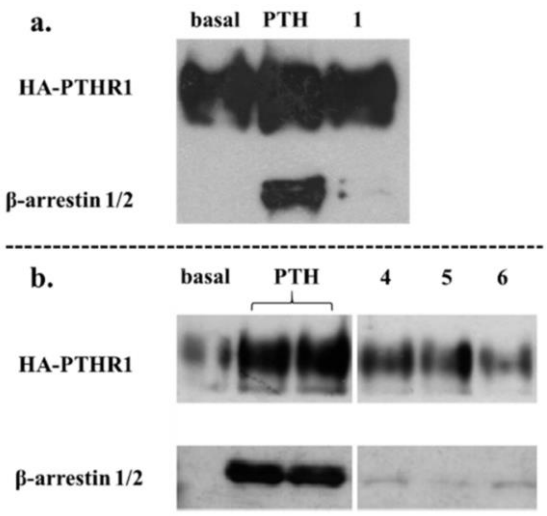

Figure 8. Recruitment of Endogenous βarr to PTHR Detected by Co-immunoprecipitation.

HEK293 cells stably expressing HA-tagged PTHR were stimulated with 100 nM of the indicated peptide. The left and right panels of B are from the same blot with unrelated data omitted from the center.

[112]. Both 2 and 3 were ~10-fold biased toward the G_s-mediated signaling pathway versus βarr recruitment relative to PTH(1-34), while peptide 1 displayed a more moderate bias.

Modifications of ABL involving positions 1 and 2 also yielded candidate analogues. Peptides 4-6 were very effective at stimulating cAMP production but significantly less effective than ABL or PTH(1-34) at recruiting βarrs (**Fig. 6B**,**C**). We evaluated βarr recruitment induced by 1, 4, 5, or 6 via co-immunoprecipitation (Co-IP) of endogenous βarr in HEK293 cells stably expressing HA-tagged PTHR. PTH(1-34) effectively induced Co-IP of the PTHR and βarr, while agonists 1, 4, 5, and 6 showed impaired interaction (**Fig. 8**).

The signaling duration of G_s-biased agonists 1-6 was evaluated with "washout" assays in which cells were stimulated with an agonist for a defined period, and then the agonist was washed away, and cAMP production was monitored (ligand-off phase) [35, 114]. Although ABL has previously been shown to induce cAMP responses that are more transient than PTH(1-34), we found that both 4 and 6 performed similarly to PTH(1-34) in this assay at the tested concentration

(**Fig**. **9B**). Interestingly, peptide 1 induced more prolonged signaling relative to PTH(1-34) (**Fig. 9A**).

To evaluate the location of the cAMP production stimulated by 1, 4, or 6, we introduced an excess of PTHR antagonist (D)Trp^{12},Tyr^{34}-bPTH(7-34) during the washout assay. We hypothesized that this antagonist should compete with agonist molecules for PTHR remaining on the cell surface, but the antagonist should not reach internalized agonist-receptor complexes [96, 115]. For 1, 4, and 6, the presence of antagonist after washout caused a profound decrease in the duration and extent of cAMP production (**Fig. 9**). In contrast, only a modest drop was observed after washout with antagonist for PTH(1-34), which is known to continue stimulating cAMP production from endosomes [31]. These observations support the conclusion that biased agonists 1, 4, and 6 are relatively ineffective at inducing βarr recruitment to the PTHR, which causes activated receptors to remain at the cell surface.

Blocking endosomal acidification was shown to prolong cAMP production of PTH [44]. We therefore conducted additional washout experiments with bafilomycin A1 (BA1), an inhibitor of endosomal acidification [116], to gain further insight into the signaling profiles of 1, 4, and 6. After agonist washout, cells were incubated in a solution containing both BA1 and the antagonist. Inclusion of BA1 after washout had very little effect on the extent of post-washout cAMP production induced by 4 or 6 (**Fig. 9C**), but BA1 caused a substantial increase in post-washout cAMP production induced by 1, relative to the level observed with the antagonist alone. This observation suggests that the single $\alpha \rightarrow \beta^2$ replacement at position 5 of PTH(1-34) (to generate 1) exerts dual effects on the agonist profile by diminishing βarr recruitment induced by 1 and rendering 1 susceptible to acidification-induced dissociation from the receptor within endosomes. In contrast to the agonist activity of 1 or ABL, the spatial restriction of cAMP

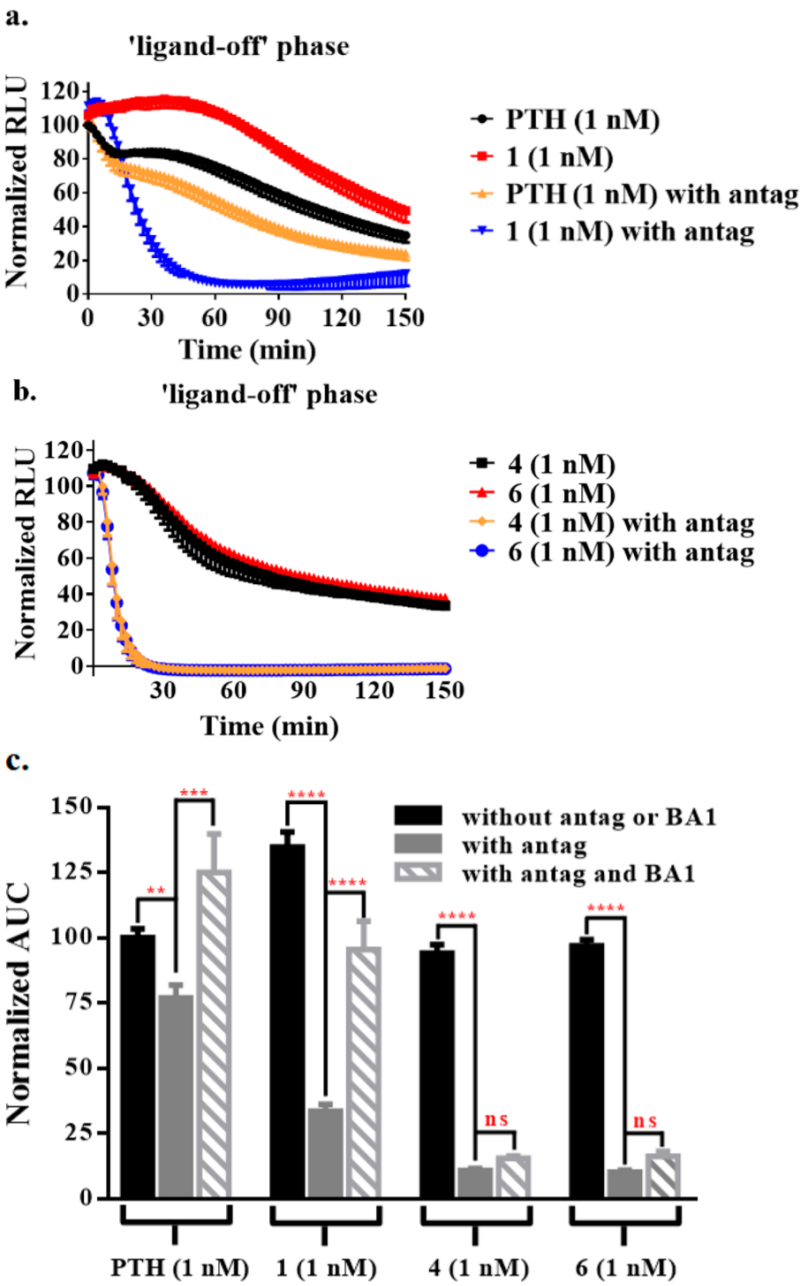

Figure 9. Effect of Competitive Antagonist and BA1 on Signal Duration.

(a, b) Post-washout cAMP production mediated by 1 nM PTH, 1, 4, or 6 in HEK293 cells stably expressing human PTHR. (c) Washout assay data from part a and b presented as area under the curve (AUC); data for measurements with BA1 are included. Data represent mean ± s.e.m. of N≥3 independent experiments. All the ligand activities are normalized to that of PTH(1-34) at 1 nM. Statistically significant difference using one-way ANOVA (**** $P < 0.0001$, *** $P < 0.001$. ** $P < 0.01$).

production induced by 4 or 6 seems to arise predominantly from their inability to induce receptor internalization.

3.4 Discussion

We have shown that introducing a single extra CH_2 unit into the backbone of a long polypeptide agonist can substantially change the signaling profile that results from engagement of a class B GPCR. Moreover, altering the position of the extra CH_2 along the backbone can lead to different signaling outcomes. Because this backbone-focused approach maintains the native side chain sequence, and because the backbone-modified peptides can be prepared via conventional solid-phase synthesis, designing and generating a "test set" of β-containing analogues based on a known polypeptide agonist is straightforward. While displaying high potency and efficacy in stimulating cAMP production, β residue-containing peptides 1, 4, and 6 are highly defective for βarr recruitment. When compared to the α peptide prototypes at equivalent concentrations, these three α/β peptides induce a longer duration of cAMP production that emanates predominantly from receptors at the cell surface. There is a long-standing belief that sustained cAMP production PTHR stimulation will lead to prolonged RANKL activation and bone resorption [117]. However, it is unclear at present whether the spatial aspect of cAMP production contributions to the RANKL activation. The highly G_s-biased agonists 4 and 6 could be useful tools to explore questions of this type.

4.0 Biased GPCR Signaling Reveals Endosomal cAMP as Determinant for Vitamin D Homeostasis

Chapter adapted from: Alex D. White, Lisa J. Clark, Karina A. Peña, Shi Liu, Saifei Lei, Fei Fang, Frédéric G. Jean-Alphonse, Zhiqiang Cheng, Chia-Ling Tu, Nicholas Szeto, Kunhong Xiao, Samuel H. Gellman, Wenhan Chang, and Jean-Pierre Vilardaga. Biased GPCR signaling reveals endosomal cAMP as determinant for vitamin D homeostasis. (manuscript in preparation)

A.D.W. performed signaling experiments with support from S.L., F.J.A., and K.P.; S.L. and S.H.G. synthesized PTH^{7d}; L.J.C. performed MD simulations; F.L. and K.X. performed MS experiments. W.C., Z.C., and C.-L.T. performed mouse studies. N.S. and C.-L.T. performed serum biochemistry, 1,25D, and/or skeletal analyses. Authors analyzed and discussed the data. J.P.V. was responsible for the overall conceptual composition and supervision of the study and wrote the manuscript with A.D.W., L.J.C., and W.C.

4.1 Introduction

GPCRs are encoded by over 800 individual genes in humans, and their expression in various tissues is paramount for proper control of a wide range of physiological processes [118]. These receptors reside predominantly at the cell surface, where they recognize and respond to an impressively diverse catalog of extracellular ligands that range from photons and ions to small molecule neurotransmitters and large peptide hormones [1]. To explain how these receptors achieve such exquisite specificity in their biological effects, previous reports have described receptor and functional selectivity as critical determinants. Functional selectivity originally referred to empirical observations that ligands for the same GPCR can possess differential propensities to activate downstream signaling pathways (i.e. biased agonism) [119, 120]. In this classical model, GPCR activation was thought to stimulate heterotrimeric G protein signaling exclusively from the cell surface in a transient manner due to subsequent recruitment of βarrs,

which was proposed to sterically block further G protein coupling and to mediate agonist-induced receptor internalization, preventing additional rounds of stimulation by extracellular ligand. This model has been challenged over the last decade by the discovery of several receptors that engage in sustained cAMP signaling from early endosomes following endocytosis [31, 53]. Observations that the location and duration of G_s-mediated cAMP responses can be dictated in a ligand-dependent manner for a single GPCR has led to the emergence of spatiotemporal regulation in GPCR signaling transduction as a novel property of functional selectivity. For example, studies involving the PTHR have shown that ligands PTH_{1-34} and its related peptide ($PTHrP_{1-36}$) stabilize distinct receptor conformations that result in cAMP responses that differ markedly in location and duration [31, 35, 36]. While both ligands stimulate transient cAMP responses from the cell surface, only PTH_{1-34} causes an additional sustained phase of cAMP generation derived from highly stable ligand-receptor-βarr complexes that remain active in early endosomes following their internalization [31, 38, 121, 122].

These findings have subsequently been used to explain ligand-specific alterations in PTHR biological outcomes observed *in vivo*, as well as a means for rational drug design. For example, early studies demonstrated that injection of PTH_{1-34} and $PTHrP_{1-36}$ into humans causes similar enhancement in the formation of new bone but discordant effects on ionized serum Ca^{2+} and vitamin D levels, with lesser effects observed for $PTHrP_{1-36}$ [45]. Additionally, the PTHrP analog abaloparatide, which triggers transient cAMP production confined to the cell surface, has been shown to efficiently promote bone formation with a reduced hypercalcemic effect when compared to PTH_{1-34}. Not surprisingly, both PTH_{1-34} and abaloparatide are FDA-approved for the treatment of osteoporosis. Despite these advancements, whether the spatial versus the temporal dimension of cAMP signaling encodes ligand-dependent PTHR biological specificity remains unknown.

Here, we addressed this question by developing a G_s-biased PTHR peptide ligand via amino acid epimerization at position 7 of PTH (PTH^{7d}). We demonstrate that this ligand fails to recruit βarrs and stimulates sustained cAMP exclusively from the cell surface. We subsequently utilize mass spectrometry, molecular dynamics simulations, and structural modeling to identify underlying determinants in PTHR and βarr that regulate the spatial organization of PTHR-mediated sustained cAMP. Studies in mice comparing the actions of PTH^{7d} and a long-acting PTH analog that potently promotes endosomal cAMP reveal that homeostatic control of active vitamin D levels specifically requires sustained cAMP generation from endosomal compartments. This study highlights the potential for delineating spatial and temporal signaling bias in rational drug design and the development of therapeutics with enhanced biological specificity.

4.2 Materials and Methods

4.2.1 Cell Culture and Transfection

Cell culture reagents were obtained from Corning (CellGro). Human embryonic kidney cells (HEK293; ATCC, Georgetown, DC) stably expressing the recombinant human PTHR were grown in selection medium (DMEM, 5% FBS, 1% penicillin/streptomycin, 500 µg/mL neomycin) at 37 °C in a humidified atmosphere containing 5% CO_2. For transient expression, cells were seeded on glass coverslips coated with poly-D-lysine in six-well plates and cultured for 24 hours prior transfection with the appropriate cDNAs using Fugene-6 (Promega) or Lipofectamine 3000 (Life Technologies) for 48-72 hours before experiments. We optimized expression conditions to

ensure the expression of fluorescently-labeled proteins was similar in examined cells by performing experiments in cells displaying comparable fluorescence levels.

4.2.2 Chemicals

Forskolin (#344270) was purchased from EMD-Millipore.

4.2.3 Peptide Synthesis, Purification, and Quantification

PTH(1-34), PTH(1-34)^{TMR}, and LA-PTH were synthesized and characterized as previously described [44].

(*D*)-Leu(7)-PTH(1-34) was synthesized by microwave-assisted reactions on NovaPEG Rink amide resin. For each coupling step, the resin was treated with 4 equivalents of protected amino acid, 4 equivalents of HATU, and 8 equivalents of *N*,*N*-diisopropylethylamine (DIEA) in DMF. Fmoc deprotection was carried out by using 20% (v/v) piperidine with 0.1 M HOBT in DMF. Upon completion of synthesis, the peptide was cleaved from the resin using a solution of 94% trifluoroacetic acid (TFA), 2.5% H_2O, 2.5% 1,2-ethanedithiol (EDT), and 1% triisopropylsilane (TIS). After cleavage, the crude peptide was precipitated by addition of cold diethyl ether. The precipitated material was purified by preparative HPLC. Peptide purity was assessed by UPLC (BEH C18 stationary phase, 2.1 mm x 100 mm, the solvent gradient was 10-60% acetonitrile over 5 minutes), and peptide mass was checked by MALDI-TOF MS. The peptide reported here was >95% pure as determined by UPLC. Since (*D*)-Leu(7)-PTH(1-34) contains one tryptophan in its sequence, the peptide concentration was determined by UV spectroscopy using the absorbance at 280 nm (the molecular extinction coefficient of tryptophan

at 280 nm is 5690 $M^{-1}cm^{-1}$). After concentration determination, the peptide was aliquoted, lyophilized to dry power, and stored at -20 °C.

4.2.4 Plasmids

DNA constructs encoding for $PTHR^{YFP}$, $PTHR^{CFP}$, and βarr-2^{YFP} were previously described by the Vilardaga lab [31, 63, 123]. βarr-1^{Rluc8} was provided by Dr. Zachary Freyberg (University of Pittsburgh).

4.2.5 Co-immunoprecipitation

HEK293 cells stably expressing HA-PTHR and cultured on a 10-cm dish were stimulated with PTH(1-34) or analogues at 100 nM at 5 minutes. Cells were then washed with ice-cold PBS prior to cross-linking for 2 hours with DSP (Covachem, #13301) in PBS at 4 °C. The reaction was stopped by addition of 10 mM Tris-HCl for 10 minutes and cell lysates were prepared using lysis buffer (1% Triton X-100, 50 mM Tris-HCl pH 7.4, 140 mM NaCl, 0.5 mM EDTA) containing protease and phosphatase inhibitors (Roche, #11873580001). Protein concentration was determined using BCA protein assay kit (ThermoFisher, #23225), and lysates were incubated with anti-HA agarose antibody beads (Sigma-Aldrich; #A2095 clone HA-7) overnight at 4 °C. Elution was done using LDS loading buffer (Life Technologies) and samples loaded on 10% SDS-PAGE and transferred to nitrocellulose membrane. We used antibodies against HA (Covance, clone 16B12), and βarr-1/2 (Cell Signaling; #4674, clone D24H9). Immunoreactive bands were visualized with Luminata Forte (EMD Millipore) and autoradiography film.

4.2.6 cAMP Accumulation Assay

HEK293 cells stably expressing the Glosensor cAMP reporter and human PTH1R were cultured in DMEM supplemented with 10% FBS. Cells were seeded into 96-well corning plates and used for cAMP assays after forming a confluent monolayer. Upon the removal of culture medium, the intact cells in 96-well plates were incubated in CO_2-independent medium containing D-luciferin (0.5 mM) for 20 minutes at room temperature. After this period, cells in each well were treated with peptides at various concentrations, and luminescence resulting from cAMP production was measured for 30 minutes on a BioTek Synergy 2 plate reader. The peak luminescence signaling (which usually appeared 14-20 minutes after peptide addition) were used to generate concentration-response curves. The concentration-response curves were fit to the data by using the sigmoidal dose-response equation in Prism 6.0. Reported EC_{50} and E_{max} values represent mean ± s.e.m of $n \geq 3$ independent measurements.

4.2.7 Washout Assay

For the washout experiments, cells preloaded with D-luciferin were treated with medium (vehicle) or agonists at the concentration of 1 nM for 14 minutes (ligand-on phase). After this period, the medium in each well was removed and the cells were rinsed twice with CO_2-independent medium to remove unbound ligand. After the addition of D-luciferin-containing fresh medium to each well, the luminescence was recorded for an additional 150 minutes (ligand-off phase). For competitive antagonist-modified washout assays, the experimental protocol was as described above except that the competitive antagonist (0.5 μM) was introduced during the ligand-off phase. For Bafilomycin A1 (BA1) and competitive antagonist-modified washout experiments,

the cells were pretreated with medium containing 0.5 mM D-luciferin for 20 minutes in the presence or absence of 50 nM BA1. After the ligand-on phase, as described above, the rinsed cells were incubated in D-luciferin-containing fresh medium with or without BA1 and competitive antagonist, and luminescence was monitored for 150 minutes.

4.2.8 cAMP Time-courses and βarr Recruitment by FRET

cAMP was assessed using FRET-based assays. Cells were transiently transfected with the FRET-based biosensor $Epac1^{CFP/YFP}$ [61] for measuring cAMP. Measurements were performed and analyzed as previously described [62]. In brief, cells plated on poly-D-lysine coated glass coverslips were mounted in Atoofluor cell chambers (Life Technologies), maintained in a HEPES buffer containing 150 mM NaCl, 20 mM HEPES, 2.5 mM KCl, 1 mM $CaCl_2$, 0.1% BSA, and pH 7.4 and transferred on the Nikon Ti-E equipped with an oil immersion 40X numerical aperture 1.30 Plan Apo objective and a moving stage (Nikon Corporation). CFP and YFP were excited using a mercury lamp. Fluorescence emissions were filtered using a 480 ± 20 nm (CFP) and 535 ± 15 nm (YFP) filter set and collected simultaneously with a LUCAS electron-multiplying charge-coupled device camera (Andor Technology) using a DualView 2 (Photometrics) with a beam splitter dichroic long pass of 505 nm. Fluorescence data were extracted from a single cell using Nikon Element Software (Nikon Corporation). The FRET ratio for single cells was calculated and corrected as previously described [63]. Individual cells were perfused with buffer or with ligand for the time indicated by the horizontal bar.

4.2.9 βarr Recruitment by BRET

CHO-FlpIn cells transfected with PTH1R-Rluc8 and βarr-1^{venus} or βarr-2^{venus} were cultured in DMEM supplemented with 10% FBS and 0.7 mg/mL hygromycin-B. Cells were seeded into 96-well plates at a density of $4x10^4$ cells/well and cultured for 24 hours before the BRET assay. Cells were rinsed twice with DPBS to remove traces of phenol red and incubated in fresh DPBS containing coelenterazine-h (at a final concentration of 5 μM) at 37 °C for 10 minutes. After this period, cells in each well were treated with peptides at various concentrations and BRET readings were collected for 25 minutes on a BioTek Synergy 2 plate reader with 460/40 and 528/20 nm emission filters. The BRET signal was calculated by subtracting the ratio of 528/20 emission over 460/40 emission for vehicle-treated cells from the same ratio for ligand-treated cells. The peak BRET signals (which usually appeared within the initial 5 minutes after the peptide addition) were used to generate concentration-response curves. The concentration-response curves were fit to the data by using sigmoidal dose-response equation in Prism 6.0. Reported EC_{50} and E_{max} values represent mean ± s.e.m of $n \geq 3$ independent experiments.

4.2.10 Saturation and Competition Binding Using PTH^{TMR}

HEK293 cells were transiently transfected with HA-PTHR and seeded in 96-well plates. Approximately 48 h after transfection, cells were incubated in HEPES buffer (137 mM NaCl/5 mM KCl/1 mM $MgCl_2$/20 mM HEPES/0.1% BSA pH 7.4) for 1 h at 4 °C, followed by 2 h incubation at 4 °C in the presence of ligand. Increasing concentration of TMR-labeled PTH (PTH^{TMR}) were utilized for saturation binding, while competition binding experiments used a constant PTH^{TMR} concentration (31.6 nM) with increasing amounts of unlabeled PTH. Cells were

washed twice with the same buffer, and fluorescence intensities were recorded at 580 ± 20 nm using an excitation wavelength of 525 ±20 nm on a Tecan Spark 20M multimode microplate reader. Nonspecific binding was determined using 1 μM of unlabeled ligand. Data were subsequently analyzed using Graphpad Prism 7.0 (GraphPad Software Inc., La Jolla, CA).

4.2.11 Receptor Internalization and Recycling

Live-imaging trafficking of $PTHR^{SEP}$ was done as described [64] using a Nikon A1 confocal microscope. Briefly, HEK293 cells stably expressing a pH-sensitive GFP variant, superecliptic pHluorin, inserted in the N-terminal domain of the human PTHR were seeded on glass coverslips coated with poly-D-lysine (Sigma #P7280) for 24 hours. Experiments were carried out at 37 °C in FRET buffer used for cAMP experiments. Cells were stimulated by ligand for 1 minute then washed out to allow recycling. Images were acquired every 30 seconds.

4.2.12 Mouse Studies

To test the impact of PTH^{7d}, LA-PTH, and PTH^{WT} (Bachem, Torrance, CA, Cat#H-5460) on serum and skeletal parameters, 3-month-old male C57BL/6J (C57/B6) mice (Jackson Laboratory, Stock No: 000664) were ear-tagged for identification, randomly assigned to groups, and injected daily with ligand (40 μg/kg body weight/injection) for 4 weeks after the mice were acclimated with house environment for 2 weeks. In this study, blood was sampled via retroorbital route under isoflurane anesthesia after 2 hours of the last drug injection. Mice were allowed to recover before another blood collection by cardiac puncture and bone collection from the mice euthanized by isoflurane overdose 24 hours after the last drug injection. Serum Ca^{2+} and phosphate

levels were assessed by an ACE Axcel bioanalyzer (Alfa Wassermann, West Coldwell, NJ) and skeletal parameters of distal femurs were assessed by an SCANCO μCT 50 scanner and analytic software (Scanco USA, Inc., Wayne, PA, USA) as detailed previously [124]. In a separate time-course study, a different group of mice were injected with a single dose of PTH^{7d} or LA-PTH for different time points before euthanization. Their serum 1,25D levels were assessed by an ELISA kit (AC-62F1; Immunodiagnostic systems, Tyne & Wear, United Kingdom) according to the manufacturer instructions. All mice were kept in a climate-controlled room (22 °C; 45-54% relative humidity) with a 12-hour light/12-hour dark cycle. Water and standard chow (1.3% calcium and 1.3% phosphate) were given ad libitum. All animal experiments (Protocol #18-013) were approved and performed according to guidelines of the Institutional Animal Care and Use Committee at the San Francisco Department of Veterans Affairs Medical Center.

4.2.13 Pharmacokinetic Analysis

Bioactive LA-PTH or PTH^{7d} peptide content of blood plasma was assessed by applying 5 μL of plasma (supplemented with protease inhibitors) to the HEK293-derived cell line GP2.3 in which human PTHR and the luciferase-derived glosensor cAMP reporter were stably expressed. Cells were seeded into 96-well white plates and assayed 24 hours later in CO_2-independent culture medium (Life Technologies, Carlsbad, CA, USA) containing 0.1% BSA. Cells were pre-incubated with D-luciferin (0.5 mM) for 2 hours, then blood plasma samples were added and cAMP-dependent luminescence was measured at 2-minute intervals. For each well, the maximum luminescence observed, which typically occurred 10-20 minutes after sample addition, was used to establish relative bioactive peptide.

4.2.14 MD simulations

System preparation. The 3.0 Å cryo-EM structure of LA-PTH-PTHR-G_s-Nb35 complex (PDB 6NBF) [109] was used to generate initial PTHR models. I-TASSER was then used to model flexible loops absent in the cryo-EM structure: ECD residues 56-104, ECL1 residues 247-275, and ICL3 residues 394-398 [125-127]. In PyMOL, structures of G_s, Nb35, palmitic acid, and cholesterol were removed. LA-PTH residues were mutated to the corresponding PTH^{WT} residues, as necessary, using the PyMOL Mutagenesis Wizard. The chirality of L7 in the PTH^{WT} model was changed in PyMOL to generate the PTH^{7d} model. Each initial model was oriented in a model membrane using the Orientations of Proteins in Membranes (OPM) PPM Server [128]. Using oriented models, inputs for Nanoscale Molecular Dynamics (NAMD) were generated using CHARMM-GUI Membrane Builder [129-135]. Disulfide bonds Cys48-Cys117, Cys108-Cys148, Cys131-Cys170, and Cys281-Cys351 were specified to ensure correct formation. A heterogeneous lipid bilayer consisting of 75% POPC and 25% cholesterol was assembled around the receptor model using the Replacement Method. The system was solvated in a box of TIP3P waters, and ions were added to a concentration of 150 mM NaCl using Monte Carlo sampling.

MD simulations. All-atom simulations were performed in triplicate for PTH^{WT}–PTHR and PTH^{7d}–PTHR simulations using NAMD with the CHARMM36m force field [136, 137]. Prior to production simulations, 10,000 steps of conjugate gradient energy minimization were performed followed by 0.675 ns equilibration in which restraints were applied and then slowly released over six steps following the protocol established by the CHARMM-GUI group [136]. Next, 200 ns production simulation with 2 fs timestep was performed. Non-bonded interactions were cut off at 12.0 Å, and van der Waals force switching was applied between 10.0 and 12.0 Å. Langevin

dynamics and Langevin piston were used to maintain temperature at 303.15 K and pressure at 1 atm.

MD trajectory analysis. MD trajectories were analyzed in Visual Molecular Dynamics (VMD) and PyMOL [138]. PTHR snapshots were aligned using receptor TM helices ($PTHR^{TMD}$ without ECLs or ICLs: residues 180 to 211, 218 to 246, 280 to 311, 317 to 343, 359 to 392, 399 to 425, 435 to 460). PTH Glu4 hydrogen bond analysis was performed using HBonds Plugin in VMD. Number of hydrogen bonds throughout the trajectories was plotted in GraphPad Prism.

4.2.15 Structural Modeling

The model of PTHR bound to βarr-1 was generated using a snapshot of PTH^{WT}−PTHR after 200 ns simulation and the crystal structure of rhodopsin bound to mouse visual arrestin-1 (PDB 4ZWJ). PyMOL was used to perform structural, sequence-independent alignment of the TMD of PTHR (residues 180 to 460) to the TMD of rhodopsin (residues 34 to 305, RMSD = 5.193 Å). A homology model of βarr-1 in the receptor core conformation was generated in SWISS-MODEL using the structure of visual arrestin-1 as a template [139, 140]. The βarr-1 model was aligned with visual arrestin-1 in PyMOL and PTH^{7d}−PTHR snapshots were then aligned with PTH^{WT}−PTHR. Distances between PTHR Val412 and βarr-1 Leu73 throughout the trajectories were calculated in VMD and plotted in GraphdPad Prism.

4.2.16 1-α(OH)ase protein expression

MDCK cells stably expressing HA-PTHR were polarized on 24 mm Transwells (Corning) with 0.4 μm pore size. Polarized cells were basolaterally stimulated with 30 nM LA-PTH or 30

nM PTH^{7d} diluted in growth media, with or without FBS, for 4 or 8 hours or left untreated. After stimulation, cells were lysed in buffer containing 50 mM Tris pH 7.4, 150 mM NaCl, 5 mM EDTA, 10% glycerol, and 1% IGEPAL (Sigma), supplemented with protease and phosphatase inhibitors, as described previously [141]. Briefly, transwells were washed in cold PBS and then membranes were cut out of their plastic supports and put in a microcentrifuge tube with 300 µL lysis buffer. Membranes were vortexed and incubated in rotation at 4 °C for 30 minutes. Lysates were then centrifuged at maximum speed for 10 minutes in a benchtop refrigerated centrifuge. Supernatants were transferred to a clean tube. Protein concentration was measured using BCA protein assay kit (ThermoFisher, #23225). For Western blot analysis, 10 µg of lysates were loaded per well in a 10% gel. Gels were transferred to a nitrocellulose membrane and blocked in TBS-T with 5% milk. For detection of 1-α(OH)ase, membranes were blotted with anti-CYP27b1 polyclonal antibody (Novus Biologicals #NBP2-29942) at 1:1000 dilution. Anti-GAPDH monoclonal antibody (Santa Crus Biotechnologies #sc-3223) at 1:1000 dilution was used as loading control. HRP-conjugated antibodies (Dako Denmark, Denmark) were used as secondary antibodies. Immunoreactive bands were visualized with immobilon forte western HRP substrate (EMD Millipore, #WBLUF0100). Band intensity quantification was performed using ImageJ software (NIH).

4.2.17 Photo-crosslinking experiments

HEK293 cells ($2x10^6$) were seeded on poly-D-lysine coated 10-cm dishes, and 24 hours later *p*-benzoyl-L-phenylalanine (Bpa) was added to the medium for 1 hour prior to transfection. Cells were co-transfected with three plasmids: one plasmid encoding for PTHR, the second plasmid containing the gene of HA-tagged βarr-1 with a TAG codon substituting for the triplet encoding Leu73, and the last plasmid (pIRE4-Bpa) encoding for the orthogonal pair incorporation

Bpa (*Ec*BpaRS/BstYam). Approximately 24-36 hours after transfection, cells were stimulated with 200 nM PTH^{WT} or PTH^{7d} for 10 minutes, washed twice with cold PBS, and irradiated for 15 minutes in PBS using UVP crosslinker (Analytik Jena) with 2000 x 100 microjoules per cm^2 energy exposure at a distance of 2.5 cm. Cell lysates were prepared with lysis buffer were prepared in buffer containing 1% Triton X-100, 50 mM Tris-HCl pH 7.4, 150 mM NaCl, and 2 mM EDTA, and protein concentration was determined using BCA protein assay kit (ThermoFisher, #23225). Lysates were incubated with Pierce™ anti-HA agarose beads (ThermoFisher, #26181) overnight at 4 °C. Beads were washed 4 times with lysis buffer and eluted with 2X loading buffer. We used antibodies against HA (Covance, clone 16B12) and βarr-1/2 (Cell Signaling, #4674, clone D24H9). Immunoreactive bands were visualized with immobilon forte western HRP substrate (EMD Millipore, #WBLUF0100).

4.2.18 Stable Isotope Labeling With Amino Acids in Cell Culture (SILAC)

We used the HEK293 cell line stably expressing the human HA-tagged PTHR previously generated in our lab [51]. Three pools of HA-PTHR/HEK293 cells were maintained side-by-side in "light", "medium", or "heavy" SILAC medium. The SILAC media were prepared from custom-ordered DMEM powder without arginine, lysine, and leucine (Gibco, formula #03-5080EB). [$^{2}H_4$]-L-lysine (50 mg/liter) and [$^{13}C_6$]-L-arginine (25 mg/liter) (Cambridge Isotope Laboratories) were added to "medium", [$^{13}C_6$, $^{15}N_2$]-L-lysine (50 mg/liter) and [$^{13}C_6$, $^{15}N_4$]-L-arginine (25 mg/liter) (Cambridge Isotope Laboratories) were added to "heavy", and equal concentrations of conventional lysine and arginine were added to "light". All versions were supplemented with L-leucine (104 mg/liter), L-proline (10 mg/liter), 10% dialyzed FBS (Hyclone), 1% penicillin/streptomycin, and G418 (150 mg/mL). The SILAC cells were cultured for at least six

doublings until the isotope incorporation rates in “medium” and “heavy” cells were higher than 95%. The SILAC cells were then expanded. When the cells reached ~80% confluence, they were serum-starved for 4 hours. To map the phosphorylation sites on the PTHR induced by PTH^{WT} or PTH^{7d}, “light” cells were treated with 30 nM PTH^{WT} for 5 minutes and “medium” cells were treated with 30 nM PTH^{7d} for 5 minutes before harvesting (“heavy” cells served as non-treated control). Equal numbers of “light”, “medium”, and “heavy” cells (generally six 150-mm culture dishes for each) were mixed, flash-frozen in liquid nitrogen, and stored at -80 °C. The SILAC experiments were repeated three times.

4.2.19 HA-PTHR Isolation, Digestion, and Peptide Desalting

HA-PTHR was isolated from SILAC cells using Pierce™ anti-HA agarose beads (Thermo Fisher Scientific, #26181). Briefly, crude membrane fractions were prepared from equally mixed (“light”:“medium”:“heavy” = 1:1:1) as previously described [142, 143]. HA-PTHR was then extracted from crude membrane preparations with buffer containing 20 mM tris-HCl pH 8.0, 100 mM NaCl, 2 mM EDTA, 1% DDM, and protease/phosphatase inhibitors. HA-PTHR was isolated from extraction solution by incubating with 200 µL anti-HA beads with rotation at 4 °C for 4 hours, and receptor was eluted with 100 µL 2X SDS-PAGE buffer (containing 100 mM DTT). The receptor was then alkylated with 30 mM iodoacetamide in the dark for 30 minutes at room temperature, and samples were then subjected to SDS-PAGE. Protein bands corresponding to HA-PTHR were excised from the gel for in-gel protein digestion. Tryptic digestion of HA-PTHR was performed as previously described [70, 144]. Briefly, excised gel bands were chopped into small pieces and de-stained with 50 mM ammonium bicarbonate in 50% acetonitrile. Sequence grade trypsin (10 ng/µL, Promega) in 50 mM ammonium bicarbonate (pH 8.0) was then added to the

tubes to cover the de-stained gel pieces. The tryptic digestion reactions were incubated at 37 °C overnight. An equal volume of 100% acetonitrile was added to the digested gel samples for peptide extraction and repeated three times. The extracted peptides were pooled into a pre-washed protein LoBind tube (Fisher, #13698793) and then dried under vacuum on a SpeedVac evaporator. The peptide samples were desalted with handmade Stage Tips was previously described [70]. The desalted peptides were lyophilized with a SpeedVac evaporator, reconstituted in 0.1% trifluoroacetic acid, 2% acetonitrile, and 25 mM citrate, and subjected to LC-MS/MS analysis.

4.2.20 MS and Data Analyses

LC-MS/MS analyses were performed on a Thermo Scientific LTQ Orbitrap Velos mass spectrometer with a Finnigan Nanospray II electrospray ionization source. The peptide samples were loaded onto a nanoViper Compatible PicoChip Column (New Object, #1PCH7515-105H354-NV) and separated with a Waters nanoACQUITY UPLC System. Instrument control and primary data processing were done with the Xcalibur software package. The LTQ Orbitrap Velos was operated in data-dependent mode using a TOP10 strategy [145]. MS/MS spectra were searched with the SEQUEST algorithm against composite database containing the human HA-PTHR sequence or HA-PTHR with its interacting proteins, as well as their reverse sequences. Search parameters allowed for three missed tryptic cleavages, a mass tolerance of ±80 ppm, a static modification of 57.02146 daltons (carboxyamidomethylation) on cysteine, and up to eight dynamic modifications: 79.96633 daltons (phosphorylation) on serine, threonine, and tyrosine; 15.99491 daltons (oxidation) on methionine; 6.02012 daltons or 10.00827 daltons on arginine; and 5.00709 daltons or 8.01420 daltons on lysine. Search results were filtered to include <1% matches to reverse sequences by restricting the mass tolerance window, and setting thresholds for Xcorr and

dCn' (defined as the normalized difference between Xcorr values of the top-ranked candidate peptide and the next candidate with a different amino acid sequence). Matches for phosphopeptides were validated manually with special consideration of intense fragment ions formed through cleave N-terminal to proline residues and neutral losses of phosphoric acid. Peptide quantification was performed with the Vista program [146] as well as by manual calculation with Qual Browser (version 3.0.63). In brief, the theoretical mass of "light", "medium", and "heavy" variants of each peptide was calculated and used to identify ion peaks in the high mass accuracy precursor scans for each. The intensity of the peaks was used to construct ion chromatograms. For each isotopic variant, the peak height and background-subtracted area under the curve were used to calculate the "light" to "heavy" (PTH^{WT}:control) and "medium" to "heavy" (PTH^{7d}:control) abundance ratios.

4.2.21 Statistical Analysis

Data were processed using Excel 2013 (Microsoft Corp. Redmond, WA) and Prism 7.0 (GraphPad Software Inc., La Jolla, CA). Data are expressed as mean ± SEM. Curves were fit to the data using a four-parameter, non-linear regression function. Statistical analyses were performed using unpaired, 2-tailed Student's *t* tests for comparisons between 2 groups and one- or two-way ANOVA with Dunnett tests for multiple group comparisons.

4.3 Results

We have previously shown that translocation of PTH−PTHR signaling complexes from the cell surface to early endosomes is βarr-dependent [38, 41]. We reasoned that a PTHR ligand that stimulates cAMP production but fails to recruit βarr would cause a shift in sustained cAMP generation from endosomes to the cell surface, thus permitting determination as to how the cellular localization of signaling responses influences PTHR biology. To this end, we explored modifications of residues in the N-terminal region of PTH_{1-34} in an effort to generate a G_s-biased agonist that promotes prolonged receptor activation and retention of ligand-receptor complexes at the cell surface. Accordingly, we determined that the diastereomer containing D-Leu, rather than L-Leu, at position 7 of (PTH^{7d}) provides the desired bias. This modification did not alter binding affinity in equilibrium competition assays utilizing tetramethylrhodamine (TMR)-labeled PTH as reporter ligand (**Fig. 10A**), nor did it cause changes in the potency (EC_{50}) or maximal efficacy (E_{max}) of cAMP production in luciferase-based accumulation assays (**Fig. 10B, black circles**). Time-course experiments of the cAMP response using the Förster resonance energy transfer (FRET)-based sensor $EPAC^{CFP/YFP}$ revealed that PTH^{7d} induces sutained cAMP responses upon ligand washout that are indistinguishable in magnitude and duration from wild-type PTH_{1-34} (hereafter referred to as PTH^{WT} (**Fig. 10C**). In contrast, PTH^{7d} displayed markedly impaired recruitment of βarrs compared to PTH^{WT} measured by bioluminescence resonance energy transfer (BRET) in cells stably expressing $PTHR^{Rluc8}$ and venus-tagged βarr-1 or βarr-2 (**Fig. 10B, orange/green circles**), and this effect was confirmed by FRET time-course experiments in cells transiently expressing $PTHR^{CFP}$ and βarr-2^{YFP} (**Fig. 10D**). These data confirm that PTH^{7d} represents a G_s-biased PTHR ligand that induces sustained cAMP responses independently of βarr recruitment.

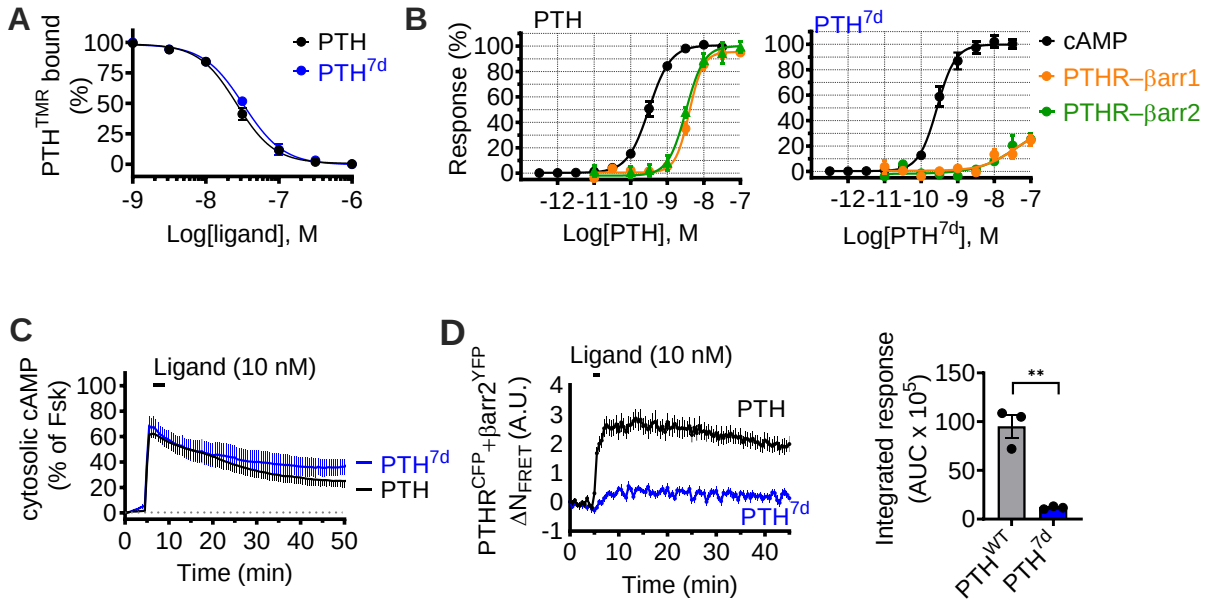

Figure 10. Characterization of Signaling by PTH^{7d}.

(a) Competition binding assays at equilibrium was performed using tetramethylrhodamine (TMR)-labeled PTH as reporter ligand and HEK293 cells stably expressing HA-tagged PTHR. Data are the mean ± s.e.m. of N=3 independent experiments with triplicate wells for each concentration point. (b) Concentration-response curves for PTH (left) or PTH^{7d} (right) in cAMP accumulation (black) or βarr recruitment (orange, green) assays. Data are the mean ± s.e.m. of N=5 independent experiments with triplicate wells for each concentration point. (c) Averaged cAMP time-course responses in HEK293 cells stably expressing PTHR following brief stimulation with 10 nM PTH or PTH^{7d}. Data are the mean ± s.e.m. of N=3 independent experiments with n = 20-26 cells per experiment. (d) Time course (left) and integrated response (right) of βarr recruitment measured by FRET in HEK293 cells transiently expressing PTHR^{CFP} and βarr2^{YFP} following brief stimulation with 10 nM PTH or PTH^{7d}. Data are the mean ± s.e.m. of N=3 independent experiments and n = 28-33 cells per experiment (**P = 0.002).

We next examined the location of PTH^{7d} signaling complexes. We have previously shown that the sustained phase of PTH^{WT}-mediated cAMP generation from endosomes requires the formation and internalization of signaling complexes comprised of ligand-bound receptor, βarr, and Gβγ subunits [38, 41]. Blockade of receptor internalization by expression of a dominant-negative dynamin mutant (DynK44A) led to significantly reduced cAMP responses induced by PTH^{WT}, while those for PTH^{7d} were unaffected (**Fig. 11A**). Additionally, live-cell confocal microscopy experiments revealed that PTH^{7d} fails to induce the subcellular co-localization of $\beta arr\text{-}2^{YFP}$ and $G\beta\gamma^{CFP}$ that is observed with PTH^{WT} and a long-acting analog (LA-PTH) previously shown to potently induce sustained cAMP signaling from endosomes [79] (**Fig. 11B**). Furthermore, real-time analysis of receptor trafficking in cells stably expressing PTHR N-terminally tagged with superecliptic pHluorin (SEP), a pH-sensitive GFP variant, showed only modest receptor internalization upon PTH^{7d} stimulation when compared to PTH^{WT} and LA-PTH (**Fig. 11C**). We subsequently confirmed that prolonged cAMP generation observed with PTH^{7d} is derived from receptor that is retained at the cell surface, as inclusion of a cell-impermeable PTHR antagonist (D-Trp^{12}, Tyr^{34}-$bPTH_{7\text{-}34}$) in the washout buffer completely abolished the sustained phase of PTH^{7d}-mediated cAMP generation (**Fig. 11D**) but had no effect in analogous experiments using PTH^{WT} or LA-PTH (**Fig. 11E,F**). Collectively, our signaling characterization data indicate that amino acid epimerization at position 7 of PTH results in a G_s-biased peptide ligand that differs from the wild-type hormone solely by the cellular localization of active signaling complexes involved in sustained cAMP responses.

Given the well-established importance of βarr coupling to the PTHR in permitting sustained cAMP generation by PTH^{WT}, we next sought to investigate the molecular mechanisms that underlie the relative inability of PTH^{7d} to promote this interaction, as well as its consequences

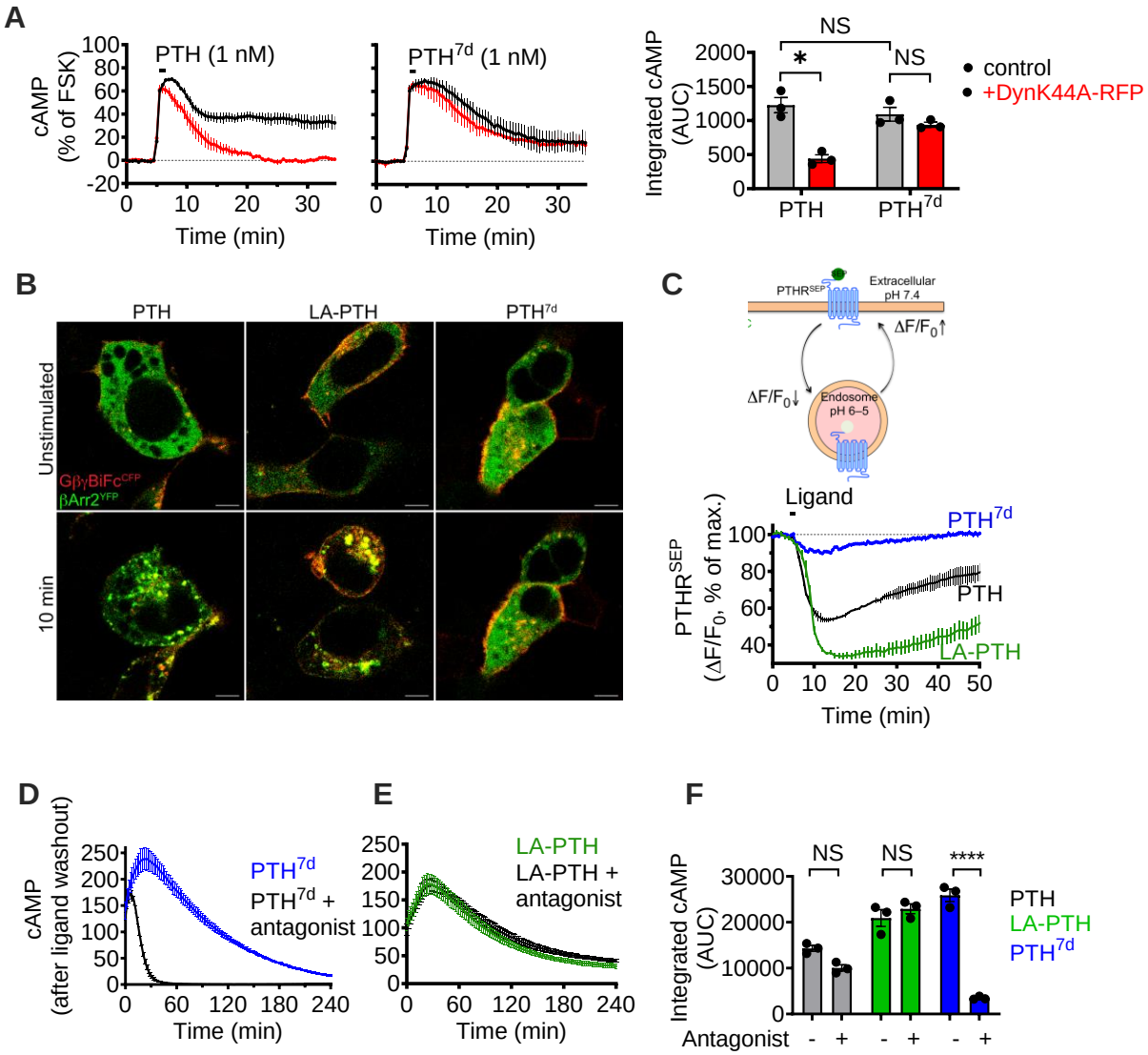

Figure 11. Localization of Signaling Complexes.

(a) Time courses (left and center panels) and integrated (right panel) cAMP responses calculated by area under the curve in cells expressing a dominant-negative dynamin mutant (DynK44A) tagged with RFP compared to control cells. Data are the mean ± s.e.m. of N = 3 independent experiments with n = 15-32 cells per experiment (***P = 0.0003). (b) Fluorescence micrographs corresponding to the merged channel data of HEK293 cells co-transfected with $G\beta\gamma^{CFP}$ (red) and βarr-2^{YFP} (green). Images were recorded at 30 s intervals for 30 minutes after a brief challenge with 100 nM PTH^{WT}, LA-PTH, or PTH^{7d}. Scale bar = 5 µm. (c) Time courses of internalization and recycling of PTHR tagged with superecliptic pHluorin (SEP) in response to ligand, measured by time-lapse confocal microscopy with images acquired every 30 seconds. The baseline was established for 5 minutes, then cells were stimulated with

100 nM PTH, PTH^{7d}, or LA-PTH for 30 seconds. Data are the mean ± s.e.m. of N=3 independent experiments with n = 11-14 cells per experiment. (d,e) cAMP time-course experiments after washout of PTH^{7d} (d) or LA-PTH (e) in the presence (black curve) or absence (blue curve) of cell-impermeable competitive antagonist. Data are the mean ± s.e.m. of N=3 independent experiments. (f) Integrated cAMP responses from panels d/e in the presence or absence of cell-impermeable competitive antagonist for PTH, LA-PTH, or PTH^{7d} (****P = 0.00000002).

for both cell biological and physiological processes. Recruitment of βarrs to activated GPCRs is thought to occur following phosphorylation of serine/threonine residues within intracellular receptor domains, specifically the third intracellular loop (ICL3) and C-terminal tail, by GPCR kinases (GRKs). Furthermore, studies in recent years have proposed that receptor phosphorylation status serves as the foremost determinant for GPCR−βarr interactions, a paradigm commonly referred to as the phosphorylation barcode hypothesis [147-149]. Accordingly, we examined whether PTH^{WT} and PTH^{7d} trigger distinct phosphorylation patterns in the PTHR that differentially permit distinct interactions with βarrs by performing Stable Isotope Labeling by Amino acids in Cell culture (SILAC)-based proteomics. We identified 10 phosphorylation sites located in the C-terminal tail and ICL3 in response to 5 minute stimulation with PTH^{WT} or PTH^{7d} at a concentration of 30 nM (**Fig. 12A**), and the quantitative changes of these phosphorylation events are listed in **Fig. 12B**. While βarr recruitment is considered driven by receptor phosphorylation status [142], we found no differences in the sites or extent of phosphorylation between PTH^{WT} and PTH^{7d} treatments (**Fig. 12C**). Despite previous work suggesting that PTHR−βarr interactions rely upon receptor phosphorylation status [150], this finding supports that alterations in βarr recruitment observed for PTH^{WT} and PTH^{7d} occur in a phosphorylation-independent manner.

In an effort to elucidate the mechanistic basis by which epimerization of Leu7 in PTH precludes association of βarr with the receptor, we subsequently utilized molecular dynamics (MD)

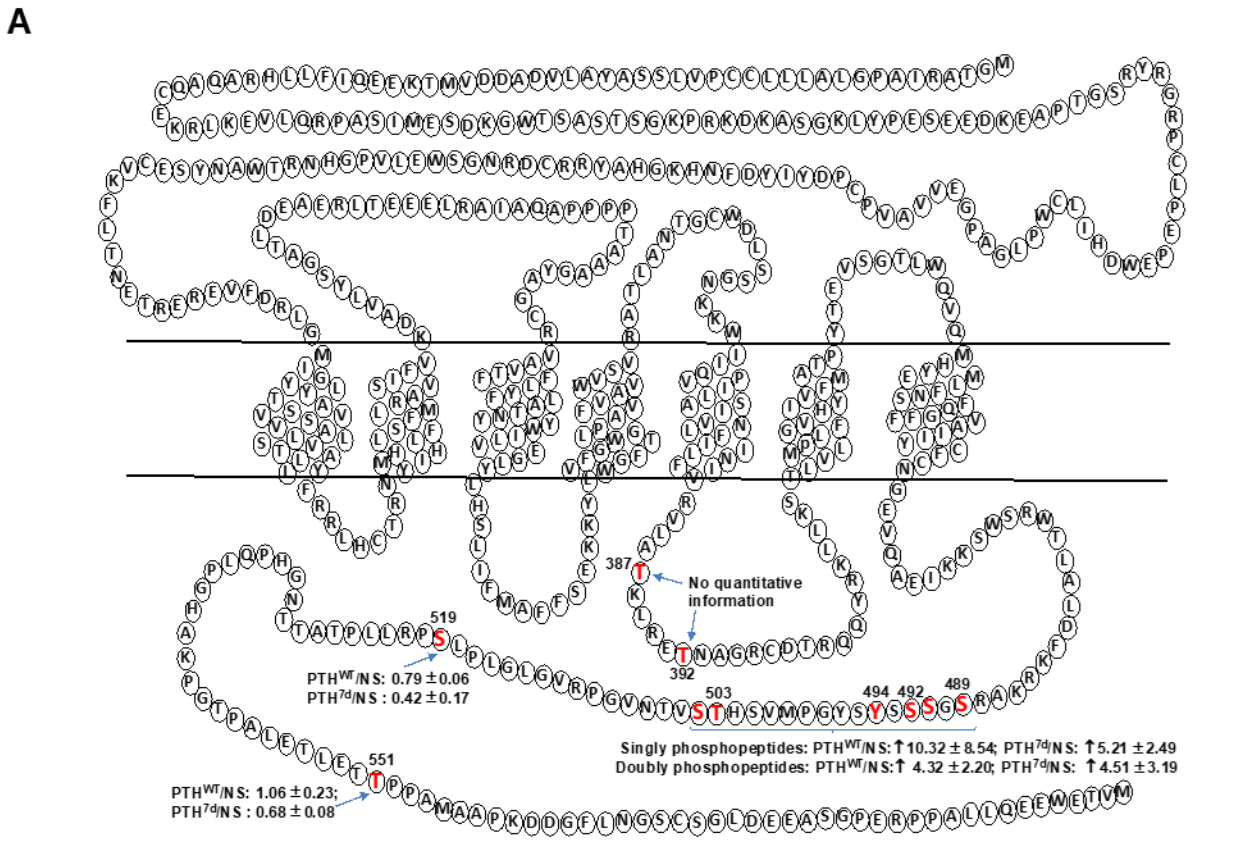

B

Phosphopeptides	PTH	PTH^{7d}
^{540}PGTPALETLET**pT**PPAM*AAPK^{559}	1.06 ± 0.23	0.68 ± 0.08
^{489}**pS**GSSSYSYGPM*VSHTSVTNVGPR^{511}	10.32 ± 8.54	5.21 ± 2.49
^{489}SG**pS**SSYSYGPM*VSHTSVTNVGPR^{511}		
^{489}SGS**pS**SYSYGPM*VSHTSVTNVGPR^{511}		
^{489}SGSSS**pY**SYGPM*VSHTSVTNVGPR^{511}		
^{489}SGSSSYSYGPM*VSH**pT**SVTNVGPR^{511}		
^{489}SGSSSYSYGPM*VSHT**pS**VTNVGPR^{511}		
^{489}SGS**pS**SYSYGPM*VSHT**pS**VTNVGPR^{511}	4.32 ± 2.20	4.51 ± 3.17
^{512}VGLGLPL**pS**PR^{521}	0.79 ± 0.06	0.42 ± 0.17
^{384}VLA**pT**KLRETNAGRCDTRQQYRK^{405}	No quantitative information	
^{384}VLATKLRE**pT**NAGR^{396}		

C

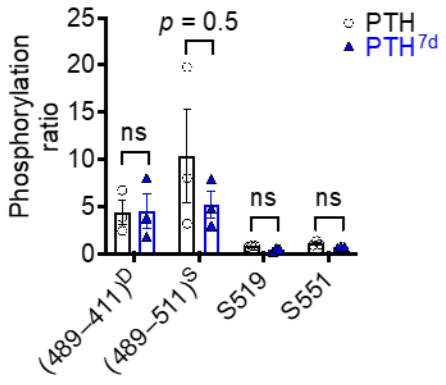

Figure 12. SILAC-based quantitative phosphorylation analysis of PTH.

(a) Summary of intracellular phosphorylation sites in PTHR and corresponding changes in response to 30 nM PTH or PTH^{7d} stimulation. Phosphorylation sites were determined by LC-MS/MS and indicated in red in the snake view map of the PTHR. The fold changes corresponding to the extents of phosphorylation were determined by SILAC-based quantitative LC-MS/MS analysis as described in the methods sections. (b,c) List of phosphopeptide sequences

identified (b) and fold changes (c) determined by SILAC-based quantitative LC-MS/MS analysis. Since isomeric single phosphorylated peptides (^{489}SGSSSYSYGPM*VSHTSVTNVGPR^{511}) with phosphorylation at different positions co-eluted from the LC column during chromatographic separation, the quantitative analysis reflects a summary of a mixture of these co-eluted single phosphorylated peptides. Data are the mean ± s.d. of N = 3 independent experiments (NS = not significant by two-way ANOVA).

simulations and structural modeling to assess PTHR conformations stabilized upon binding of either PTH^{WT} or PTH^{7d}. We utilized the recently reported 3.0 Å cryo-EM structure of active PTHR bound to G_s and LA-PTH (PDB 6NBF) [109] to generate initial models of PTH^{WT}- and PTH^{7d}-bound PTHR for triplicate 200 ns MD simulations. In the initial PTH^{7d}–PTHR model, D-Leu7 is unfavorably close to neighboring transmembrane helix (TM) 7 residues Trp437 and Met441 of the receptor (**Fig. 13A**), and simulations revealed that the D-Leu7 side chains shifts to mirror L-Leu7 nonpolar interactions in the PTH^{WT}–PTHR model (**Fig. 13B**). We found that this shift induces a kink in the PTH^{7d} helix toward TM6 (**Fig. 13B**), which subsequently permits additional polar interactions between Glu4 of PTH^{7d} and PTHR residues that are not observed for PTH^{WT} (**Fig. 13C, 13D**). In the active-state cryo-EM structure of PTHR, Glu4 promotes an extensive polar interaction network that stabilizes the outward kink of TM6 that is considered prerequisite for coupling to G proteins [109, 122]. The increased polar contacts by Glu4 of PTH^{7d} further extend this polar interaction network relative to PTH^{WT}-bound receptor.

These observations, combined with previous reports that an inward movement of TM6 is essential for efficient βarr coupling [151], led us to hypothesize that the increased stabilization of the outward TM6 kink by PTH^{7d} relative to PTH^{WT} may provide the structural basis for differences in βarr recruitment. To test this possibility, we generated a homology model of βarr-1 using the conformation of visual-arrestin-1 bound to rhodopsin (PDB 4ZWJ) as a template [139, 140]. We

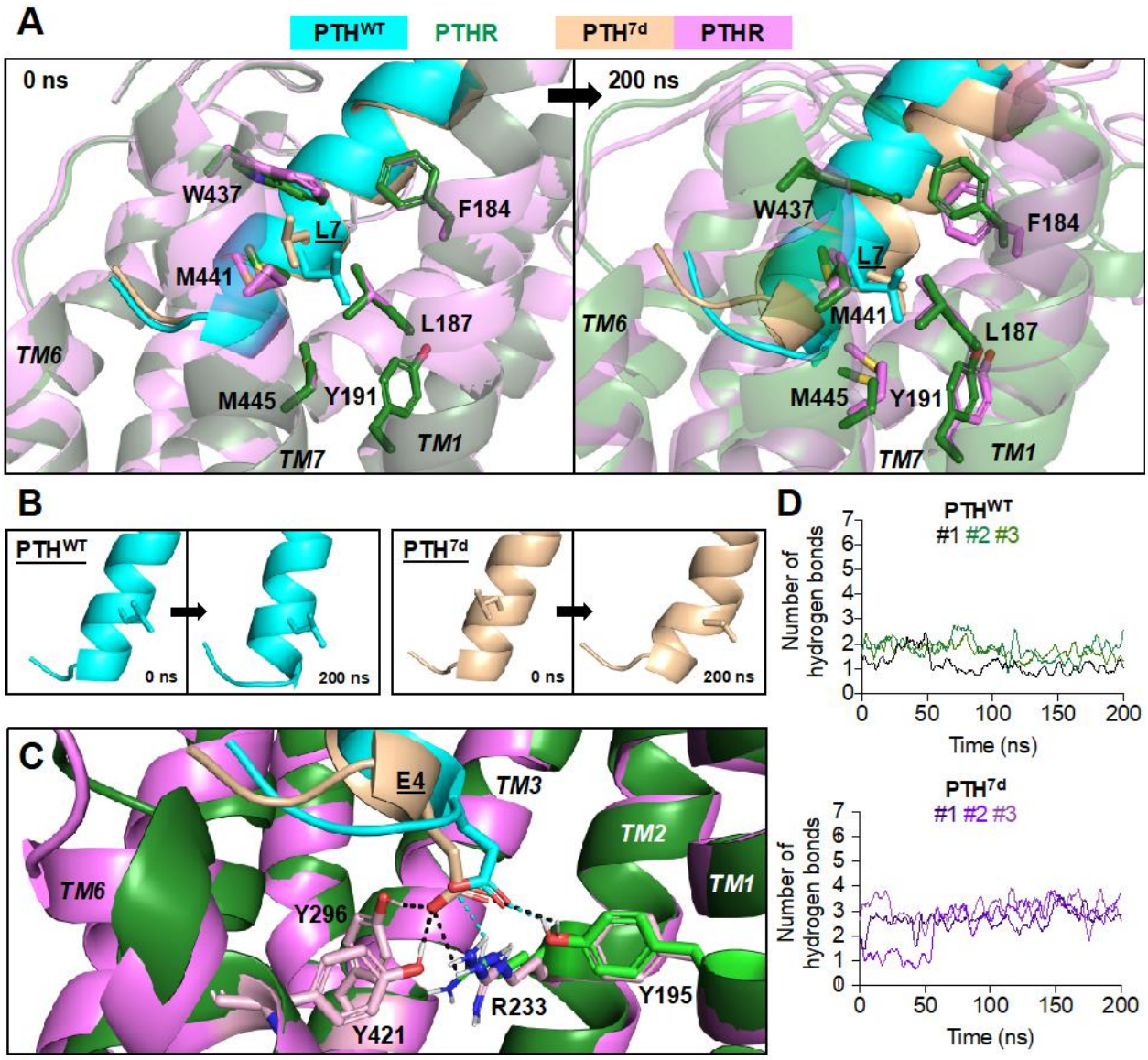

Figure 13. Molecular changes induced by PTH^{7d}.

(a) PTH^{WT} and PTH^{7d} are colored cyan and wheat, respectively. PTH^{WT}- and PTH^{7d}-bound receptor are colored dark green and violet, respectively. PTH Leu7 and receptor residues within 4 Å of Leu7 are shown as sticks. The left panel shows initial MD models of PTH^{WT}–PTHR and PTH^{7d}–PTHR. In the initial model of PTH^{7d}–PTHR, D-Leu7 is unfavorably close to PTHR residues W437 and M441. The right panel shows MD models after 200 ns, where the D-Leu7 side chain has shifted to promote more favorable interactions with nonpolar residues in TM1 and TM7. (b) Snapshots of PTH^{WT} and PTH^{7d} peptide helices at the start (0 ns) and end (200 ns) of MD simulations. PTH Leu7 side chain is shown as sticks. At 200 ns, note the break in the PTH^{7d} helix and the resulting outward push of the

peptide N-terminus. (c) Polar contacts between PTH Glu4 and receptor residues. Residues interacting with PTH^{WT} Glu4 are green sticks, and interactions are cyan dashes. Residues interacting with PTH^{7d} Glu4 are light pink sticks, and interactions are black dashes. (d) Number of hydrogen bonds between Glu4 (PTH^{WT}, top; PTH^{7d}, bottom) and receptor residues over triplicate simulations. Raw data are connected by thin lines. Second-order smoothened data (over 20 neighbors) are shown as thick lines.

then structurally aligned the transmembrane domain (TMD) of rhodopsin from the rhodopsin-visual-arrestin-1 crystal structure to the TMD of PTH^{WT}–PTHR after 200 ns simulation, followed by alignment of our βarr-1 model to visual-arrestin-1 (**Fig. 14A**). In this model, residue Leu73 of βarr-1 engages in nonpolar interactions with TM6 residue Val412 of PTH^{WT}-bound receptor (**Fig. 14A**); however, the extended TM6 kink induced by PTH^{7d} precludes these contacts by shifting Val412 of the receptor away from Leu73 of βarr-1 (**Fig. 14A, 14B**). To confirm the ability of PTH^{WT} to differentially promote interaction between Leu73 of βarr and the receptor, we performed photo-crosslinking experiments in cells transiently expressing PTHR and a photoreactive HA-tagged βarr-1 analog in which residue Leu73 was substituted with *p*-benzoylphenylalanine (Bpa) (**Fig. 14C**). This assay permits selective detection of Bpa73-dependent PTHR−βarr1 complexes via co-immunoprecipitation and Western blot, as UV-induced covalent linkage of Bpa with the receptor is required to maintain the complex in the presence of sodium dodecyl sulfate (SDS). In agreement with results from MD simulations and structural modeling, the Leu73Bpa βarr-1 mutant formed a complex with PTHR in response to PTH^{WT}, but this effect was completely absent in cells treated with PTH^{7d} compared to vehicle control (**Fig. 14C**). Collectively, these data identify novel phosphorylation-independent, nonpolar contacts that are determinant for PTHR−βarr interactions and provide the structural basis by which amino acid epimerization at position 7 of PTH leads to impaired βarr recruitment to the receptor.

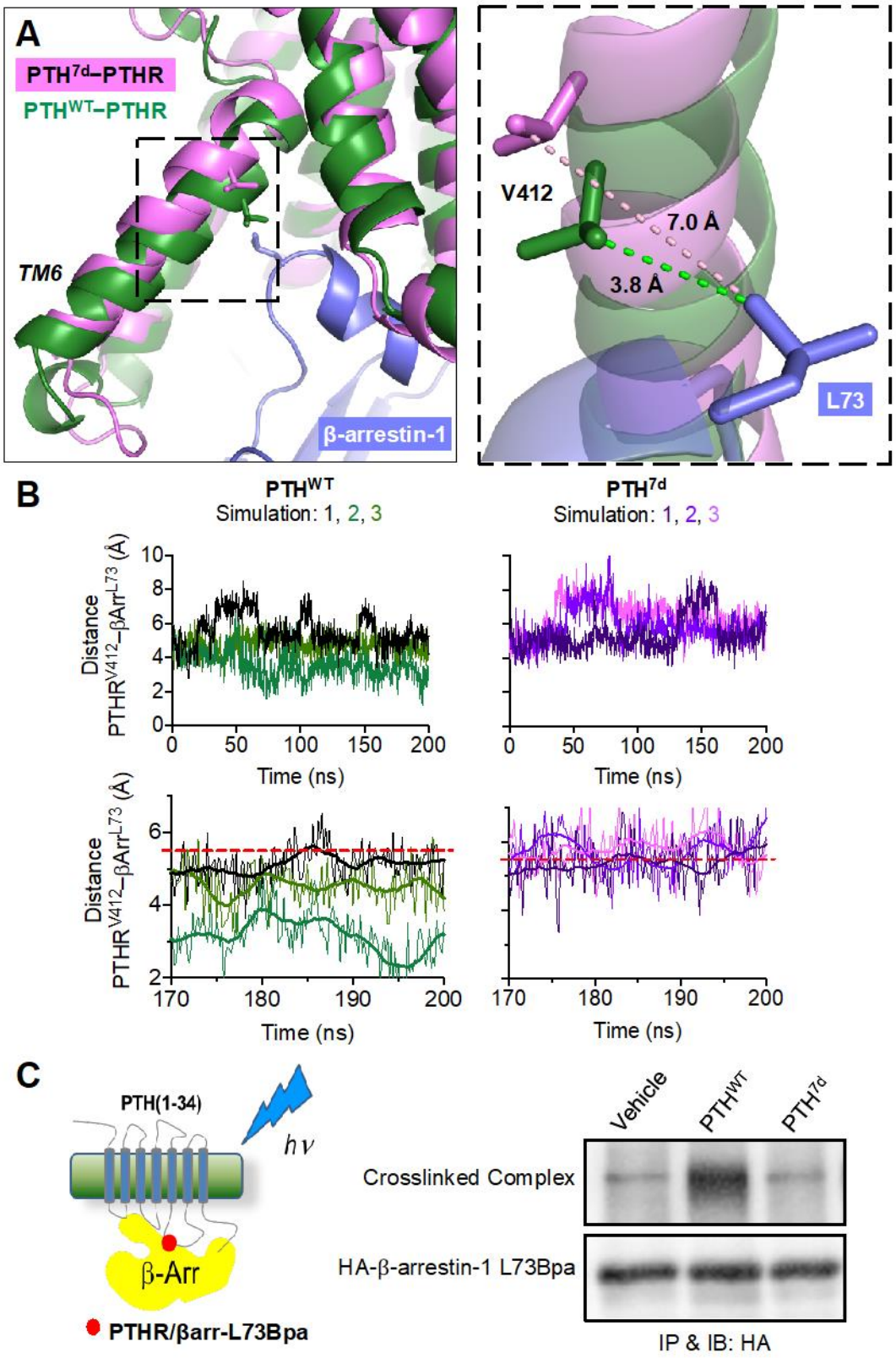

Figure 14. Structural basis for impaired βarr coupling by PTH^{7d}.

(a) Snapshots of PTH^{WT}–PTHR (dark green) and PTH^{7d}–PTHR (violet) MD simulations after 200 ns were aligned by receptor transmembrane helices. A model of βarr-1 (slate blue) was positioned based on the structural alignment of rhodopsin (from rhodopsin-visual-arrestin-1) to PTH^{WT}-bound PTHR. The dashed box highlights potential interactions of PTHR TM6 residues Val412 with βarr-1 Leu73. (b) Distance distributions between PTHR Val412 CG1 and βarr Leu73 CD1 side chain atoms over triplicate MD simulations of PTH^{WT}- and PTH^{7d}-bound receptor. Raw data are shown as thin lines. Second order smoothened data (over 20 neighbors) are shown as thick lines (top, distance data over 200 ns simulations; bottom, distance data over the last 30 ns of each simulation). Distances greater than 5.5 Å (red dashed line) prevent nonpolar interactions. (c) Photo-crosslinking between βarr-1 Leu73Bpa and PTHR (left, schematic procedure; right, co-immunoprecipitation of HA-tagged βarr-1 Leu73Bpa and photo-crosslinked PTHR−βarr-1 complexes. Samples were immunoprecipitated and immunoblotted using an anti-HA antibody.

The PTHR is the main regulator of bone remodeling and serum mineral-ion (inorganic phosphate and Ca^{2+}) homeostasis [54]. Despite previous reports demonstrating ligand-dependent modulation of these physiological processes, whether the location or the duration of the cAMP response is determinant remains unclear. We thus compared the effects of PTH^{7d}, PTH^{WT}, and LA-PTH on these parameters in mice following four weeks of daily injection (40 μg/kg body weight). Examination of skeletal parameters via micro-computed tomography (**Fig 15A**) further highlighted the physiological significance of spatial organization in PTHR-mediated signaling. While all three ligands caused expansion of metaphysis at their distal femurs (**Fig. 15B**, TV), only PTH^{WT} and LA-PTH led to a significant increase in trabecular (Tb) bone fractions (Tb.BV/TV) and thickness (Tb.Th) when compared to vehicle control (**Fig**. **15B**). Additionally, LA-PTH treatment resulted in an increase in trabecular number (Tb.N) that was markedly distinct from that observed for PTH and PTH^{7d} (**Fig. 15B**). Analysis of effects on mineral-ion homeostasis revealed that each ligand caused similar reductions in serum Pi levels (**Fig. 15C**, top panel) consistent with

the previously reported regulation of phosphate uptake by PKA-dependent phosphorylation NHERF1 in the cytoplasm [152], while acute elevations in serum Ca^{2+} levels occurred only in response to PTH^{WT} and LA-PTH, but not PTH^{7d}, when compared to vehicle control (**Fig. 15C**, bottom panel). In addition to direct effects on bone remodeling and Ca^{2+} homeostasis, previous studies have established that PTHR ligands can indirectly influence these processes via upregulation of the 25-hydroxyvitamin D 1-α hydroxylase [referred to as 1-α(OH)ase], the rate-limiting enzyme that catalyzes the conversion of 25-hydroxyvitamin D to the active form of vitamin D (1,25D) in renal cells [153]. Our previous report that endosomal cAMP production enhances and prolongs phosphorylation and activation of the downstream transcription factor cAMP response element binding protein (CREB), coupled with observations that PTHR-mediated upregulation of 1-α(OH)ase occurs in a cAMP/PKA/CREB-dependent manner, led us to hypothesize that the impaired actions of PTH^{7d} compared to PTH^{WT} and LA-PTH arise from deficient nuclear cAMP/PKA signaling and thus reduced alterations in 1-α(OH)ase expression and circulating 1,25D. Indeed, consistent with previous studies showing that cAMP, rather than PKA, diffusion into the nucleus represents the rate-limiting step for nuclear PKA activation [58, 154], we found that cAMP accumulates and activates PKA in the nucleus more efficiently over time when it originates from endosomes compared to the cell surface (**Fig. 15D, 15E**). Additionally, we determined that basolateral stimulation with LA-PTH, but not PTH^{7d}, caused a significant increased in expression of 1-α(OH)ase in polarized MDCK cells (**Fig. 15F, 15G**). Remarkably consistent with this result was the sustained increase in circulating 1,25D upon injection of LA-PTH into mice that was completely absent in mice treated with PTH^{7d} (**Fig. 15H**). Importantly, pharmacokinetic analysis of serum from mice treated with LA-PTH or PTH^{7d} confirmed that biological effects were not influenced by differential degradation of these peptides (**Fig. 16**).

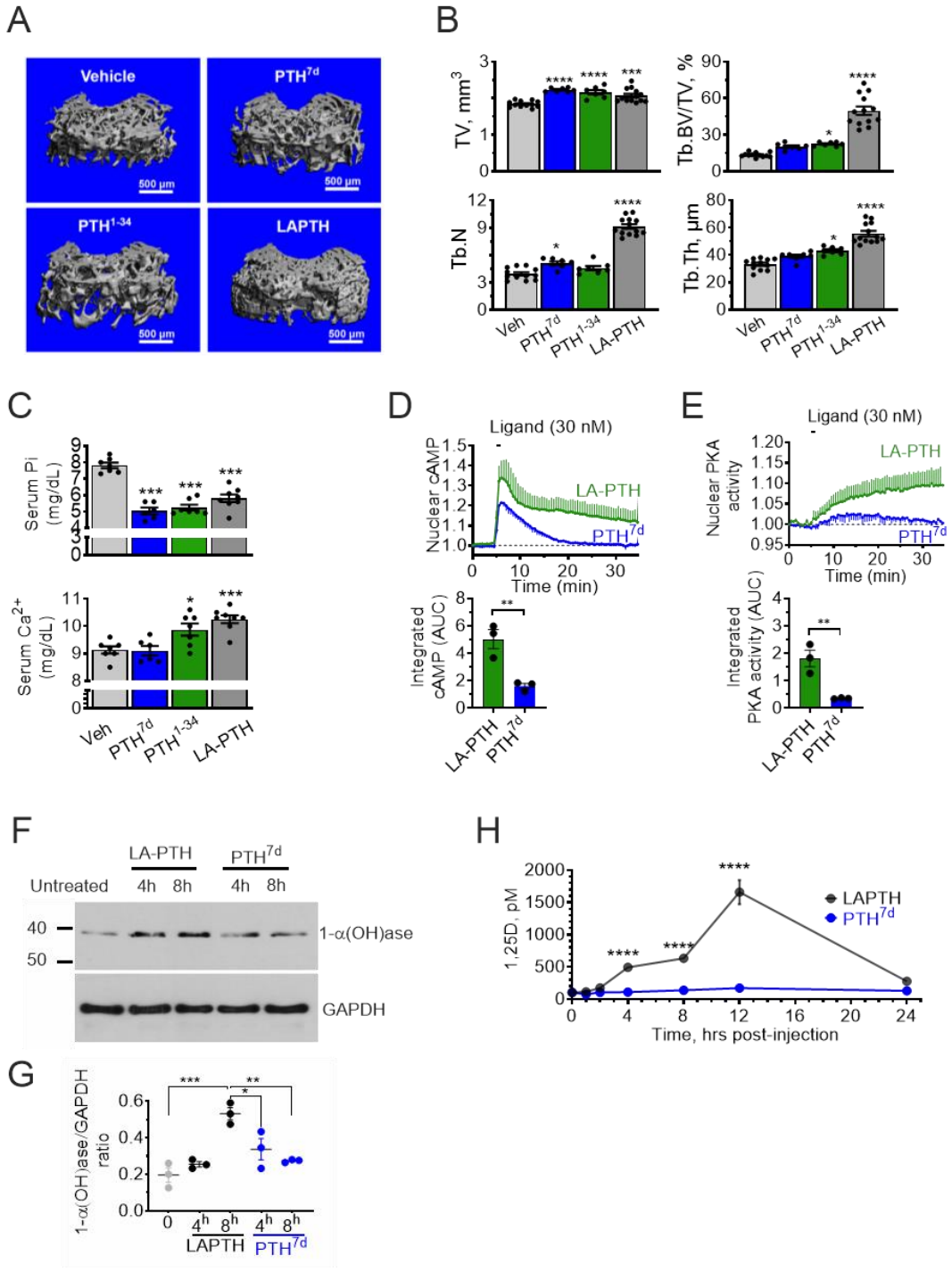

Figure 15. Differential physiological actions of PTH^{7d}, PTH^{WT}, and LA-PTH in mice.

(a,b) 3-D reconstructed µCT images (a) and quantifications of skeletal parameters in trabecular (Tb) bone of distal femur (b), including: TV, Tb total volume; Tb.BV/TV, Tb bone

fraction over total bone volume; Tb.N, Tb number; and Tb.Th, Tb thickness. Parameters were assessed in mice subjected to 4-week daily injections of PTH^{7d}, PTH^{WT}, LA-TPh, or vehicle (Veh) as described in panels (a) and (b). N = 7 mice/group for PTH^{7d} and PTH^{WT} injections and N = 14 mice/group for LA-PTH and Veh injections. Data are the mean ± s.e.m. (*P < 0.05; ***P < 0.01; and ****P < 0.0001 vs Veh control mice by one-way ANOVA with Dunnett test). (c) Serum phosphate (top panel) and Ca^{2+} (bottom panel) levels were measured 2 hours after the last of the 4-week daily injections of PTH^{7d}, PTH^{WT}, and LA-PTH (40 µg/kg body weight/injection) or vehicle (Veh). N = 7 mice/group; mean ± s.e.m. (*P < 0.05; **P < 0.01; and ****P < 0.0001 vs Veh control mice by one-way ANOVA with Dunnett test). (d,e) Averaged time courses and integrated responses of nuclear cAMP (h) and PKA activation (i) in response to 30 nM LA-PTH or PTH^{7d}. Data are the mean ± s.e.m. of N = 3 independent experiments with n = 10-28 cells per experiment (**P = 0.009 and 0.008 for panels for panels d and e, respectively). (f,g) Representative Western blot showing 1-α(OH)ase levels (top) in polarized PTHR-expressing MDCK cells after basolateral stimulation with either LA-PTH or PTH^{7d} for 4 or 8 hours. GAPDH was used as loading control. Quantification of three independent Western blot experiments is shown in the bottom panel. 1-α(OH)ase levels were normalized to GAPDH levels (bottom). Graph shows individual data points and mean ± s.e.m. (*P = 0.0195; **P = 0.003; and ***P = 0.0004 by one-way ANOVA with Tukey test. (h) In a separate time-course study, serum 1,25D levels were measured in mice before or 1, 2, 4, 8, 12, or 24 hours after a single injection of PTH^{7d} or LA-PTH. N = 7 mice/time point/drug and 14 mice for time "0" controls. Mean ± s.e.m. (****P < 0.0001 vs time "0" controls by two-way ANOVA with Dunnett test).

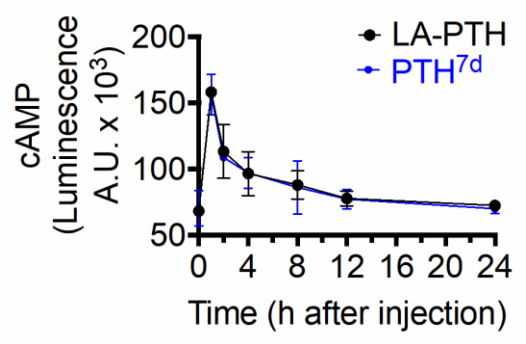

Figure 16. Pharmacokinetic Analysis of PTH^{7d} and LA-PTH.

Blood plasma was assessed for LA-PTH or PTH^{7d} bioactive peptide content by applying 5 µL of plasma to GP2.3 cells and measuring cAMP-dependent changes in luminescence. Data are the mean ± s.e.m. of N=3 experiments and n=5 mice per time point for each ligand.

4.4 Discussion

Previous studies have proposed a paradigm whereby the duration of the cAMP response serves as the sole determinant for PTHR-mediated regulation of serum Ca^{2+} and bone remodeling, and this model has served as the premise for the development of therapeutics targeting the receptor [155]. Our findings reveal that a shift in spatial bias of cAMP signaling from endosomes to the cell surface is sufficient to abolish PTH-induced effects on serum Ca^{2+} elevation, vitamin D activation, and bone formation, without alteration of serum Pi reduction.

The present work identifies that amino acid epimerization at a single position in a GPCR peptide ligand may provide a means to exquisitely probe ligand-dependent signaling determinants and physiological consequences, without significantly altering ligand binding affinity or stability *in vivo*. In the case of PTH^{7d}, L→D isomerization at position 7 of PTH revealed significant

modulation of PTHR−βarr interactions and thus a shift in the cellular localization of sustained cAMP signaling from endosomes to the plasma membrane. The formation of ternary PTHR-βarr-Gβγ complexes and their translocation to early endosomes permits a prolonged phase of cAMP signaling from this intracellular compartment, and it is this response that is considered the primary determinant for driving distinct biological outcomes; however, sustained G protein-independent signaling by βarrs (e.g. ERK phosphorylation) in early endosomes has been reported. Thus, it remains possible that the differences observed in this study between PTH^{7d} and PTH^{WT}/LA-PTH may involve βarr signaling that occurs independently of G proteins, an intriguing hypothesis to probe in future investigations.

Our study also raises the prospect of selectively modulating mineral-ion levels when there are pathophysiological aberrations. For example, chronic kidney disease and poorly controlled diabetes have been shown to cause hyperphosphatemia [156]. PTH^{7d} may prove useful therapeutically in this setting, as it possesses the ability to selectively reduce systemic phosphate levels without concomitant effects on serum Ca^{2+} and bone remodeling observed for traditional PTHR ligands. In addition to the PTHR, several other GPCRs have been reported to engage in cAMP signaling from intracellular compartments, including the vasopressin type 2 receptor (V_2R) [157], glucagon-like peptide 1 receptor (GLP-1R) [158], the β_1-adrenergic receptor (β_1AR) [159], among others, each of which hold potential biological and clinical significance: the V_2R is a major regulator of water homeostasis via actions in the kidneys, and has been implicated in nephrogenic diabetes insipidus and heart failure; the GLP-1R is well-known to modulate insulin secretion from the pancreas and currently serves as a therapeutic target for the treatment of type 2 diabetes; and the β_1AR contributes to a wide variety of physiological processes, including cardiac function and blood pressure, and currently represents a main therapeutic target for the treatment of hypertension

and heart failure. This study thus presents interesting implications for other GPCRs that may aid understanding of human physiology and facilitate rational drug design in the future.

5.0 $G_{q/11}$-dependent Regulation of Endosomal cAMP Generation by Parathyroid Hormone Class B GPCR

Chapter adapted from: Alex D. White, Frédéric G. Jean-Alphonse, Fei Fang, Karina A. Peña, Shi Liu, Asuka Inoue, Despoina Aslanoglou, Samuel H. Gellman, Evi Kostenis, Kunhong Xiao, and Jean-Pierre Vilardaga. $G_{q/11}$-dependent regulation of endosomal cAMP generation by parathyroid hormone class B GPCR. *PNAS* (in press 2020).

A.D.W., F.J-A, F.F., K.A.P., D.A., Z.F., and K.X. performed and/or designed experiments. E.K. and G.M.K. provided FR900359. A.I. provided CRISPR cells. S.L. and S.H.G. contributed reagents that led to the studies here. Authors analyzed and discussed the data. J.P.V. was responsible for the overall conceptual composition and supervision of the study and wrote the manuscript with A.D.W.

5.1 Introduction

The PTHR is a class B GPCR that mediates the biological effects of endogenous peptide ligands PTH and PTHrP [160]. While the receptor functions to regulate growth and development of various tissues in response to PTHrP, PTH-induced activation of the PTHR serves as a critical role in homeostatic control of systemic Ca^{2+} and phosphate levels, as well as bone remodeling [161]. Although both ligands exert their physiological effects via binding to the same receptor and subsequent activation of G_s/cAMP and G_q/Ca^{2+} signaling pathways [91], PTH and PTHrP are distinguished by cAMP responses that differ markedly in duration and cellular localization [31, 55]. Association of PTHrP with the receptor permits only transient cAMP production from the cell membrane that is consistent with the classical model of GPCR signaling [55]. The receptor is also capable of promoting sustained cAMP generation following internalization of highly stable PTH-PTHR complexes that remain active in early endosomes. Furthermore, accumulating

evidence suggests that these differential modes of signaling may give rise to distinct biological outcomes. For example, a recently identified point mutation in PTH (Arg25→ Cys) that abolishes endosomal signaling causes severe hypocalcemia in patients harboring this mutation [51, 52]. In agreement with this finding, injection of a long-acting PTH (LA-PTH) analog into mice causes prolonged hypercalcemic responses that correlate with the propensity to promote sustained cAMP from endosomes [36]. Despite significant advancements in identifying the physiological relevance of PTHR endosomal signaling, its underlying molecular mechanisms and regulation remain incompletely understood.

We recently reported on the development of G_s-biased PTH analogs that stimulate cAMP production but fail to engage in endosomal cAMP signaling due to impaired recruitment of βarrs [162]. Observation that these same ligands also show deficient G_q signaling as measured by reduced intracellular Ca^{2+} mobilization in HEK293 cells stably expressing PTHR (HEK-PTHR) led us to question whether G_q signaling serves as a regulator of PTHR-mediated endosomal cAMP responses.

5.2 Materials and Methods

5.2.1 Cell Culture and Transfection

Cell culture reagents were obtained from Corning (CellGro). Human embryonic kidney cells (HEK293; ATCC, Georgetown, DC) stably expressing the recombinant human PTHR were grown in selection medium (DMEM, 5% FBS, 1% penicillin/streptomycin, 500 µg/mL neomycin) at 37 °C in a humidified atmosphere containing 5% CO_2. Primary mouse calvarial osteoblast (Ob)

cells were isolated and cultured as described [58]; RPTEC were grown in DMEM/F12 supplemented with 5 pM triiodo-L-thyronine, 10 ng/mL recombinant human epidermal growth factor, 25 ng/mL prostaglandin E_1, 3.5 µg/mL ascorbic acid, 1 mg/mL insulin, 0.55 mg/mL transferrin, 0.5 µg/mL sodium selenite, 25 ng/mL hydrocortisone, 1% penicillin/streptomycin). For transient expression, cells were seeded on glass coverslips coated with poly-D-lysine in six-well plates and cultured for 24 hours prior transfection with the appropriate cDNAs using Fugene-6 (Promega) or Lipofectamine 3000 (Life Technologies) for 48-72 hours before experiments. We optimized expression conditions to ensure the expression of fluorescently labeled proteins was similar in examined cells by performing experiments in cells displaying comparable fluorescence levels.

5.2.2 Peptides and Chemicals

PTH(1-34) and PTH(1-34)^{TMR} were synthesized and characterized as previously described [44]. Forskolin (#344270) was purchased from EMD-Millipore. FR900359 (known as UBO-QIC former commercial name) was extracted from *Ardisia crenata* following a previously published protocol [163].

5.2.3 Plasmids

DNA constructs encoding for PTHR^{YFP}, PTHR^{CFP}, and βarr-2^{YFP} were previously described by the Vilardaga lab [31, 41, 123]. βarr-1^{Rluc8} was provide by Dr. Zachary Freyberg (University of Pittsburgh); $G\alpha_q{}^{YFP}$, $G\beta_1{}^{BiFC}$ (Cer(1-158)-$G\beta_1$) and $G\gamma_2{}^{BiFC}$ (CFP-(159-238)-$G\gamma_2$)

were a gift from Dr. Catherine Berlot and can be found in Addgene (#55782, #55707, and #55707, respectively); masGRK3ct was a kind gift from Dr. Nevin Lambert (Augusta University).

5.2.4 Co-immunoprecipitation

HEK293 cells stably expressing HA-PTHR and cultured on a 10-cm dish were pre-incubated with serum-free DMEM ± 100 nM TGX-221, then stimulated with 100 nM PTH for 5 minutes. Cells were then washed with ice-cold PBS prior to cross-linking for 2 hours with 1 mM DSP (Covachem, #13301) in PBS at 4 °C. The reaction was stopped by addition of 10 mM Tris-HCl for 10 minutes and cell lysates were prepared using lysis buffer (1 % Triton X-100, 50 mM Tris-HCl pH 7.4, 140 mM NaCl, 0.5 mM EDTA) containing protease and phosphatase inhibitor (Roche, #11873580001). Protein concentration was determined using BCA protein assay kit (ThermoFisher, #23225), and lysates were incubated with anti-HA agarose antibody beads (Sigma-Aldrich; #A2095 clone HA-7) overnight at 4 °C. Elution was done using LDS loading buffer (Life Technologies) and samples were loaded on 10% SDS gels, followed by transfer to nitrocellulose membranes. We used antibodies against HA (Covance, clone 16B12), and βarr-1/2 (Cell Signaling; #4674 clone D24H9). Immunoreactive bands were visualized with Luminata Forte (EMD Millipore) and autoradiography film.

5.2.5 Time-course Measurements of cAMP Production and βarr Recruitment in Live Cells

cAMP was assessed using FRET-based assays. Cells were transiently transfected with the FRET-based biosensor $Epac1^{CFP/YFP}$ [61] for measuring cAMP. Measurements were performed and analyzed as previously described [62]. In brief, cells plated on poly-D-lysine coated glass

coverslips were mounted in Atoofluor cell chambers (Life Technologies), maintained in a HEPES buffer containing 150 mM NaCl, 20 mM HEPES, 2.5 mM KCl, 0.1-10 mM $CaCl_2$, 0.1% BSA, and pH 7.4 and transferred on the Nikon Ti-E equipped with an oil immersion 40X numerical aperture 1.30 Plan Apo objective and a moving stage (Nikon Corporation). CFP and YFP were excited using a mercury lamp. Fluorescence emissions were filtered using a 480 ± 20 nm (CFP) and 535 ± 15 nm (YFP) filter set and collected simultaneously with a LUCAS electron-multiplying charge-coupled device camera (Andor Technology) using a DualView 2 (Photometrics) with a beam splitter dichroic long pass of 505 nm. Fluorescence data were extracted from a single cell using Nikon Element Software (Nikon Corporation). The FRET ratio for single cells was calculated and corrected as previously described [63]. Individual cells were perfused with buffer or with ligand for the time indicated by the horizontal bar.

5.2.6 Saturation and Competition Binding at Equilibrium

HEK293 cells were transiently transfected with HA-PTHR and seeded in 96-well plates. Approximately 48 h after transfection, cells were incubated in HEPES buffer (137 mM NaCl/5 mM KCl/1 mM $MgCl_2$/20 mM HEPES/0.1% BSA pH 7.4) for 1 h at 4 °C, followed by 2 h incubation at 4 °C in the presence of ligand. Increasing concentration of TMR-labeled PTH (PTH^{TMR}) were utilized for saturation binding, while competition binding experiments used a constant PTH^{TMR} concentration (31.6 nM) with increasing amounts of unlabeled PTH. Cells were washed twice with the same buffer, and fluorescence intensities were recorded at 580 ± 20 nm using an excitation wavelength of 525 ±20 nm on a Tecan Spark 20M multimode microplate reader. Nonspecific binding was determined using 1 μM of unlabeled ligand. Data were subsequently analyzed using Graphpad Prism 7.0 (GraphPad Software Inc., La Jolla, CA).

5.2.7 Laser Scanning Confocal Microscopy

Cells plated on coverslips were mounted in Attofluor cell chambers (Life Technologies) and incubated with HEPES buffer (150 mM NaCl, 20 mM HEPES, 2.5 mM KCl, varied [Ca^{2+}], 0.1% BSA, pH 7.4) and transferred on the Nikon Ti-E microscope (Nikon) equipped with a Z-driven piezo motor. Imaging was performed using Nikon A1 confocal unit, through a 60X N.A. = 1.45 objective (Nikon). Fluorescent antibody (anti-HA-Alex488, Cell Signaling, #2350), proteins or peptides containing CFP, Turqoise, GFP, FITC, YFP, tetramethylrhodamine (TMR) were excited with 440 nm (CFP, Turquoise), 488 nm (Alexa488, GFP, FITC), 514 nm (YFP) or 561 nm (TMR) lasers (Melles Griot). Data acquisitions were done using Nikon Element Software (Nikon Corporation). After acquisition, raw data were analyzed using ImageJ software. Each different analysis was done at the single-cell level.

5.2.8 BRET Recordings of PTHR-βarr Interaction.

HEK293 cells were transiently transfected with βarr-1^{Rluc8} and $PTHR^{YFP}$ and seeded in 96-well plates. Approximately 48 hours after transfection, cells were incubated in HEPES buffer (137 mM NaCl/5 mM KCl/1 mM $MgCl_2$/20 mM HEPES/0.1% BSA pH 7.4) at 37 °C in the presence of 5 µM coelenterazine-*h* for 10 minutes, followed by addition of increasing concentrations of PTH. Donor and acceptor luminescence (466 and 535 nm, respectively) were measured at 2.5-minute intervals using a Tecan Spark 20M multiplate reader. For each well, the maximum luminescence observed, which typically occurred 10 minutes after PTH stimulation, was utilized to calculate BRET ratios (acceptor/donor). Data were subsequently analyzed using Graphpad

Prism 7.0 (GraphPad Software Inc., La Jolla, CA) and expressed as ΔBRET, which was determined by subtracting ratios obtained in control wells containing cells with donor alone.

5.2.9 Statistical Analysis

Data were processed using Excel 2013 (Microsoft Corp. Redmon, WA) and Prism 7.0 (GraphPad Software Inc. La Jolla, CA). Data are expressed as mean ± SEM. Curves were fitted to the data using a four-parameter, non-linear regression function. Statistical analyses were performed using unpaired, 2-tailed Student's *t* tests for comparisons between 2 groups.

5.3 Results

In support of this hypothesis, the selective $G_{q/11}$ inhibitor FR900359 markedly decreased the duration of PTH-induced cAMP responses in HEK-PTHR cells (**Fig. 17A**), and this effect was recapitulated in bone and kidney cells endogenously expressing the receptor (**Fig. 17B-D**). Similar effects were observed on cAMP generation using another $G_{q/11}$ inhibitor, GP2A (**Fig. 17E**), as well as in HEK293 cells lacking $G\alpha_{q/11}$ (HEK-$G_{q/11}^{KO}$) (**Fig. 17F**). Inhibition of the $G_{q/11}$ downstream effector PLC by U73122 had no effect on PTH-induced cAMP (**Fig. 17G**), thus these results collectively demonstrate that $G_{q/11}$ activation, as opposed to PLC-dependent signaling, is determinant for endosomal PTHR cAMP generation.

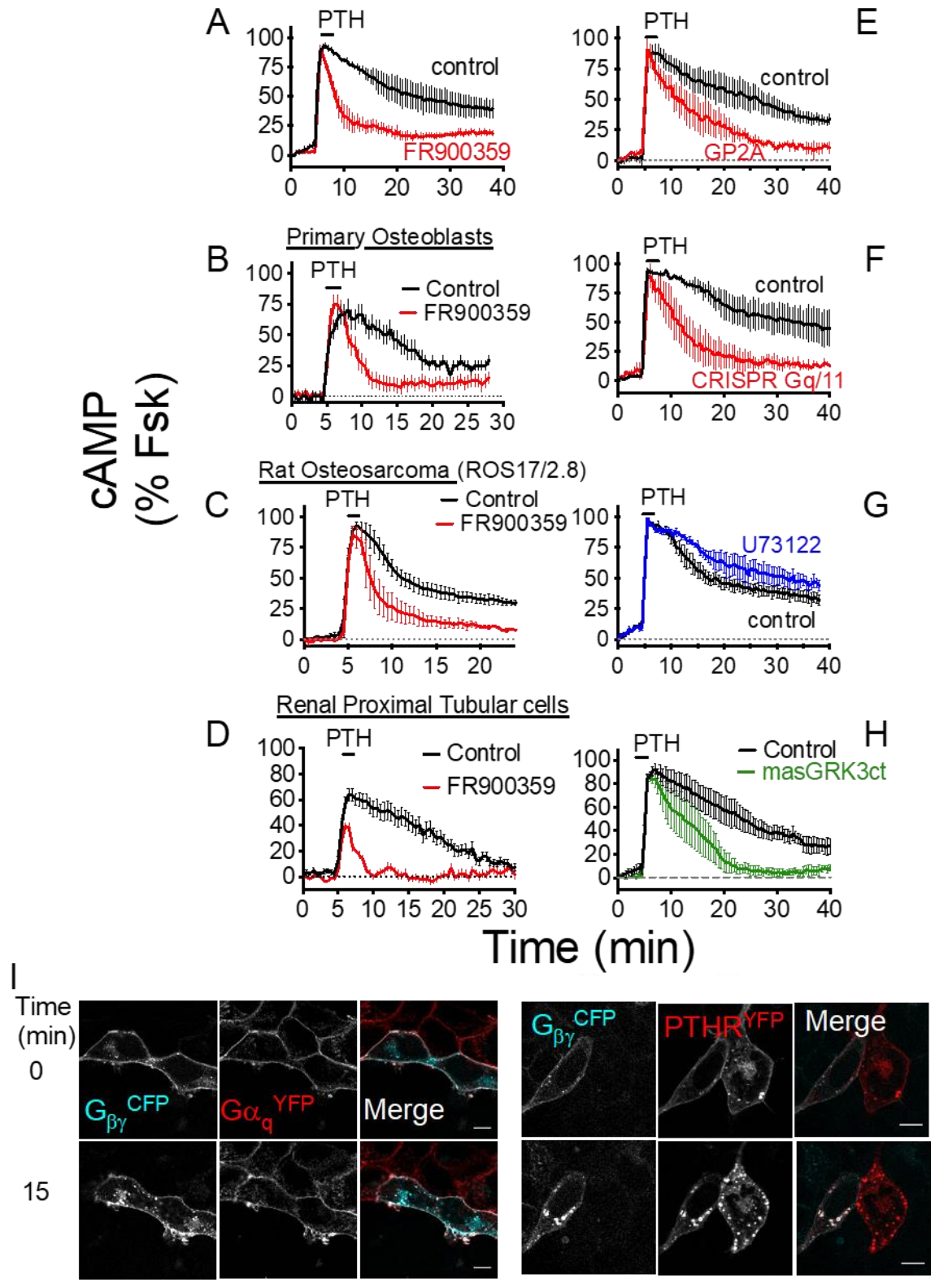
A
PTH
control
FR900359
E
GP2A
B
Primary Osteoblasts
Control
F
CRISPR Gq/11
C
Rat Osteosarcoma (ROS17/2.8)
G
U73122
D
Renal Proximal Tubular cells
H
masGRK3ct
cAMP (% Fsk)
Time (min)
I
Time (min)
0
15
Merge
PTHR

Figure 17. $G_{q/11}$-dependent cAMP Production by PTH.

(A) Time courses of cAMP production recorded by FRET in response to 10 nM PTH in single HEK-PTHR cells +/- FR900359. (B-D) Similar assay as in panel A in response to 100 nM PTH in primary osteoblasts isolated from mice (B), rat osteosarcoma (ROS) 17/2.8 cells (C), and renal proximal tubular epithelial cells (RPTEC) (D). (E-H) Similar as in panel A +/- GP2A €, in parental and HEK-$G_{q/11}^{KO}$ cells (F), and as in panela A with the PLC inhibitor U73122 (G), or in the absence (control) or presence of masGRK3ct (H). cAMP data represent mean values ± SEM of N=3-4 independent experiments and n=15-45 cells per experiment. (I) Fluorescence micrographs corresponding to the individual and merged channel data of HEK cells co-transfected with $G\beta\gamma^{CFP}$ (cyan) and either $G\alpha_q^{YFP}$ or $PTHR^{YFP}$ (red). Images were recorded at 30 second intervals for 15 minutes after a brief challenge with 100 nM PTH. Scale bar = 10 μm.

To delineate the roles of Gα and Gβγ subunits in $G_{q/11}$-mediated regulation of cAMP, we utilized live-cell confocal microscopy to monitor the localization of fluorescently-labeled G protein subunits. Under basal conditions, both $G\alpha_q^{YFP}$ and $G\beta\gamma^{CFP}$ were observed primarily at the plasma membrane along with a small fraction located in subcellular compartments (**Fig. 17I**); however, brief stimulation with PTH induced translocation of Gβγ intracellularly that colocalized with the receptor, while $G\alpha_q$ remained at the cell surface (**Fig. 17I**). Subsequent cAMP time-course experiments revealed that translocation of Gβγ originating from the cell surface is critical for endosomal signaling, as expression of masGRK3ct, a Gβγ scavenger that localizes exclusively to the plasma membrane [164], completely abolished sustained signaling induced by PTH (**Fig. 17H**). We reasoned that $G_{q/11}$ activation, via provision of Gβγ subunits, may promote assembly of signaling complexes at the cell surface comprised of receptor, βarr, and Gβγ that have previously been reported as key components of PTHR-mediated endosomal cAMP production [36]. Indeed, time-course experiments measuring FRET between $\beta arr\text{-}2^{YFP}$ and either $G\beta\gamma^{CFP}$ or $PTHR^{CFP}$ in response to PTH showed significantly impaired interactions in HEK-$G_{q/11}^{KO}$ cells compared with

the parental cell line (**Fig. 18A, 18B**). The unexpected effect of $G_{q/11}$ activation on βarr recruitment was confirmed in subsequent BRET-based assays using $PTHR^{YFP}$ and βarr-1^{Rluc8}, which showed reduced potency (EC_{50}) of PTH-induced recruitment of βarr in HEK-$G_{q/11}{}^{KO}$ (19.2 ± 0.44 nM) compared to parental cells (6.95 ± 0.44 nM) (**Fig. 18C**). Consistent with data obtained for cAMP responses, additional FRET recordings showed that the reduced interaction between PTHR and βarr is not due to lack of PLC activity (**Fig. 18D**), but rather the availability of liberated Gβγ subunits at the cell surface derived from heterotrimeric $G_{q/11}$ proteins (**Fig. 18E**).

The well-established ability of Gβγ to activate class I PI3K isoforms PI3Kβ/γ [165] coupled to the previously reported enhanced binding affinity of βarrs for phosphatidylinositol-(3,4,5)-triphosphate (PtdIns(3,4,5)P_3) compared to PtdIns(4,5)P_2 led us to hypothesize that βarr coupling to the PTHR may be regulated by activation of $G_{q/11}$ heterotrimeric proteins through liberation of Gβγ subunits and subsequent activation of class I PI3K. We tested this possibility using the PI3K inhibitor wortmannin in time-course experiments measuring βarr interaction by FRET between $PTHR^{CFP}$ and βarr-2^{YFP} in response to PTH. Indeed, we observed significantly slower kinetics and decreased magnitude of βarr-2 association with the receptor in wild-type HEK293 cells pre-incubated with wortmannin compared to control cells (**Fig. 19A, 19B**); however, this effect was completely abolished in analogous experiments performed in HEK-$G_{q/11}{}^{KO}$ cells (**Fig. 19A**). Due to the relative non-selectivity of wortmannin, we repeated these experiments using the PI3Kβ-specific inhibitor TGX-221 [166], which similarly reduced βarr recruitment to the PTHR in wild-type but not $G_{q/11}{}^{KO}$ cells (**Fig. 19C**). Furthermore, the effect of TGX-221 on PTHR− βarr interactions in wild-type cells was confirmed by co-immunoprecipitation assays (**Fig. 19D**). Consistent with a role in endosomal signaling, wortmannin and TGX-221 also markedly reduced the duration of PTH-induced cAMP responses in wild-type cells (**Fig. 19E, 19F**). Altogether,

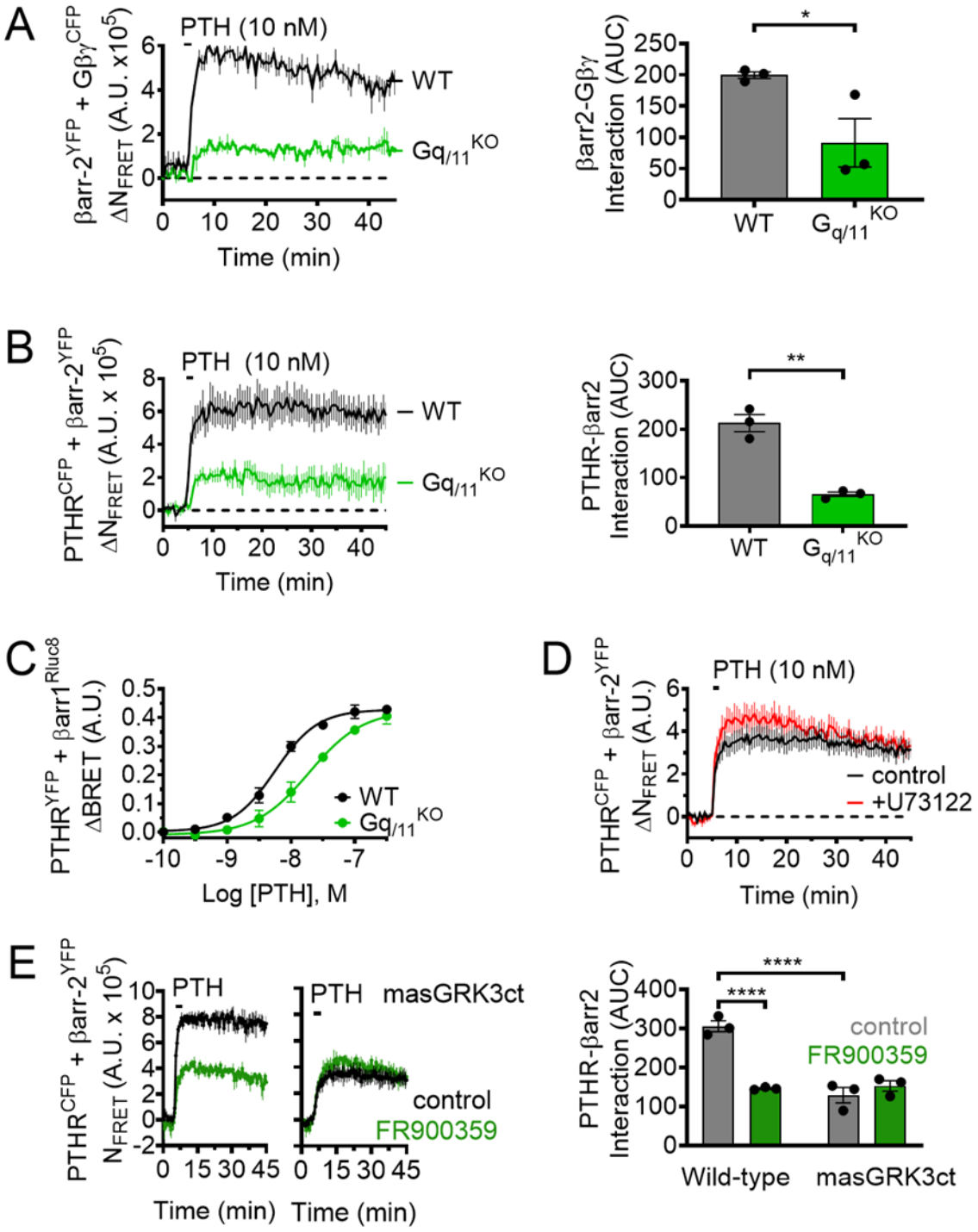

Figure 18. Effect of Gq/11 Activation on the Formation of PTHR Endosomal Signaling Complexes.

(A,B) Time-course experiments measuring FRET between βarr-2^{YFP} and either Gβγ^{CFP} (A) or PTHR^{CFP} (B) in response to 10 nM PTH in wild-type (WT) HEK293 cells or cells lacking $G\alpha_{q/11}$ ($G_{q/11}{}^{KO}$). Data represent the mean value ± SEM of N = 3 experiments and n = 17-31 cells per experiment (*P < 0.05; **P < 0.01). (C) Recruitment of βarr to the

PTHR as a function of PTH concentration measured by BRET in cells co-transfected with βarr-1^{Rluc8} and PTHR^{YFP}. Data represent the mean ± SEM of N=3 experiments. (D) Similar experiments as in panels A and B with the PLC inhibitor U73122. Data represent the mean value ± SEM of N=3 experiments and n=23-30 cells per experiment. (E) Effect of masGRK3ct on βarr recruitment to the receptor upon exposure to 10 nM PTH +/- FR900359 in cells transfected with PTHR^{CFP} and βarr-2^{YFP}. Data represent the mean value ± SEM of N=3 experiments and n=16-18 cells per experiment (****$P < 0.0001$).

these results provide evidence that $G_{q/11}$-dependent PI3K activation via Gβγ represents a major mechanism for both the kinetics and magnitude of βarr interaction with the PTHR, which, in turn, regulates endosomal cAMP signaling.

In addition to its lipid kinase function, PI3Kβ has been shown to phosphorylate effector proteins as well [167]. To differentiate lipid versus protein kinase actions of PI3Kβ in mediating βarr recruitment, we utilized chemically-induced dimerization between FK506 binding protein 12 (FKBP) and the FKBP12 rapamycin binding (FRB) domain of mTOR [168] to recruit PTEN to the plasma membrane. PTEN is a lipid phosphatase that dephosphorylates predominantly PtdIns(3,4,5)P_3, but also PtdIns(3,4)P_2 to some extent, at the 3' position [169]. By expressing mcherry-tagged PTEN-FKBP and FRB fused to the plasma membrane-targeting sequence Lyn_{11}, addition of rapamycin results in acute depletion of PtdIns(3,4,5)P_3 specifically at the plasma membrane (**Fig. 19G, left**). We confirmed the efficacy of this approach using confocal imaging with cells co-expressing PTEN-FKBP-mcherry, Lyn_{11}-FRB, and the venus-conjugated PH domain from Akt (PH-Akt-venus) that binds selectively to the 3'-phosphate of PtdIns(3,4,5)P_3 [169]. Under basal conditions, PH-Akt-venus localized almost exclusively at the plasma membrane, but rapidly translocated to the cytoplasm upon addition of rapamycin (**Fig. 19G, middle and right**).

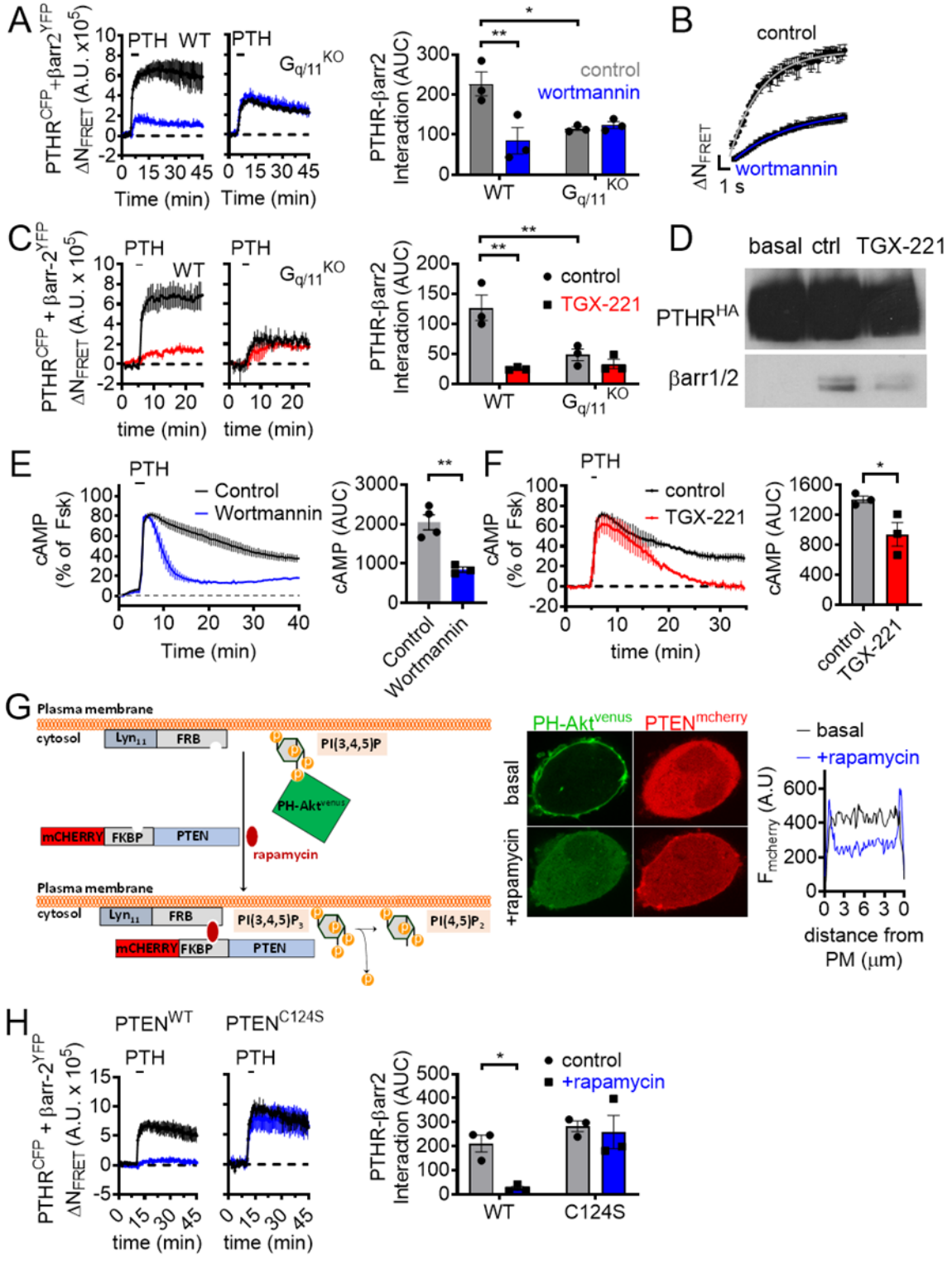

Figure 19. Recruitment of βarr is Regulated by $G_{q/11}$-dependent Activation of PI3Kβ.

We subsequently used this system in FRET-based time courses of βarr recruitment, which revealed a significant reduction in PTHR−βarr interactions in the presence of rapamycin in cells expressing wild-type PTEN ($PTEN^{WT}$) but not in those expressing a catalytically dead mutant of PTEN ($PTEN^{C124S}$) [170] (**Fig. 19H**). Taken together, these findings suggest that $G_{q/11}$-dependent generation of PtdIns(3,4,5)P_3 by PI3Kβ at the plasma membrane serves as a critical regulator of βarr recruitment to the PTHR and thus the propensity of the receptor to engage in endosomal cAMP signaling in response to PTH.

5.4 Discussion

Initially thought to induce signaling exclusively from the plasma membrane, several GPCRs are now recognized for eliciting responses from intracellular compartments, including the Golgi apparatus [159] and endosomes [55]. Notably, studies involving the class B PTHR have shown that binding of PTH causes sustained cAMP responses attributed to ligand-receptor complexes that remain active in early endosomes following βarr-mediated internalization. Accordingly, endosomal cAMP responses are thus considered to be regulated by G_s- and βarr-dependent signaling pathways. While the PTHR also activates $G_{q/11}$ in response to PTH, the role of this pathway in endosomal cAMP generation has been ignored because of its foremost association with the PLC/Ca^{2+} pathway. Mechanistically, our findings unveil that $G_{q/11}$ promotes PI3Kβ-mediated generation of PtdIns(3,4,5)P_3 (PIP_3) at the plasma membrane and that this represents a critical determinant for association of βarr with the PTHR. Further understanding of how PIP_3 can be used to promote the association between arrestin and PTHR will require, for example, structural studies to determine whether PIP_3 directly binds to the PTHR to stabilize a

functional active state that favors formation of the PTHR−arrestin complex. Another question to be explored is whether the PIP_3-dependent recruitment of arrestin is restricted to either the PTHR or receptors with $G_s/G_{q/11}$ signaling pleiotropy, such as class B GPCRs. This is particularly pertinent given that PIP_3 was previously reported to have no effect on βarr recruitment to the class A β_2-adrenergic receptor [171]. Thus, future investigations into other receptors that couple to $G_{q/11}$ and engage in sustained cAMP signaling from intracellular compartments may provide insight into the breadth of PIP_3-mediated regulation of GPCR−βarr interactions. Collectively, our findings identify a regulatory mechanism of PTH-induced cAMP wherein $G_{q/11}$-derived Gβγ subunits enhance the assembly of ternary PTHR-βarr-Gβγ complexes at the cell surface, which permits endosomal cAMP generation. While previous studies have implicated Gβγ-dependent modulation of adenylyl cyclase activity in the context of receptor functional crosstalk [58], our results provide a novel instance of a single GPCR that utilizes $G_{q/11}$-dependent formation of signaling complexes to control the spatial organization and duration of G_s-mediated cAMP production.

6.0 Final Conclusions

Since initial reports of the PTHR as a GPCR that deviates from the classical signaling paradigm, significant efforts have been made to elucidate the molecular mechanisms underlying the receptor's ligand-specific spatiotemporal regulation of cAMP signaling, as well as its biological and disease relevance. Herein we investigated the role of extracellular Ca^{2+} concentration in PTHR-mediated cAMP responses and identified this divalent cation as a positive allosteric modulator that increases the propensity of PTH to engage in endosomal signaling (**Fig. 21**). We determined that Ca^{2+} allostery is coordinated by ECL1 residues of the receptor and R25 of PTH, and further demonstrated that loss of sensitivity to Ca^{2+} for the hypocalcemia-associated R25C mutant results in ablation of endosomal cAMP generation (**Fig. 21**). We subsequently presented the development of G_s-biased PTHR ligands that enabled evaluation of the biological information encoded in the spatial versus temporal dimension of cAMP signaling (**Fig. 21**). We found that sustained cAMP specifically from endosomes is required for PTH-mediated regulation of serum Ca^{2+}, vitamin D activation, and particular aspects of bone remodeling processes (**Fig. 21**). We then probed the role of $G_{q/11}$ signaling in PTH-induced endosomal cAMP, and demonstrated that $G_{q/11}$-derived Gβγ subunits at the cell surface act in a PI3K-dependent manner to promote the assembly of signaling complexes compatible with sustained cAMP generation from endosomes (**Fig. 22**). These findings will provide key insights toward understanding PTHR signaling and biology, as well as rational drug design.

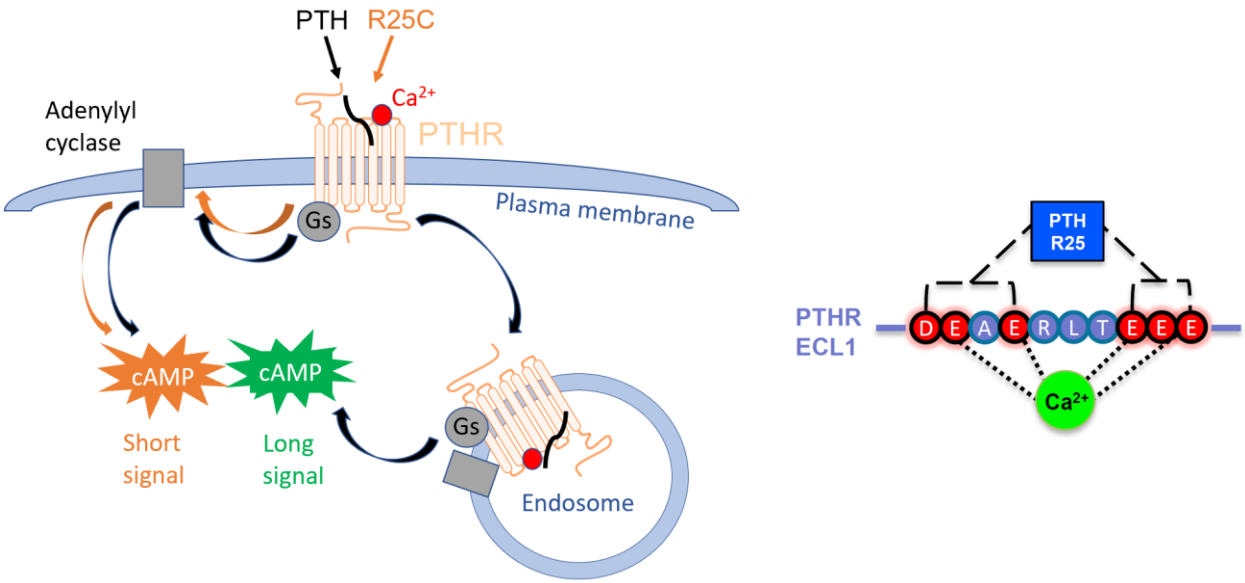

Figure 20. Ca^{2+} Allostery in PTHR Signaling.

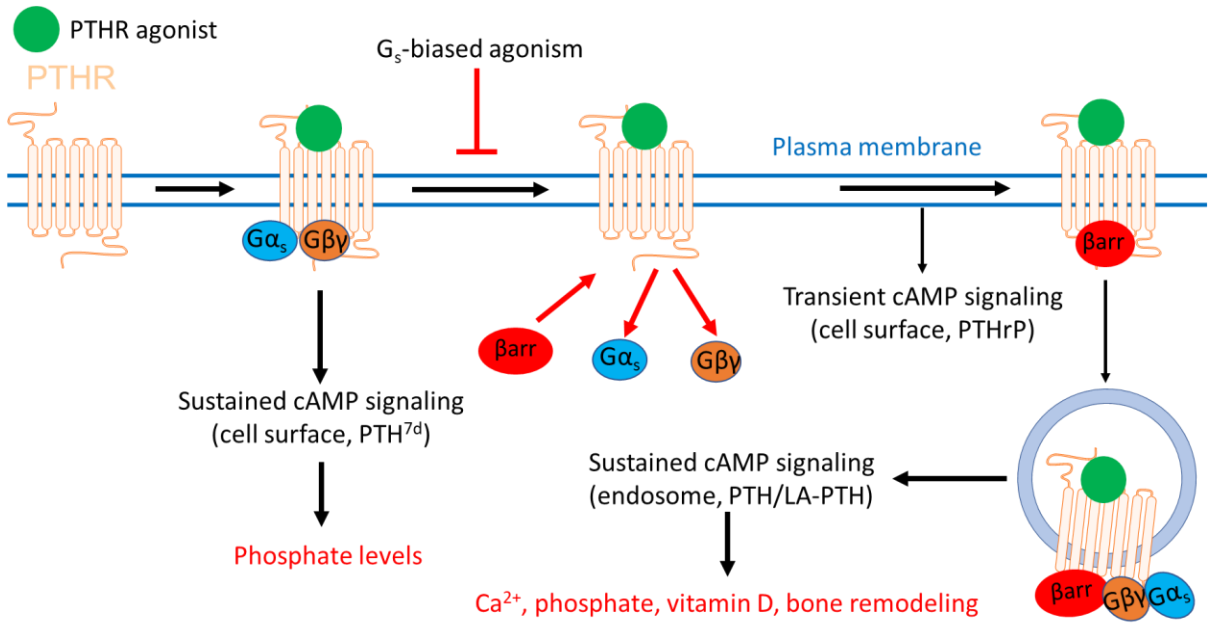

Figure 21. Decoding Spatial From Temporal Information of cAMP Signaling via PTH Receptor Biased Agonism.

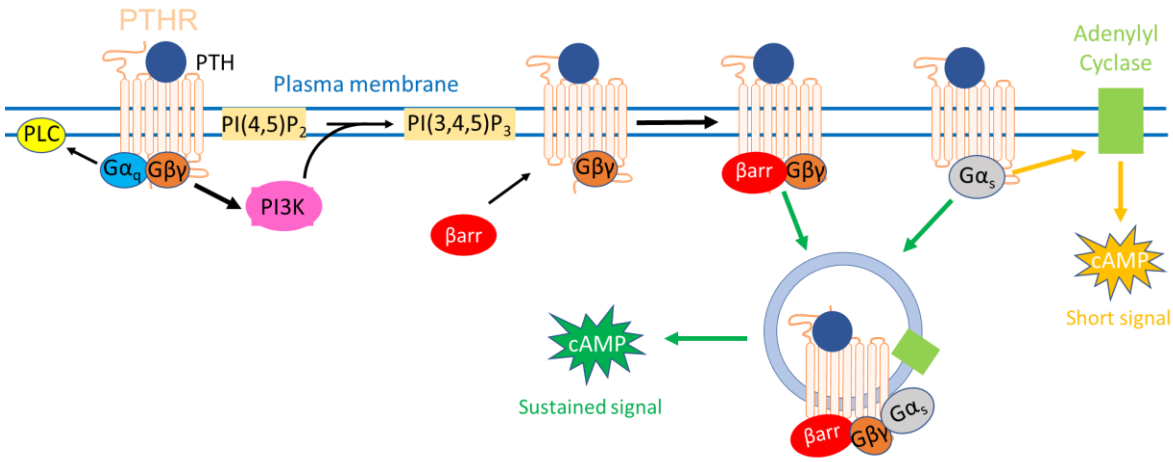

Figure 22. $G_{q/11}$-dependent Regulation of Endosomal cAMP Generation by PTH Class B GPCR.

Bibliography

1. Bockaert, J. and J.P. Pin, *Molecular tinkering of G protein-coupled receptors: an evolutionary success.* Embo j, 1999. **18**(7): p. 1723-9.

2. Hill, C.A., et al., *G protein-coupled receptors in Anopheles gambiae.* Science, 2002. **298**(5591): p. 176-8.

3. Insel, P.A., et al., *GPCR expression in tissues and cells: are the optimal receptors being used as drug targets?* Br J Pharmacol, 2012. **165**(6): p. 1613-1616.

4. Versele, M., K. Lemaire, and J.M. Thevelein, *Sex and sugar in yeast: two distinct GPCR systems.* EMBO Rep, 2001. **2**(7): p. 574-9.

5. Vernier, P., et al., *An evolutionary view of drug-receptor interaction: the bioamine receptor family.* Trends Pharmacol Sci, 1995. **16**(11): p. 375-81.

6. Bargmann, C.I., *Neurobiology of the Caenorhabditis elegans genome.* Science, 1998. **282**(5396): p. 2028-33.

7. Milligan, G. and J.C. McGrath, *GPCR theme editorial.* Br J Pharmacol, 2009. **158**(1): p. 1-4.

8. Schioth, H.B. and R. Fredriksson, *The GRAFS classification system of G-protein coupled receptors in comparative perspective.* Gen Comp Endocrinol, 2005. **142**(1-2): p. 94-101.

9. Pal, K., K. Melcher, and H.E. Xu, *Structure and mechanism for recognition of peptide hormones by Class B G-protein-coupled receptors.* Acta Pharmacol Sin, 2012. **33**(3): p. 300-11.

10. Palczewski, K., et al., *Crystal structure of rhodopsin: A G protein-coupled receptor.* Science, 2000. **289**(5480): p. 739-45.

11. Malbon, C.C., *G proteins in development.* Nature Reviews Molecular Cell Biology, 2005. **6**(9): p. 689-701.

12. Hamm, H.E., *How activated receptors couple to G proteins.* Proceedings of the National Academy of Sciences of the United States of America, 2001. **98**(9): p. 4819-4821.

13. Neves, S.R., P.T. Ram, and R. Iyengar, *G protein pathways.* Science, 2002. **296**(5573): p. 1636-9.

14. Urena, P., et al., *Parathyroid hormone (PTH)/PTH-related peptide receptor messenger ribonucleic acids are widely distributed in rat tissues.* Endocrinology, 1993. **133**(2): p. 617-23.

15. Silva, B.C., et al., *Catabolic and anabolic actions of parathyroid hormone on the skeleton.* J Endocrinol Invest, 2011. **34**(10): p. 801-10.

16. Boyce, B.F., et al., *The osteoclast, bone remodelling and treatment of metabolic bone disease.* Eur J Clin Invest, 2012. **42**(12): p. 1332-41.

17. O'Brien, C.A., T. Nakashima, and H. Takayanagi, *Osteocyte control of osteoclastogenesis.* Bone, 2013. **54**(2): p. 258-63.

18. Saini, V., et al., *Parathyroid hormone (PTH)/PTH-related peptide type 1 receptor (PPR) signaling in osteocytes regulates anabolic and catabolic skeletal responses to PTH.* J Biol Chem, 2013. **288**(28): p. 20122-34.

19. van Abel, M., et al., *Coordinated control of renal Ca(2+) transport proteins by parathyroid hormone.* Kidney Int, 2005. **68**(4): p. 1708-21.

20. de Groot, T., et al., *Parathyroid hormone activates TRPV5 via PKA-dependent phosphorylation.* J Am Soc Nephrol, 2009. **20**(8): p. 1693-704.

21. Biber, J., et al., *Regulation of phosphate transport in proximal tubules.* Pflugers Arch, 2009. **458**(1): p. 39-52.

22. Picard, N., et al., *Acute parathyroid hormone differentially regulates renal brush border membrane phosphate cotransporters.* Pflugers Arch, 2010. **460**(3): p. 677-87.

23. Nagai, S., et al., *Acute down-regulation of sodium-dependent phosphate transporter NPT2a involves predominantly the cAMP/PKA pathway as revealed by signaling-selective parathyroid hormone analogs.* J Biol Chem, 2011. **286**(2): p. 1618-26.

24. Suva, L.J., et al., *A parathyroid hormone-related protein implicated in malignant hypercalcemia: cloning and expression.* Science, 1987. **237**(4817): p. 893-6.

25. Nissenson, R.A., D. Diep, and G.J. Strewler, *Synthetic peptides comprising the amino-terminal sequence of a parathyroid hormone-like protein from human malignancies. Binding to parathyroid hormone receptors and activation of adenylate cyclase in bone cells and kidney.* J Biol Chem, 1988. **263**(26): p. 12866-71.

26. McCauley, L.K. and T.J. Martin, *Twenty-five years of PTHrP progress: from cancer hormone to multifunctional cytokine.* J Bone Miner Res, 2012. **27**(6): p. 1231-9.

27. Karaplis, A.C., et al., *Lethal skeletal dysplasia from targeted disruption of the parathyroid hormone-related peptide gene.* Genes Dev, 1994. **8**(3): p. 277-89.

28. Wysolmerski, J.J. and A.F. Stewart, *The physiology of parathyroid hormone-related protein: an emerging role as a developmental factor.* Annu Rev Physiol, 1998. **60**: p. 431-60.

29. Philbrick, W.M., et al., *Parathyroid hormone-related protein is required for tooth eruption.* Proc Natl Acad Sci U S A, 1998. **95**(20): p. 11846-51.

30. Mullershausen, F., et al., *Persistent signaling induced by FTY720-phosphate is mediated by internalized S1P1 receptors.* Nat Chem Biol, 2009. **5**(6): p. 428-34.

31. Ferrandon, S., et al., *Sustained cyclic AMP production by parathyroid hormone receptor endocytosis.* Nat Chem Biol, 2009. **5**(10): p. 734-42.

32. De Lean, A., J.M. Stadel, and R.J. Lefkowitz, *A ternary complex model explains the agonist-specific binding properties of the adenylate cyclase-coupled beta-adrenergic receptor.* J Biol Chem, 1980. **255**(15): p. 7108-17.

33. Jacobs, J.W., et al., *Structural analysis of human proparathyroid hormone by a new microsequencing approach.* Nature, 1974. **249**(453): p. 155-7.

34. Hamilton, J.W., et al., *The N-terminal amino-acid sequence of bovine proparathyroid hormone.* Proc Natl Acad Sci U S A, 1974. **71**(3): p. 653-6.

35. Dean, T., et al., *Altered selectivity of parathyroid hormone (PTH) and PTH-related protein (PTHrP) for distinct conformations of the PTH/PTHrP receptor.* Mol Endocrinol, 2008. **22**(1): p. 156-66.

36. Okazaki, M., et al., *Prolonged signaling at the parathyroid hormone receptor by peptide ligands targeted to a specific receptor conformation.* Proc Natl Acad Sci U S A, 2008. **105**(43): p. 16525-30.

37. Maeda, A., et al., *Critical role of parathyroid hormone (PTH) receptor-1 phosphorylation in regulating acute responses to PTH.* Proc Natl Acad Sci U S A, 2013. **110**(15): p. 5864-9.

38. Wehbi, V.L., et al., *Noncanonical GPCR signaling arising from a PTH receptor-arrestin-Gbetagamma complex.* Proc Natl Acad Sci U S A, 2013. **110**(4): p. 1530-5.

39. Mahon, M.J., et al., *A docking site for G protein betagamma subunits on the parathyroid hormone 1 receptor supports signaling through multiple pathways.* Mol Endocrinol, 2006. **20**(1): p. 136-46.

40. Hoffmann, R., et al., *The MAP kinase ERK2 inhibits the cyclic AMP-specific phosphodiesterase HSPDE4D3 by phosphorylating it at Ser579.* The EMBO journal, 1999. **18**(4): p. 893-903.

41. Feinstein, T.N., et al., *Retromer terminates the generation of cAMP by internalized PTH receptors.* Nat Chem Biol, 2011. **7**(5): p. 278-84.

42. Collins, B.M., et al., *Structure of Vps26B and mapping of its interaction with the retromer protein complex.* Traffic, 2008. **9**(3): p. 366-79.

43. Bonifacino, J.S. and R. Rojas, *Retrograde transport from endosomes to the trans-Golgi network.* Nat Rev Mol Cell Biol, 2006. **7**(8): p. 568-79.

44. Gidon, A., et al., *Endosomal GPCR signaling turned off by negative feedback actions of PKA and v-ATPase.* Nat Chem Biol, 2014. **10**(9): p. 707-9.

45. Horwitz, M.J., et al., *Continuous PTH and PTHrP infusion causes suppression of bone formation and discordant effects on 1,25(OH)2 vitamin D.* J Bone Miner Res, 2005. **20**(10): p. 1792-803.

46. Horwitz, M.J., et al., *Short-term, high-dose parathyroid hormone-related protein as a skeletal anabolic agent for the treatment of postmenopausal osteoporosis.* J Clin Endocrinol Metab, 2003. **88**(2): p. 569-75.

47. Horwitz, M.J., et al., *Direct comparison of sustained infusion of human parathyroid hormone-related protein-(1-36) [hPTHrP-(1-36)] versus hPTH-(1-34) on serum calcium, plasma 1,25-dihydroxyvitamin D concentrations, and fractional calcium excretion in healthy human volunteers.* J Clin Endocrinol Metab, 2003. **88**(4): p. 1603-9.

48. Neer, R.M., et al., *Effect of parathyroid hormone (1-34) on fractures and bone mineral density in postmenopausal women with osteoporosis.* N Engl J Med, 2001. **344**(19): p. 1434-41.

49. Leder, B.Z., et al., *Effects of abaloparatide, a human parathyroid hormone-related peptide analog, on bone mineral density in postmenopausal women with osteoporosis.* J Clin Endocrinol Metab, 2015. **100**(2): p. 697-706.

50. Shimizu, M., et al., *Pharmacodynamic Actions of a Long-Acting PTH Analog (LA-PTH) in Thyroparathyroidectomized (TPTX) Rats and Normal Monkeys.* J Bone Miner Res, 2016. **31**(7): p. 1405-12.

51. White, A.D., et al., *Ca(2+) allostery in PTH-receptor signaling.* Proc Natl Acad Sci U S A, 2019. **116**(8): p. 3294-3299.

52. Lee, S., et al., *A Homozygous [Cys25]PTH(1-84) Mutation That Impairs PTH/PTHrP Receptor Activation Defines a Novel Form of Hypoparathyroidism.* J Bone Miner Res, 2015. **30**(10): p. 1803-13.

53. Calebiro, D., et al., *Persistent cAMP-signals triggered by internalized G-protein-coupled receptors.* PLoS Biol, 2009. **7**(8): p. e1000172.

54. Gardella, T.J. and J.P. Vilardaga, *International Union of Basic and Clinical Pharmacology. XCIII. The parathyroid hormone receptors--family B G protein-coupled receptors.* Pharmacol Rev, 2015. **67**(2): p. 310-37.

55. Vilardaga, J.P., F.G. Jean-Alphonse, and T.J. Gardella, *Endosomal generation of cAMP in GPCR signaling.* Nat Chem Biol, 2014. **10**(9): p. 700-6.

56. Eichel, K. and M. von Zastrow, *Subcellular Organization of GPCR Signaling.* Trends Pharmacol Sci, 2018. **39**(2): p. 200-208.

57. Kotowski, S.J., et al., *Endocytosis promotes rapid dopaminergic signaling.* Neuron, 2011. **71**(2): p. 278-90.

58. Jean-Alphonse, F.G., et al., *β(2)-adrenergic receptor control of endosomal PTH receptor signaling via Gβγ.* Nature chemical biology, 2017. **13**(3): p. 259-261.

59. Silver, I.A., R.J. Murrills, and D.J. Etherington, *Microelectrode studies on the acid microenvironment beneath adherent macrophages and osteoclasts.* Exp Cell Res, 1988. **175**(2): p. 266-76.

60. Mitra, N., et al., *Calcium-dependent ligand binding and G-protein signaling of family B GPCR parathyroid hormone 1 receptor purified in nanodiscs.* ACS Chem Biol, 2013. **8**(3): p. 617-25.

61. Nikolaev, V.O., et al., *Novel single chain cAMP sensors for receptor-induced signal propagation.* J Biol Chem, 2004. **279**(36): p. 37215-8.

62. Gidon, A., et al., *Studying the regulation of endosomal cAMP production in GPCR signaling.* Methods Cell Biol, 2016. **132**: p. 109-26.

63. Vilardaga, J.P., *Studying ligand efficacy at G protein-coupled receptors using FRET.* Methods Mol Biol, 2011. **756**: p. 133-48.

64. McGarvey, J.C., et al., *Actin-Sorting Nexin 27 (SNX27)-Retromer Complex Mediates Rapid Parathyroid Hormone Receptor Recycling.* J Biol Chem, 2016. **291**(21): p. 10986-1002.

65. Rasmussen, S.G., et al., *Crystal structure of the beta2 adrenergic receptor-Gs protein complex.* Nature, 2011. **477**(7366): p. 549-55.

66. Zhang, J., et al., *GPCR-I-TASSER: A Hybrid Approach to G Protein-Coupled Receptor Structure Modeling and the Application to the Human Genome.* Structure, 2015. **23**(8): p. 1538-1549.

67. Pioszak, A.A. and H.E. Xu, *Molecular recognition of parathyroid hormone by its G protein-coupled receptor.* Proc Natl Acad Sci U S A, 2008. **105**(13): p. 5034-9.

68. Jin, L., et al., *Crystal structure of human parathyroid hormone 1-34 at 0.9-A resolution.* J Biol Chem, 2000. **275**(35): p. 27238-44.

69. Castro, M., et al., *Turn-on switch in parathyroid hormone receptor by a two-step parathyroid hormone binding mechanism.* Proceedings of the National Academy of Sciences of the United States of America, 2005. **102**(44): p. 16084-16089.

70. Kahsai, A.W., et al., *Monitoring protein conformational changes and dynamics using stable-isotope labeling and mass spectrometry.* Nat Protoc, 2014. **9**(6): p. 1301-19.

71. Katritch, V., et al., *Allosteric sodium in class A GPCR signaling.* Trends Biochem Sci, 2014. **39**(5): p. 233-44.

72. Pasternak, G.W., A.M. Snowman, and S.H. Snyder, *Selective enhancement of [3H]opiate agonist binding by divalent cations.* Mol Pharmacol, 1975. **11**(6): p. 735-44.

73. Johansson, B., F.E. Parkinson, and B.B. Fredholm, *Effects of mono- and divalent ions on the binding of the adenosine analogue CGS 21680 to adenosine A2 receptors in rat striatum.* Biochem Pharmacol, 1992. **44**(12): p. 2365-70.

74. Rodriguez, F.D., E. Bardaji, and J.R. Traynor, *Differential effects of Mg2+ and other divalent cations on the binding of tritiated opioid ligands.* J Neurochem, 1992. **59**(2): p. 467-72.

75. Mazzoni, M.R., C. Martini, and A. Lucacchini, *Regulation of agonist binding to A2A adenosine receptors: effects of guanine nucleotides (GDP[S] and GTP[S]) and Mg2+ ion.* Biochim Biophys Acta, 1993. **1220**(1): p. 76-84.

76. Burgmer, U., et al., *Interaction of Mg2+ with the allosteric site of muscarinic M2 receptors.* Naunyn Schmiedebergs Arch Pharmacol, 1998. **357**(4): p. 363-70.

77. Ye, L., et al., *Mechanistic insights into allosteric regulation of the A2A adenosine G protein-coupled receptor by physiological cations.* Nat Commun, 2018. **9**(1): p. 1372.

78. Urwyler, S., *Allosteric modulation of family C G-protein-coupled receptors: from molecular insights to therapeutic perspectives.* Pharmacol Rev, 2011. **63**(1): p. 59-126.

79. Hattersley, G., et al., *Binding Selectivity of Abaloparatide for PTH-Type-1-Receptor Conformations and Effects on Downstream Signaling.* Endocrinology, 2016. **157**(1): p. 141-9.

80. Broichhagen, J., et al., *Optical Control of Insulin Secretion Using an Incretin Switch.* Angew Chem Int Ed Engl, 2015. **54**(51): p. 15565-9.

81. Fremaux, J., et al., *Peptide-oligourea hybrids analogue of GLP-1 with improved action in vivo.* Nat Commun, 2019. **10**(1): p. 924.

82. Kroll, C., et al., *Hybrid bombesin analogues: combining an agonist and an antagonist in defined distances for optimized tumor targeting.* J Am Chem Soc, 2013. **135**(45): p. 16793-6.

83. Liu, Y., et al., *Triblock peptide-linker-lipid molecular design improves potency of peptide ligands targeting family B G protein-coupled receptors.* Chem Commun (Camb), 2015. **51**(28): p. 6157-60.

84. Cheloha, R.W., et al., *Backbone modification of a polypeptide drug alters duration of action in vivo.* Nat Biotechnol, 2014. **32**(7): p. 653-5.

85. Cheloha, R.W., et al., *Development of Potent, Protease-Resistant Agonists of the Parathyroid Hormone Receptor with Broad beta Residue Distribution.* J Med Chem, 2017. **60**(21): p. 8816-8833.

86. Johnson, L.M., et al., *A potent alpha/beta-peptide analogue of GLP-1 with prolonged action in vivo.* J Am Chem Soc, 2014. **136**(37): p. 12848-51.

87. Liu, S., et al., *Receptor selectivity from minimal backbone modification of a polypeptide agonist.* Proc Natl Acad Sci U S A, 2018. **115**(49): p. 12383-12388.

88. Hager, M.V., et al., *beta-Arrestin-Biased Agonists of the GLP-1 Receptor from beta-Amino Acid Residue Incorporation into GLP-1 Analogues.* J Am Chem Soc, 2016. **138**(45): p. 14970-14979.

89. Mary, S., et al., *Ligands and signaling proteins govern the conformational landscape explored by a G protein-coupled receptor.* Proc Natl Acad Sci U S A, 2012. **109**(21): p. 8304-9.

90. Rajagopal, S., K. Rajagopal, and R.J. Lefkowitz, *Teaching old receptors new tricks: biasing seven-transmembrane receptors.* Nat Rev Drug Discov, 2010. **9**(5): p. 373-86.

91. Abou-Samra, A.B., et al., *Expression cloning of a common receptor for parathyroid hormone and parathyroid hormone-related peptide from rat osteoblast-like cells: a single receptor stimulates intracellular accumulation of both cAMP and inositol trisphosphates and increases intracellular free calcium.* Proc Natl Acad Sci U S A, 1992. **89**(7): p. 2732-6.

92. Gesty-Palmer, D., et al., *Distinct beta-arrestin- and G protein-dependent pathways for parathyroid hormone receptor-stimulated ERK1/2 activation.* J Biol Chem, 2006. **281**(16): p. 10856-64.

93. Cheloha, R.W., et al., *PTH receptor-1 signalling-mechanistic insights and therapeutic prospects.* Nat Rev Endocrinol, 2015. **11**(12): p. 712-24.

94. Tsvetanova, N.G. and M. von Zastrow, *Spatial encoding of cyclic AMP signaling specificity by GPCR endocytosis.* Nat Chem Biol, 2014. **10**(12): p. 1061-5.

95. Ricarte, F.R., et al., *Parathyroid hormone(1-34) and its analogs differentially modulate osteoblastic Rankl expression via PKA/SIK2/SIK3 and PP1/PP2A-CRTC3 signaling.* J Biol Chem, 2018. **293**(52): p. 20200-20213.

96. Ferrari, S.L., et al., *Endocytosis of ligand-human parathyroid hormone receptor 1 complexes is protein kinase C-dependent and involves beta-arrestin2. Real-time monitoring by fluorescence microscopy.* J Biol Chem, 1999. **274**(42): p. 29968-75.

97. Bisello, A., et al., *Selective ligand-induced stabilization of active and desensitized parathyroid hormone type 1 receptor conformations.* J Biol Chem, 2002. **277**(41): p. 38524-30.

98. Cupp, M.E., et al., *Parathyroid hormone (PTH) and PTH-related peptide domains contributing to activation of different PTH receptor-mediated signaling pathways.* J Pharmacol Exp Ther, 2013. **345**(3): p. 404-18.

99. Peggion, E., et al., *Structure-function studies of analogues of parathyroid hormone (PTH)-1-34 containing beta-amino acid residues in positions 11-13.* Biochemistry, 2002. **41**(25): p. 8162-75.

100. Schievano, E., et al., *Conformational and biological characterization of human parathyroid hormone hPTH(1-34) analogues containing beta-amino acid residues in positions 17-19.* Biopolymers, 2003. **70**(4): p. 534-47.

101. Berg, C., K. Neumeyer, and P. Kirkpatrick, *Teriparatide.* Nat Rev Drug Discov, 2003. **2**(4): p. 257-8.

102. Shirley, M., *Abaloparatide: First Global Approval.* Drugs, 2017. **77**(12): p. 1363-1368.

103. Chi, Y. and S.H. Gellman, *Enantioselective organocatalytic aminomethylation of aldehydes: a role for ionic interactions and efficient access to beta2-amino acids.* Journal of the American Chemical Society, 2006. **128**(21): p. 6804-6805.

104. Chi, Y., et al., *Practical synthesis of enantiomerically pure beta2-amino acids via proline-catalyzed diastereoselective aminomethylation of aldehydes.* J Am Chem Soc, 2007. **129**(18): p. 6050-5.

105. Kuipers, B.J. and H. Gruppen, *Prediction of molar extinction coefficients of proteins and peptides using UV absorption of the constituent amino acids at 214 nm to enable quantitative reverse phase high-performance liquid chromatography-mass spectrometry analysis.* J Agric Food Chem, 2007. **55**(14): p. 5445-51.

106. Liang, Y.L., et al., *Phase-plate cryo-EM structure of a biased agonist-bound human GLP-1 receptor-Gs complex.* Nature, 2018. **555**(7694): p. 121-125.

107. Liang, Y.L., et al., *Phase-plate cryo-EM structure of a class B GPCR-G-protein complex.* Nature, 2017. **546**(7656): p. 118-123.

108. Zhang, Y., et al., *Cryo-EM structure of the activated GLP-1 receptor in complex with a G protein.* Nature, 2017. **546**(7657): p. 248-253.

109. Zhao, L.H., et al., *Structure and dynamics of the active human parathyroid hormone receptor-1.* Science, 2019. **364**(6436): p. 148-153.

110. Gardella, T.J., et al., *Parathyroid hormone (PTH)-PTH-related peptide hybrid peptides reveal functional interactions between the 1-14 and 15-34 domains of the ligand.* J Biol Chem, 1995. **270**(12): p. 6584-8.

111. Vilardaga, J.P., et al., *Differential conformational requirements for activation of G proteins and the regulatory proteins arrestin and G protein-coupled receptor kinase in the G protein-coupled receptor for parathyroid hormone (PTH)/PTH-related protein.* J Biol Chem, 2001. **276**(36): p. 33435-43.

112. Kenakin, T., et al., *A simple method for quantifying functional selectivity and agonist bias.* ACS Chem Neurosci, 2012. **3**(3): p. 193-203.

113. Black, J.W. and P. Leff, *Operational models of pharmacological agonism.* Proc R Soc Lond B Biol Sci, 1983. **220**(1219): p. 141-62.

114. Tamura, T., et al., *Identification of an orally active small-molecule PTHR1 agonist for the treatment of hypoparathyroidism.* Nat Commun, 2016. **7**: p. 13384.

115. Thomsen, A.R.B., et al., *GPCR-G Protein-beta-Arrestin Super-Complex Mediates Sustained G Protein Signaling.* Cell, 2016. **166**(4): p. 907-919.

116. Yoshimori, T., et al., *Bafilomycin A1, a specific inhibitor of vacuolar-type H(+)-ATPase, inhibits acidification and protein degradation in lysosomes of cultured cells.* J Biol Chem, 1991. **266**(26): p. 17707-12.

117. Qin, L., L.J. Raggatt, and N.C. Partridge, *Parathyroid hormone: a double-edged sword for bone metabolism.* Trends Endocrinol Metab, 2004. **15**(2): p. 60-5.

118. Fredriksson, R. and H.B. Schioth, *The repertoire of G-protein-coupled receptors in fully sequenced genomes.* Mol Pharmacol, 2005. **67**(5): p. 1414-25.

119. Galandrin, S., G. Oligny-Longpre, and M. Bouvier, *The evasive nature of drug efficacy: implications for drug discovery.* Trends Pharmacol Sci, 2007. **28**(8): p. 423-30.

120. Maudsley, S., B. Martin, and L.M. Luttrell, *The origins of diversity and specificity in g protein-coupled receptor signaling.* J Pharmacol Exp Ther, 2005. **314**(2): p. 485-94.

121. Feinstein, T.N., et al., *Retromer terminates the generation of cAMP by internalized PTH receptors.* Nature chemical biology, 2011. **7**(5): p. 278-284.

122. Sutkeviciute, I., et al., *PTH/PTHrP Receptor Signaling, Allostery, and Structures.* Trends Endocrinol Metab, 2019. **30**(11): p. 860-874.

123. Vilardaga, J.P., et al., *Measurement of the millisecond activation switch of G protein-coupled receptors in living cells.* Nat Biotechnol, 2003. **21**(7): p. 807-12.

124. Burghardt, A.J., et al., *Multicenter precision of cortical and trabecular bone quality measures assessed by high-resolution peripheral quantitative computed tomography.* Journal of bone and mineral research : the official journal of the American Society for Bone and Mineral Research, 2013. **28**(3): p. 524-536.

125. Roy, A., A. Kucukural, and Y. Zhang, *I-TASSER: a unified platform for automated protein structure and function prediction.* Nat Protoc, 2010. **5**(4): p. 725-38.

126. Yang, J., et al., *The I-TASSER Suite: protein structure and function prediction.* Nat Methods, 2015. **12**(1): p. 7-8.

127. Zhang, Y., *I-TASSER server for protein 3D structure prediction.* BMC Bioinformatics, 2008. **9**: p. 40.

128. Lomize, M.A., et al., *OPM database and PPM web server: resources for positioning of proteins in membranes.* Nucleic Acids Res, 2012. **40**(Database issue): p. D370-6.

129. Brooks, B.R., et al., *CHARMM: the biomolecular simulation program.* Journal of computational chemistry, 2009. **30**(10): p. 1545-1614.

130. Jo, S., T. Kim, and W. Im, *Automated builder and database of protein/membrane complexes for molecular dynamics simulations.* PloS one, 2007. **2**(9): p. e880-e880.

131. Jo, S., et al., *CHARMM-GUI: a web-based graphical user interface for CHARMM.* J Comput Chem, 2008. **29**(11): p. 1859-65.

132. Jo, S., et al., *CHARMM-GUI Membrane Builder for mixed bilayers and its application to yeast membranes.* Biophys J, 2009. **97**(1): p. 50-8.

133. Lee, J., et al., *CHARMM-GUI Input Generator for NAMD, GROMACS, AMBER, OpenMM, and CHARMM/OpenMM Simulations Using the CHARMM36 Additive Force Field.* J Chem Theory Comput, 2016. **12**(1): p. 405-13.

134. Lee, J., et al., *CHARMM-GUI Membrane Builder for Complex Biological Membrane Simulations with Glycolipids and Lipoglycans.* J Chem Theory Comput, 2019. **15**(1): p. 775-786.

135. Wu, E.L., et al., *CHARMM-GUI Membrane Builder toward realistic biological membrane simulations.* J Comput Chem, 2014. **35**(27): p. 1997-2004.

136. Huang, J., et al., *CHARMM36m: an improved force field for folded and intrinsically disordered proteins.* Nat Methods, 2017. **14**(1): p. 71-73.

137. Phillips, J.C., et al., *Scalable molecular dynamics with NAMD.* J Comput Chem, 2005. **26**(16): p. 1781-802.

138. Humphrey, W., A. Dalke, and K. Schulten, *VMD: visual molecular dynamics.* J Mol Graph, 1996. **14**(1): p. 33-8, 27-8.

139. Kang, Y., et al., *Crystal structure of rhodopsin bound to arrestin by femtosecond X-ray laser.* Nature, 2015. **523**(7562): p. 561-7.

140. Waterhouse, A., et al., *SWISS-MODEL: homology modelling of protein structures and complexes.* Nucleic Acids Res, 2018. **46**(W1): p. W296-w303.

141. Oztan, A., et al., *Exocyst requirement for endocytic traffic directed toward the apical and basolateral poles of polarized MDCK cells.* Mol Biol Cell, 2007. **18**(10): p. 3978-92.

142. Nobles, K.N., et al., *Distinct phosphorylation sites on the beta(2)-adrenergic receptor establish a barcode that encodes differential functions of beta-arrestin.* Sci Signal, 2011. **4**(185): p. ra51.

143. Xiao, K. and S.K. Shenoy, *Beta2-adrenergic receptor lysosomal trafficking is regulated by ubiquitination of lysyl residues in two distinct receptor domains.* J Biol Chem, 2011. **286**(14): p. 12785-95.

144. Xiao, K., et al., *Revealing the architecture of protein complexes by an orthogonal approach combining HDXMS, CXMS, and disulfide trapping.* Nat Protoc, 2018. **13**(6): p. 1403-1428.

145. Haas, W., et al., *Optimization and use of peptide mass measurement accuracy in shotgun proteomics.* Mol Cell Proteomics, 2006. **5**(7): p. 1326-37.

146. Bakalarski, C.E., et al., *The impact of peptide abundance and dynamic range on stable-isotope-based quantitative proteomic analyses.* J Proteome Res, 2008. **7**(11): p. 4756-65.

147. Liggett, S.B., *Phosphorylation Barcoding as a Mechanism of Directing GPCR Signaling.* Science Signaling, 2011. **4**(185): p. pe36.

148. Mayer, D., et al., *Distinct G protein-coupled receptor phosphorylation motifs modulate arrestin affinity and activation and global conformation.* Nature Communications, 2019. **10**(1): p. 1261.

149. Staus, D.P., et al., *Sortase ligation enables homogeneous GPCR phosphorylation to reveal diversity in beta-arrestin coupling.* Proc Natl Acad Sci U S A, 2018. **115**(15): p. 3834-3839.

150. Zindel, D., et al., *Identification of key phosphorylation sites in PTH1R that determine arrestin3 binding and fine-tune receptor signaling.* The Biochemical journal, 2016. **473**(22): p. 4173-4192.

151. Shiraishi, Y., et al., *Phosphorylation-induced conformation of β(2)-adrenoceptor related to arrestin recruitment revealed by NMR.* Nature communications, 2018. **9**(1): p. 194-194.

152. Wang, B., et al., *Ezrin-anchored protein kinase A coordinates phosphorylation-dependent disassembly of a NHERF1 ternary complex to regulate hormone-sensitive phosphate transport.* The Journal of biological chemistry, 2012. **287**(29): p. 24148-24163.

153. Brenza, H.L., et al., *Parathyroid hormone activation of the 25-hydroxyvitamin D3-1alpha-hydroxylase gene promoter.* Proc Natl Acad Sci U S A, 1998. **95**(4): p. 1387-91.

154. Sample, V., et al., *Regulation of nuclear PKA revealed by spatiotemporal manipulation of cyclic AMP.* Nature chemical biology, 2012. **8**(4): p. 375-382.

155. Jilka, R.L., *Molecular and cellular mechanisms of the anabolic effect of intermittent PTH.* Bone, 2007. **40**(6): p. 1434-46.

156. Askar, A.M., *Hyperphosphatemia. The hidden killer in chronic kidney disease.* Saudi medical journal, 2015. **36**(1): p. 13-19.

157. Feinstein, T.N., et al., *Noncanonical control of vasopressin receptor type 2 signaling by retromer and arrestin.* The Journal of biological chemistry, 2013. **288**(39): p. 27849-27860.

158. Kuna, R.S., et al., *Glucagon-like peptide-1 receptor-mediated endosomal cAMP generation promotes glucose-stimulated insulin secretion in pancreatic beta-cells.* Am J Physiol Endocrinol Metab, 2013. **305**(2): p. E161-70.

159. Irannejad, R., et al., *Functional selectivity of GPCR-directed drug action through location bias.* Nat Chem Biol, 2017. **13**(7): p. 799-806.

160. Juppner, H., et al., *A G protein-linked receptor for parathyroid hormone and parathyroid hormone-related peptide.* Science, 1991. **254**(5034): p. 1024-6.

161. Potts, J.T., H.M. Kronenberg, and M. Rosenblatt, *Parathyroid Hormone: Chemistry, Biosynthesis, and Mode of Action*, in *Advances in Protein Chemistry*, C.B. Anfinsen, J.T. Edsall, and F.M. Richards, Editors. 1982, Academic Press. p. 323-396.

162. Liu, S., et al., *Use of Backbone Modification To Enlarge the Spatiotemporal Diversity of Parathyroid Hormone Receptor-1 Signaling via Biased Agonism.* Journal of the American Chemical Society, 2019. **141**(37): p. 14486-14490.

163. Schrage, R., et al., *The experimental power of FR900359 to study Gq-regulated biological processes.* Nat Commun, 2015. **6**: p. 10156.

164. Hollins, B., et al., *The c-terminus of GRK3 indicates rapid dissociation of G protein heterotrimers.* Cell Signal, 2009. **21**(6): p. 1015-21.

165. Kurosu, H., et al., *Heterodimeric phosphoinositide 3-kinase consisting of p85 and p110beta is synergistically activated by the betagamma subunits of G proteins and phosphotyrosyl peptide.* J Biol Chem, 1997. **272**(39): p. 24252-6.

166. Jackson, S.P., et al., *PI 3-kinase p110beta: a new target for antithrombotic therapy.* Nat Med, 2005. **11**(5): p. 507-14.

167. Thomas, D., et al., *Protein kinase activity of phosphoinositide 3-kinase regulates cytokine-dependent cell survival.* PLoS Biol, 2013. **11**(3): p. e1001515.

168. Belshaw, P.J., et al., *Controlling protein association and subcellular localization with a synthetic ligand that induces heterodimerization of proteins.* Proceedings of the National Academy of Sciences, 1996. **93**(10): p. 4604.

169. Goulden, B.D., et al., *A high-avidity biosensor reveals plasma membrane PI(3,4)P2 is predominantly a class I PI3K signaling product.* The Journal of Cell Biology, 2018. **218**(3): p. 1066-1079.

170. Myers, M.P., et al., *P-TEN, the tumor suppressor from human chromosome 10q23, is a dual-specificity phosphatase.* Proc Natl Acad Sci U S A, 1997. **94**(17): p. 9052-7.

171. Gaidarov, I., et al., *Arrestin function in G protein-coupled receptor endocytosis requires phosphoinositide binding.* Embo j, 1999. **18**(4): p. 871-81.